University of South-Eastern Norway
Faculty of Technology, Natural Sciences and Maritime Studies

Doctoral dissertation no. 7
2018

Anjana Malagalage

N l c s k _rga am l t cwg l e _ l b qrmp_ec md u cr n_prgajcq rm gjj s qrp_rc mddq f mpc bpgjj a s rrg l e f _ l bjg l e

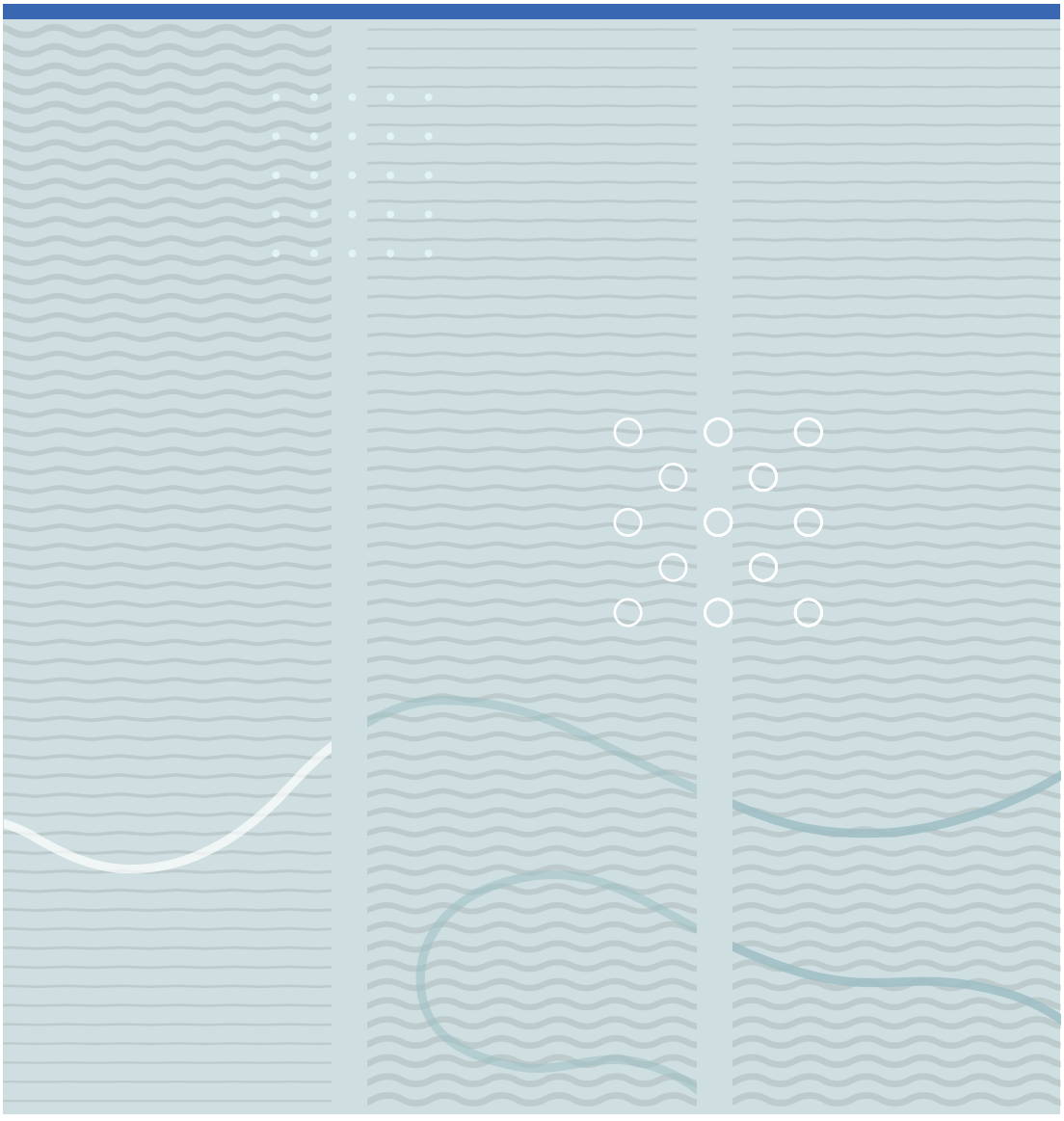

Anjana Malagalage

Pneumatic conveying and storage of wet particles to illustrate offshore drill cutting handling

A PhD dissertation in
Process, Energy and Automation Engineering

Faculty of Technology, Natural Sciences and Maritime Studies
University of South-Eastern Norway
Porsgrunn, 2018

Doctoral dissertations at the University of South-Eastern Norway no.7

ISSN: 2535-5244 (print)
ISSN: 2535-5252 (online)

ISBN: 978-82-7206-481-4 (print)
ISBN: 978-82-7206-482-1 (online)

Print: University of South-Eastern Norway

Preface

This thesis is submitted as a partial fulfilment of the requirements for the degree of philosophiae doctor (PhD) at the University of South-Eastern Norway (USN). I had the pleasure of working as a PhD student at SINTEF Tel-Tek (formerly Tel-Tek) from August 2014 to December 2017 and my PhD study was funded by the Norwegian Research Council (NRF) and Aker BP ASA (formerly Det norske oljeselskap ASA) under the PETROMAKS II project. The PhD study was carried out at SINTEF Tel-Tek with the collaboration of USN and Aker BP. Apart from them, CUBILITY AS and Powder Power AS also participated in the project.

The experimental study described in this dissertation would not have become a reality without the support of many individuals and organizations. Therefore, I would like to take this opportunity to thank and express my gratitude to,

- Prof.Chandana Rathnayake, my supervisor, and Prof.Arild Saasen at University of Stavenger (formerly at Aker BP), my co-supervisor, for their invaluable guidance, encouragement, support given in obtaining relevant test materials and interesting discussions that we had throughout this project amidst their busy schedules.
- Prof.Morten C. Melaaen and Dr.Hiromi Ariyarathna at USN for their many valuable comments and suggestions on my experimental work.
- Prof.Britt E. Moldestad at USN for providing me with the fluidization test apparatus at USN and also for her valuable comments and suggestions with regarding my experimental work.
- Prof.Gisle Enstad at Powder Power As for answering my questions and giving me valuable suggestions with regarding bulk solid shear tests.
- Mr.Richard Gyland at M-I Swaco (Schlumberger) for providing me with the required drilling fluids.
- Dr.Frode Brakstad, department manager of the Powder science and technology (POSTEC) at SINTEF Tel-Tek, for all the support given to me in the administrative matters and for the guidance given to me with regarding the application of process analytical technologies (PAT) in my research work. I must also express my sincere gratitude for him as he was always concerned about my well-being during this hard working period.

- All the colleagues at SINTEF Tel-Tek including Dr.Klaus Schöffel, our managing director, Liv Axelsen, administrative manager,Marit Larsen, senior advisor, Eksath de Silva, IT coordinator who supported me in various ways throughout my PhD career. I must also thank Dr. Kristian Aas and Ms.Ingrid Haugland who were very collaborative and helpful in sharing laboratory resources (compressed air) at the POSTEC hall. The support given to me by Lars Ellingsen with regarding the IT matters during the final days of thesis writing is also highly appreciated.
- Mr.Franz Hafenbrädl at SINTEF Tel-Tek for his great technical support for my experimental work. I must also thank him and Ms.Tonje Thomassen at SINTEF Tel-Tek for conducting some experimental tests (Jenike shear cell) on behalf of me.
- Mr.Bovinda Ahangama and Mr.Widuramini Sameendranath, my PhD assistants for their immense support given to me during the experimental tests.
- Mr.Mahesh Ediriweera at SINTEF Tel-Tek, Mr.Jørgen Vangen at Vangen Welding AS for their immense support in modification and repairing of the pneumatic conveying test rig.
- The staff of the library and the IT department at USN for providing me all the articles and software that I required for my study.
- The academic staff of the department of chemical and process engineering at the University of Moratuwa, Sri Lanka, specially Dr.P.G.Rathnasiri and Dr.Shantha Amarasinghe for providing me the opportunity to achieve my higher studies in Norway.
- All the Sri Lankan friends in Norway for their social support that made my stay in Norway a very enjoyable one. I must specially mention Chameera ayya, Manjula ayya, Ajith ayya and their families who were there with me all the time since the very first day that I came to Norway.
- My beloved parents, my brother and my sister-in-law for standing by me and encouraging me all the time with love and care.
- My loving wife Jayalanka, for taking care of me and my son with love and care. She was very patient, understanding and morally supportive during the difficult time periods that I was going through. No words can express my gratitude to her for the burden that she took on behalf of me throughout my PhD career. A big hug to my little son Pubud, for being patient with me when I was busy with my work. Love you so much!

Porsgrunn, 18th June 2018

Anjana Malagalage

Abstract

In this thesis, the pneumatic conveying and storage characteristics of particles mixed with a drilling fluid are studied based on the pilot scale experiments. The objective of this research is to investigate the impact of the presence of a drilling fluid towards the pneumatic conveying and storage properties of a bulk solid, which can be utilized in offshore drill cuttings handling.

Fluidization tests were conducted for sand samples with different particle size distributions and for a treated drill cuttings sample. Tests were conducted for both dry and wet (mixed with a drilling fluid) conditions. For this study two drilling fluids were considered namely, EDC 95/11 (a base oil) and a premix based on EDC 95/11. The comparison of the results shows that the minimum fluidization velocity of a particular dry particle system is significantly increased when a small amount of drilling fluid (1.5% by weight) is introduced to particle mixture. However, there was no significant deviation of the fluidization behaviour when the drilling fluid concentration was increased from 1.5% up to 6.3% but when it was further increased up to 10 %, the minimum fluidization velocity started to increase. The phenomenon was observed in both sand and treated drill cuttings sample with both drilling fluids.

The same sand mixtures were used in the pilot scale pneumatic conveying tests in dilute state both under dry and wet (mixed with the premix) conditions. Horizontal pneumatic conveying pressure drop displayed a similar behaviours as the minimum fluidization velocity with the drilling fluid concentration. That is, the pressure drop corresponding to the sand-drilling fluid mixture at concentration of 1.5% was significantly low compared to the pressure drop of the same dry sand mixture. It was also observed that the deviation of the minimum fluidization velocity of a wet sand mixture with respect to its dry condition and the the deviation of the horizontal pneumatic pressure drop of the same wet sand mixture with respect to its dry condition are closely correlated.

An empirical model was developed to predict the pressure drop of horizontal pneumatic conveying under dilute conditions. The model can successfully predict the pressure drop of the same dry material with different size distributions. It was shown that by incorporating the reduction of the minimum fluidization velocity which was obtained by the fluidization tests, the proposed model can predict the horizontal pneumatic conveying pressure drop of sand-drilling fluid mixtures approximately.

Bulk solid flow properties of a sand-drilling fluid mixture with different drilling fluid concentrations were analysed by using Jenike shear tester. The study shows that the flowability of the bulk solid depends on the fluid concentration, type of the fluid and the time period which the bulk solid is subjected under stress. With increasing fluid concentration, the flowability of the bulk solid reduce and reaches a minimum and beyond that the flowability improves as the bulk solid starts to behave as a slurry. Sand sample mixed with water displayed a lower flowability compared to the sand-drilling fluid mixtures. A sand-soap mixtures displayed a similar behaviour to the sand-drilling fluids approximately. It was also observed that the 7 days time consolidation has reduced the flowability of all the sand samples with different fluid types and concentrations.

Contents

List of Figures

List of Tables

Nomenclature

Symbols

Symbol	Explanation	Units
A	Area	[m^2]
Ar	Archimedes number	[-]
C_d	Drag coefficient	[-]
D	Pipe diameter	[m]
D90	Particle diameter at the 90% of the cumulative distribution	[mm]
d	Particle diameter	[m]
d_m	Mean particle diameter	[m]
Fr	Frode number	[-]
f_c	Unconfined yield strength	[Pa] / [$kgm^{-1}s^{-2}$]
f_D	Darcy friction factor	[-]
f_p	Impact and friction coefficient	[-]
g	Acceleration due to gravity	[ms^{-2}]
K_1, K_2	Numerical constants	[-]
k	Permeability	[m^2]
L	Distance	[m]
$\dot{m}$	Mass flow rate	[kgs^{-1}]
ΔP	Pressure drop	[Pa] / [$kgm^{-1}s^{-2}$]
P_i	Initial pressure	[Pa]
Re	Reynolds number	[-]
ΔT	Change in tensile strength	[Pa] / [$kgm^{-1}s^{-2}$]
u_c	Superficial fluid velocity	[ms^{-1}]
u	Velocity	[ms^{-1}]
u_r	Relative velocity	[ms^{-1}]
$u - u_{mf}$	Excess gas velocity	[ms^{-1}]
$\dot{V}$	Volumetric flow rate	[m^3s^{-1}]
w	Weight fraction	[-]
W_b	Weight of the bed	[kg]

Greek letters

Symbol	Explanation	Units
β_A	Fluid particle friction coefficient	[Pa.s.m^{-2}] / [kgm^{-3}s^{-1}]
δ	Effective angle of internal friction	[^{0}]
ε	Void fraction / voidage	[-]
η	Solid loading ratio	[-]
θ	Hopper angle	[^{0}]
λ_p	Additional pressure drop factor	[-]
λ_t	Global pressure drop factor	[-]
μ	Dynamic viscosity of fluid	[Pa.s] / [kgm^{-1}s^{-1}]
ρ	Density	[kgm^{-3}]
σ	Normal stress	[Pa] / [kgm^{-1}s^{-2}]
σ_1	Major principal stress	[Pa] / [kgm^{-1}s^{-2}]
σ_2	Minor principal stress	[Pa] / [kgm^{-1}s^{-2}]
σ_c	Unconfined yield strength	[Pa] / [kgm^{-1}s^{-2}]
$\sigma_{c,crit}$	Critical unconfined yield strength	[Pa] / [kgm^{-1}s^{-2}]
$\Delta\sigma$	Isostatic tensile strength	[Pa] / [kgm^{-1}s^{-2}]
τ	Shear stress	[Pa] / [kgm^{-1}s^{-2}]
ϕ	Kinematic angle of internal friction	[^{0}]
ϕ'	Static angle of surface friction	[^{0}]
ϕ_s	Sphericity	[-]

Subscripts

Symbol	Explanation
b	Bulk solid
D	Based on pipe diameter
g	Gas
mf	Minimum fluidization
mp	Minimum pressure drop
p	Particle
s	Solids
t	Total
∞	At terminal velocity conditions

Abbrivations

Symbol	Explanation
CFD	Computational Fluid Dynamics
FF	Flow function
ff	Flow factor
MFV	Minimum Fluidization Velocity
OBM	Oil Based Mud
PCA	Principle Component Analysis
WBM	Water Based Mud

1 Introduction

1.1 Background

The statistics published by the U.S. Energy Information Administration [1] show that the offshore oil production has been contributing for around 30% of the global oil production during the last decade.The first reported offshore oil well was drilled in Santa Barbara Channel at Summerland, California in 1897 and the offshore oil exploration in the Gulf of Mexico commenced in early 1930s. However, the commercial oil production in the Gulf of Mexico started in the period of 1960-70. Oil exploration in North Sea initiated after 1958 and the first oil reservoir in North Sea was discovered in 1965 in the sector of United Kingdom. The first commercially viable oil reservoir in the Norwegian sector was discovered in 1967 [2]. Currently, Saudi Arabia, Brazil, Mexico, Norway and USA are the five-major offshore oil producing countries and around 43% of the total offshore oil are produced by them [1].

1.1.1 Offshore drilling process

The first step in drilling an oil well is to conduct proper surveys to explore and locate suitable oil fields and to identify suitable drilling sites. Once all the technical, legal and environmental requirements are being fulfilled the drilling process can be commenced. Depending on the depth of the drilling site, different drilling rigs are used. Jack-up rigs are used in relatively shallow waters while the semi-submersible platforms are used in depths around 80-1800 m. In North Sea both Norway and United Kingdom use both types of these platforms. In deep waters, drill ships are being used and they are quite common in USA and Asia [3].

Both onshore and offshore wells are drilled by using a rotating drill bit. The drill bit is connected to the drill platform through a hollow pipe known as the drill string. The drill string is rotated by the top drive either by using an electric or hydraulic motor. The drill string is also used to pump the drilling fluid (drilling mud) to the drill bit. The main functions of a drilling fluid are to maintain the pressure inside the borehole, to lubricate the drill bit, to function as a cooler to reduce the temperature of the drill bit and to to transport the drill cuttings out from the well (well cleaning). The pumped drilling fluid is returned to the platform through the annulus between the drill string and the casing

or the wall of the drilled hole. Drilling fluids can be categorized as water based drilling fluids which is traditionally known as Water Based Muds (WBM) and oil based drilling fluids which is traditionally known as Oil Based Muds (OBM) depending on the base fluid. As the drill bit rotates and grinds the rock formations, small rock particles known as cuttings are generated. These cuttings get suspended in the drilling fluid and comes to the platform through the annulus. Reuse of returned drilling fluid in the drilling process is both economical and environmental friendly. Hence, drill cuttings are separated from the returning drilling fluids by using solid control devices such as shale shakers. Separated drilling fluid are collected in the mud pit. This drilling fluid can be contaminated with fine clay particles and its properties have been altered from its initial values. Hence chemicals are added to it to correct the properties such as density and viscosity before being reused in the drilling process. The separated drill cuttings from the solid control devices are considered as drilling waste [4].

1.1.2 Offshore drilling waste handling

Offshore drilling operations generate significant amount of drilling waste which mainly consists of drill cuttings and drilling fluid. Figure 1.1 shows the amount of drill cuttings generated in the Norwegian Continental Shelf (NCS) during the last decade. The amount of OBM associated cuttings generated has been in a steady state at around 100 000 tonnes per year. During the period of 2008-11 the amount of WBM associated cuttings generation has been increased exponentially and since then it has been reducing gradually.

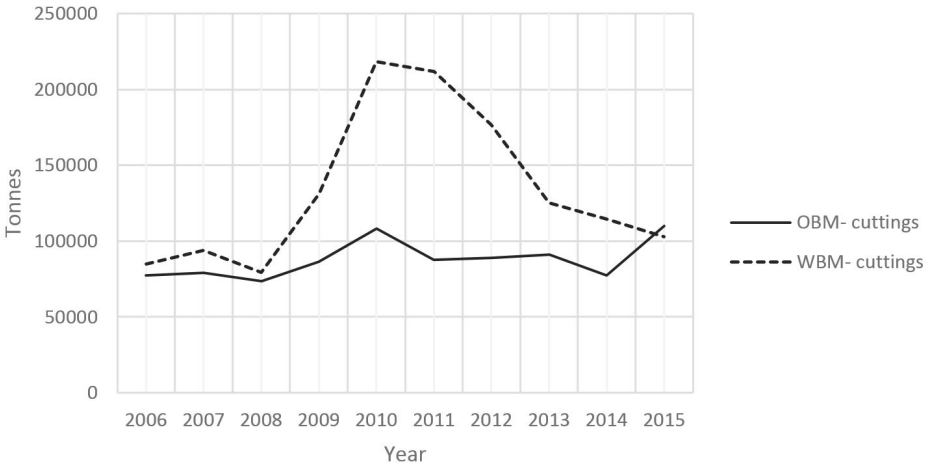

Figure 1.1: Total amount of cuttings generated in Norwegian Continental Shelf [5]

As mentioned in section 1.1, offshore oil exploration and production developed exponentially in the period of 1960-70. The concern over the environmental impact due to

offshore waste also grew simultaneously. Offshore drilling waste management has three approaches.

- Offshore discharge
- Re-injection
- Onshore treatment and disposal

Figure 1.2 and Figure 1.3 show the percentage of the disposal methods of the OBM and WBM associated cuttings respectively. It can be clearly seen that no OBM-cuttings have been discharged to sea except in 2015 where 2460 tonnes of extensively treated OBM-cuttings have been discharged [5]. On the other hand, around 96% of the WBM-cuttings have been disposed through offshore discharge.

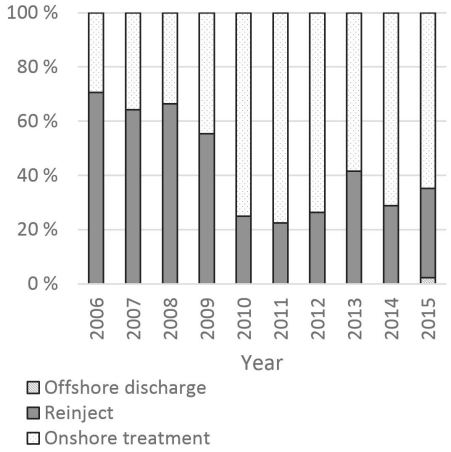

Figure 1.2: Disposal of cuttings with OBM in Norwegian Continental Shelf [5]

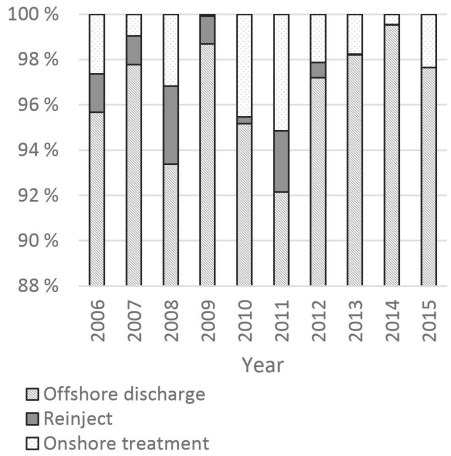

Figure 1.3: Disposal of cuttings with WBM in Norwegian Continental Shelf [5]

Offshore discharge

Prior to 1990, cuttings associated with WBM were allowed to be discharged into marine environments under existing environmental regulations. Offshore disposal of cuttings contaminated with OBM were not allowed in the USA, but in North Sea countries (Norway, Netherland and The United Kingdom) it was allowed [2]. In early 1980s high concentrations of hydrocarbons in the sediments closer to several production platforms in North Sea were discovered. This discovery led the governments to impose controls over offshore discharge. The usage of diesel based muds were prohibited in 1980s and the permissible amount of mineral oil associated with cuttings was gradually reduced [6]. According to the OSPAR decision 2000/3, offshore discharge of cuttings contaminated with organic phase fluids with a concentration above 1% of weight is completely prohibited. Other offshore oil producing countries such as USA and Canada have also imposed similar strict control over offshore discharge [2]. Therefore, no cuttings associated with OBM has been allowed to be discharged into Norwegian continental shelf during the last decade while around 96% of the cuttings associated with WBM has been allowed for offshore discharge. Compared to the other oil fields, Norwegian continential shelf has the most strict regulations with regarding the discharges. Even though WBMs are environmental friendly and cuttings associated with them are easy to be discharged, many drilling operators still prefer to use OBM due to its superior drilling performances such as better shale stability, higher lubricity and higher thermal stability [7].

Re-injection

Re-injection was considered as the most economical and environmental friendly disposal method for OBM-cuttings as they are not permitted for offshore discharge. A slurry is made by mixing finely ground drill cuttings with water. This slurry can be pumped into the re-injecting wells. The advantage of this method is that the treatment method is close to the source which reduces the requirement for transportation. The energy consumption and the emissions associated with re-injection was relatively less [8]. However, in 2009 it was discovered that certain wells in Norwegian Continental Shelf have lost the integrity causing the fractures to form up to the sea bed [9]. Therefore currently re-injection is allowed to be carried out at dedicated re-injection wells which are drilled at suitable locations. Drilling of dedicated re-injection wells and transportation of the slurry to the disposal location has increased the waste handling cost significantly [10]. Therefore, cuttings re-injection has been reduced significantly since 2009 and it can also be clearly seen in Figure 1.2.

Onshore treatment and disposal

The focus on onshore treatment and disposal of drill cuttings is continuously increasing as the control over offshore discharge and re-injection are tightened. The most common onshore disposal methods are burial and land farming. Before the final disposal it is essential to further treat the drill cuttings to convert them into non-hazardous waste. Stabilization combined with solidification, vermiculture, thermal desorption and incineration are such treatment methods [11][12]. Once completely treated, cuttings are disposed at burial sites or seldomly used as road construction material [13].

Drill cuttings storage and transportation

Drill cuttings storage and transportation is one of the major challenges that must be overcome in offshore waste handling. Conventionally skip-and-ship method was used to transfer drill cuttings from the drilling platform to the conveying vessels. This operation is slow, requires large amount of space to store the skips on the drilling platform and is associated with several health and safety issues [8]. Within the drilling platform gravity collection methods, screw conveyors and auger belts are used to convey the drill cuttings from the solid control devices to the storage locations. These mechanical conveying systems have low capital cost but higher maintenance cost. Depending on the drilling fluid concentration of the cuttings screw conveyors tend to get stuck and fail. Mechanical conveying systems in a drilling platform are associated with higher health and safety risks. A detailed description of the challenges of offshore drill cuttings handling is presented in Appendix A.

1.2 Problem statement

The conventional drill cuttings storage equipment such as skips and the conventional transportation systems such as conveyor belts and screw conveyors are unreliable and have low capacity. Therefore, these conventional systems are being replaced by novel techniques. Among the new conveying technologies, pneumatic conveying is claimed to be applied successfully [14][15].

Pneumatic conveying has several advantages such as, flexible routing, closed conveying system (less health and safety issues), potential to collect material from several pick up points and the ability to discharge the material at several discharge locations. The disadvantages of pneumatic conveying are the higher energy consumptions and the sensitivity of the conveying performances to the slight changes in the properties of the material to be conveyed and/or slight changes in the operating conditions. Pneumatic conveying has been developed and applied mostly for conveying of dry material. Pneumatic conveying

of wet material is itself a challenging task. Therefore, a proper scientific study is required to study the conveying characteristics of oil wet material to optimize the pneumatic conveying of drill cuttings.

1.3 Aim of the project

The main objectives of this study can be listed as,

- Increase the reliability and applicability of wet particle (drill cuttings) transfer
  - Identify the influential properties on wet particle (drill cuttings) transfer
  - Establish a scientific method to design wet particle (drill cuttings) transfer system
- Investigate the influence of wet particle (drill cuttings) properties in effective and reliable storage and reclaiming process
  - Investigate the influence of characteristic properties in flowability
  - Identify the major challenges in storage of drill cuttings

1.4 Outline of the thesis

This thesis is divided into six main chapters. In Chapter **2** the theoretical background and related work with regarding particle fluidization, pneumatic conveying and flow properties of bulk solids are presented. The experimental setups, instrumentation and procedures corresponding to fluidization, pneumatic conveying and and bulk solid shear tests are described in Chapter **3**. The selection of experimental material is also described in this chapter.

Chapter **4** includes the results and analysis of the fluidization and pneumatic conveying tests. Based on the results a method to develop a model to predict the pressure drop of horizontal pneumatic conveying is also presented. The results and the finding of the fluidization and pneumatic conveying tests are also discussed in this chapter. Chapter **5** presents the results and analysis of the bulk solid shear test. The discussion corresponding to the findings is also included in the same Chapter. The conclusion and the recommendation for future work is presented in the Chapter **6**. The graphical representation of the experimental data are given in the Appendix C - Appendix H

2 Theoretical background and related work

The objective of this chapter is to give the reader an overall background knowledge corresponding to the experimental work carried out in this research project. The experimental work can be categorized into three main fields, that is, pneumatic conveying, particle fluidization and bulk solid flow properties. A brief theoretical background on those fields is also provided in this chapter to facilitate the readers who are not familiar with the principles of powder handling.

2.1 Particle fluidization

The term particle fluidization is used to describe the process of suspending a bed of particles in a fluid to form a fluid-solid mixture that behaves as a fluid-like state [16].

2.1.1 Phenomenon of fluidization

When a fluid is flowing upwards through a bed of solids, the pressure drop across the bed is directly proportional to the fluid velocity at relatively low fluid flow rates. Under this condition the bed is considered as a *packed (fixed) bed*. The frictional drag forces exerted on the particles by the fluid flow increase with the fluid flow rate. When the fluid velocity approaches the minimum fluidization velocity (u_{mf}), the frictional drag forces acting on the particles get closer to the apparent weight of the particles (actual weight - buoyancy force). Then the particles tend to rearrange in a manner to reduce the resistance to the fluid flow. As a result the solid bed expands and the voidage of the bed increases. This phenomenon continues with increasing fluid flow rate until the frictional drag forces are equal to the apparent weight of the particles. At this point the individual particles get separated from one another as the vertical compression forces between the particles diminish. At this point the fluid bed is considered to be at the *minimum fluidization condition* [17].

Both liquid-solid and gas-solid systems behave similarly until the minimum fluidization condition. When the fluid flow rate is increased above the minimum fluidization conditions, the liquid-solid systems tend to expand the bed smoothly and continuously. On the contrary, gas-solid systems tend to behave rather differently at gas flow rates above the

minimum fluidization conditions. Gas bubbles and channelling can be observed within the bed and with further increase of gas flow, solid particles start to move vigorously. However, the expansion of the bed is relatively low for gas-solid systems beyond the minimum fluidization condition. When the gas flow rate is increased beyond the terminal velocity (settling velocity) of the solid particles, the particles in the upper boundary of the bed starts to get entrained with the gas flow. With further increase of gas flow rate, the solid particles start to get carried away with the gas flow, initiating pneumatic transport of solids [16].

In this research project fluidization behaviour of a gas-solid system where the solid particles are contaminated with drilling fluids is considered. The fluidization behaviour of the gas - dry particle systems is well studied relative to the fluidization behaviour of the gas - wet particle systems. Therefore, the well established fundamentals of fluidization of gas - dry particle systems are presented in the Section 2.1.2. The impact of the presence of a liquid in the packed bed towards the fluidization behaviour is discussed in the Section 2.1.4.

2.1.2 Theoretical background

In Figure 2.1 the total pressure drop across the particle bed is plotted against the superficial gas velocity (u_c). The pressure drop increases with increasing gas velocity until the bed initiates to expand (A-B). With further increase in gas velocity, the pressure drop passes through a maximum (C) and reaches a constant value. At the maximum pressure drop, the bed gets fluidized and the voidage of the bed increases, resulting a reduction in the pressure drop across the bed. Therefore, beyond the maximum pressure drop, a slight reduction in the pressure drop is observed and the pressure drop reaches a static condition with increasing gas velocity (D-E) [16].

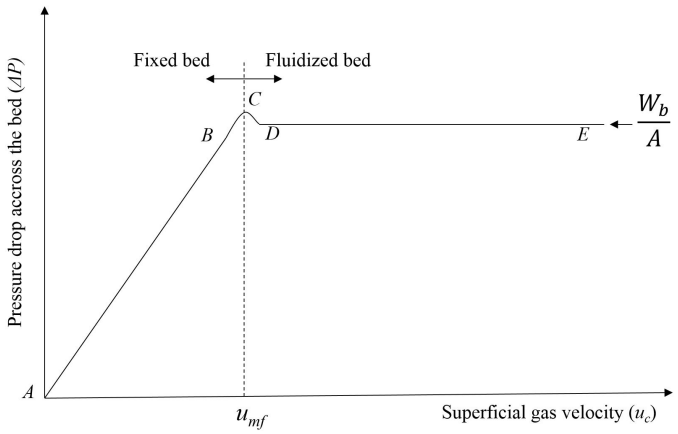

Figure 2.1: Pressure drop vs. superficial air velocity diagram for particle fluidization

In the packed (fixed) bed condition where the air velocity is less than the minimum fluidization velocity, the pressure drop across the bed can be obtained by the Ergun's equation as follows,

$$\frac{\Delta P}{L} = 150\frac{\mu u_c}{d^2}\frac{(1-\varepsilon)^2}{\varepsilon^3} + 1.75\frac{\rho_g u_c^2}{d}\frac{(1-\varepsilon)}{\varepsilon^3} \tag{2.1}$$

The first term in the right-hand side of the equation describes the viscous effects towards the pressure gradient and the second term describes the kinetic effects towards the pressure gradient in the bed. In the Ergun's equation the term μ represents the dynamic viscosity of the gas. The voidage in the packed bed (ε) is defined as the fraction of the bed volume occupied by the voids (the gas spaces between the particles).

In a fluidized bed, the frictional drag forces acting on the particles due to the gas flow are equal to the apparent weight of the particles. Therefore, the pressure drop across the fluidized bed balances the weight of the bed and it can be represented as [16],

$$\frac{\Delta P}{L_{mf}} = (1-\varepsilon_{mf})(\rho_p - \rho_g)g \tag{2.2}$$

Where L_{mf} and ε_{mf} are the height and the voidage of the bed at the minimum fluidization condition respectively.

The pressure drop in A-B region can also be expressed in terms of a friction coefficient (β_A) using the Darcy's law [18]. It is assumed that the effect of wall friction, acceleration and gravity on the momentum balance of gas phase is negligible [18].

$$\frac{dP}{dL} = -\frac{1}{\varepsilon}\beta_A u_r \tag{2.3}$$

$$\frac{1}{\beta_A} = \frac{k}{\mu} \tag{2.4}$$

Where k is the permeability of the solid particle bed. In Equation 2.3, u_r is the relative velocity defined as, $u_r = u_g - u_p$. In the region of A-B, the bed is fixed and the solid particles are stationary. Hence, $u_p = 0$.

Based on the extended version of the Ergun equation for fluidized bed (Equation 2.1) and Equation 2.2, the superficial air velocity at minimum fluidization condition can be found by solving the equation,

$$\frac{1.75}{\varepsilon_{mf}^3\phi_s}Re_{p,mf}^2 + \frac{150(1-\varepsilon_{mf})}{\varepsilon_{mf}^3\phi_s^2}Re_{p,mf} = \frac{d_p^3\rho_g(\rho_s-\rho_g)g}{\mu^2} \tag{2.5}$$

Where $Re_{p,mf}$ is the particle Reynolds number at minimum fluidization conditions and the Re_p is defined as,

$$Re_p = \frac{d_p u_c \rho_g}{\mu} \tag{2.6}$$

The sphericity of a particle (ϕ_s) is defined as the ratio of the surface area of a sphere which has the same volume of the given particle to the surface area of that particle.

The solution of the Equation 2.5 for small particles or low Reynolds value ($Re_{p,mf}$ <20) is given by,

$$u_{mf} \approx \frac{d_p^2(\rho_s - \rho_g)g}{150\mu} \frac{\varepsilon_{mf}^3 \phi_s^2}{1-\varepsilon_{mf}} \tag{2.7}$$

For larger particles where, $Re_{p,mf} > 1000$, the solution for the Equation 2.5 is given by,

$$u_{mf}^2 \approx \frac{d_p(\rho_s - \rho_g)g}{1.75\rho_g} \varepsilon_{mf}^3 \phi_s \tag{2.8}$$

For the systems where the voidage at minimum fluidization condition (ε_{mf}) and the sphericity of the particles (ϕ_s) is not known, the Equation 2.5 can be expressed as,

$$K_1 \; Re_{p,mf}^2 + K_2 \; Re_{p,mf} = Ar \tag{2.9}$$

K_1 and K_2 are numerical constants and Ar is the Archimedes number and they are defined as follows,

$$K_1 = \frac{1.75}{\varepsilon_{mf}^3 \phi_s} \tag{2.10}$$

$$K_2 = \frac{150(1-\varepsilon_{mf})}{\varepsilon_{mf}^3 \phi_s^2} \tag{2.11}$$

$$Ar = \frac{d_p^3 \rho_g (\rho_s - \rho_g) g}{\mu^2} \tag{2.12}$$

Numerical values for the constants K_1 and K_2 can be found in literature which have been defined empirically. The reported values for K_1 and K_2 are given in Table 2.1 . These values can be used to simplify Equation 2.7 and Equation 2.8. It must be noted that this method only gives a rough estimation of the minimum fluidization velocity.

For more accurate prediction of the minimum fluidization velocity, the information with regarding the voidage at minimum fluidization state and the sphericity of the particles are required.

Table 2.1: Values for the two constants in Equation 2.9

Investigators	K_1	K_2
Wen and Yu (1966) [19] *from 284 data points from literature*	24.5	1651.3
Richardson (1971) [20]	27.4	1408.4
Saxena and Vogel (1977) [21] *for dolomite at high temperature and pressure*	17.5	885.5
Babu et al. (1978) [22] *for reported data until 1977*	15.4	779.24
Grace (1982) [23]	24.5	1332.8
Chitester et al. (1982) [24] *for coal, char, Ballotini up to 64 bar*	20.25	1162.4

2.1.3 Material properties on fluidization behaviour

The behaviour of particles in a fluidized bed depends on the particle properties such as density, particle size and cohesiveness. Based on those properties, solid particles can be classified into groups representing different fluidization characteristics.

Geldart's classification of powders

Powders consisting uniformly sized particles are classified into four groups by Geldart based on their fluidization behaviour, mean particle size and the density difference between the solid and fluid. This classification has been conducted based on fluidization with air under ambient conditions and the classification is graphically represented in the Figure 2.2 [18].

Group A (Aerated)-Powders with a small mean particle diameter (30 μm - 100μm) and a low particle density (<1400 kgm^{-3}) are classified into this group. These powders can be fluidized easily and they tend to expand the bed significantly after the minimum fluidization condition. Until the air velocity is increased to a significantly higher value than the minimum fluidization velocity, air bubbles will not be formed. The air velocity at which the air bubbles will be formed is denoted as the *bubbling velocity* (u_b).

Group B (Bubbling)-The powders in this group have the mean particle diameter in the range of 40 μm - 500 μm. The particle density lies in the range of 1400 kgm^{-3} to 4000

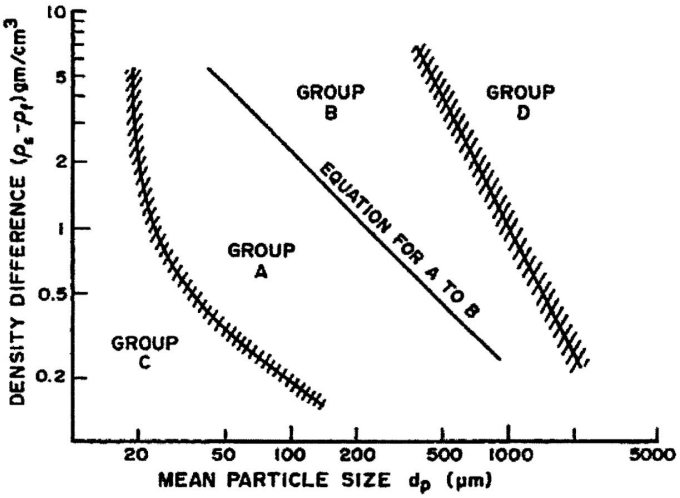

Figure 2.2: Geldart's classification of particles [18]

kgm^{-3}. Sand is a typical material that represent the *Group B* type powders. In these powders, bubbling occurs at the minimum fluidization velocity and the bed expansion is not significant. The boundary between *Group A* and *Group B* is given by the following equation [25].

$$(\rho_p - \rho_g) d_p = 225 \times 10^{-3} \tag{2.13}$$

Group C (Cohesive)-Cohesive and very fine powders are classified into the *Group C*. Fluidization of these powders are difficult due to the significant interparticle forces.

Group D (Spoutable)-*Group D* consists of large and/or dense powders. These are also difficult to be fluidized and with increasing air velocity exploding bubbles and spouting occurs. The boundary between the *Group B* and *Group D* is given by the following relation [25].

$$(\rho_p - \rho_g) d_p^2 = 10^{-3} \tag{2.14}$$

Based on the Ergun's equation given in the Equation 2.1 the pressure gradient across a packed bed for the different Geldart's groups has been analysed and it is given by Figure 2.3.

According to the Figure 2.3 the pressure gradient for *Group A* shows a linear relationship and for the *Group D* it shows a parabolic relationship. The pressure gradient curve can be almost linear or slightly parabolic for different *Group B* materials [26]. Since *Group C* material are difficult to be fluidized, a general form of the pressure gradient for the *Group C* materials is not presented by the authors.

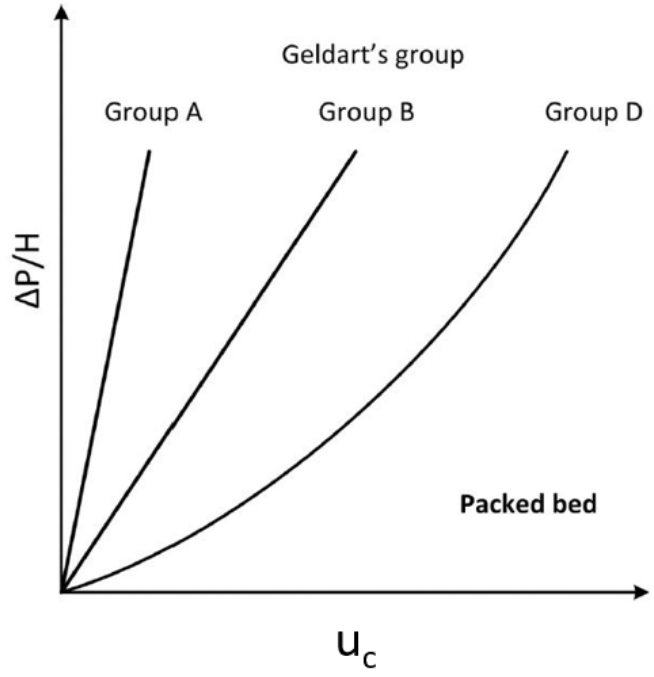

Figure 2.3: Theoretical pressure gradient curve for packed bed state for different Geldart's groups [26]

2.1.4 Influence of presence of liquid for fluidization

Geldart's classification of powders is done under the assumption that the interparticle forces are negligible compared to the drag forces and weight of the particles at fluidized conditions. Generally, this assumption is acceptable but according to Molerus [27] the difference in the fluidization behaviour in the Geldart's powder groups can be explained through the relative dominance of inter-particle forces and fluid drag forces. The difference between *Group A* and *Group C* occurs due to the dominance of cohesive forces in *Group C* type powders which limit the free motion of particles. *Group A* and Group B is separated due to the insignificance of interparticle forces in *Group B* type powders under fluidized conditions. The main inter-particle forces present in powders are Van der Waals forces, electrostatic forces and liquid bridges (when a liquid is present in powders). A brief description of these forces is presented in Section 2.3.1.

Group B powders which demonstrate good fluidization behaviour are transferred to *Group C* via *Group A* with continuous addition of liquid to the fluidized bed. This phenomenon was observed by Seville and Clift [28], McLaughlin and Rhodes [29] whom studied the influence of non-volatile thin liquid layers on fluidization behaviour. However, according to the experimental studies it was observed that the impact towards the fluidization behaviour of *Group B* is negligible when only a very little amount of liquid is present. Both these studies support the hypothesis that the boundary of *Group A* and *Group C*

occurs at a fixed ratio of inter-particle forces to the fluid drag forces. The numerical value of this ratio between interparticle forces and fluid drag forces obtained by different researchers deviate significantly due to the challenges of estimating the magnitude of inter-particle forces accurately [29]. Addition of liquid to a fluidized bed can make the bed more compact as the voidage of the fluidized bed is reduced compared to the dry conditions [30].

The minimum fluidization velocity also increases with the addition of liquid to the fluidized bed. The difference between the fluidization velocities of the wet system and the dry system can be expressed as, $u - u_{mf}$ which represents the excess air velocity that is required to overcome the defluidizing impact due to the addition of liquid to the fluidized bed. Hartman et. al. [31] conducted fluidization experiments with sand contaminated with a high viscous oil and low viscous oil separately. It was observed that the de-fluidization effect of the heavy oil is higher compared to the light oil. They have also proposed two correlations for the excess air velocity and oil concentration as follows,

Light oil

$$u - u_{mf} = 17900 \frac{w}{Ar^{1/2}} \tag{2.15}$$

Heavy oil

$$\frac{u - u_{mf}}{u_{mf}} = 9030 \frac{w}{Ar^{1/2}} \tag{2.16}$$

Where w is the oil mass fraction in the fluidized bed and this study has been conducted with $w < 0.02$.

2.2 Pneumatic conveying

Pneumatic transportation of solids is commonly used in many industrial applications. A wide range of powders and granular particles can be successfully conveyed pneumatically. According to Molerus [32] pneumatic transportation of solids is a brutal misuse of the principle which is basically suitable for transportation of fluids. Therefore, pneumatic conveying has its own advantages, disadvantages and pitfalls. The main advantages of pneumatic conveying are potential to have flexible routes and to have several pick up and discharge points. Higher power consumption, particle degradation and wearing of the conveying line are among the main disadvantages. The main pitfall associated with pneumatic conveying is its high dependability on the conveying system parameters and on the material properties. A slight variation of these parameters can cause severe problems in the conveying process and even might cause complete system failure [32][33]. Therefore,

a pilot scale tests covering the whole range of potential air flow rates and the potential solid mass flow rates are recommended for each conveying material and it will provide required information of the conveying system within the considered operating region [34].

The experimental data are plotted in the state diagram (pressure drop per unit length vs. superficial air velocity). A typical state diagram for horizontal conveying is shown in Figure 2.4. $\dot{m}_{s0}$ shows the pressure drop curve corresponding to no solid flow (air only). Other five pressure drop curves denoted by $\dot{m}_{si}$ represent pressure drop corresponding to different solid mass flow rates. The solid mass flow rate increases from $\dot{m}_{s1}$ to $\dot{m}_{s5}$. The point c on each curve corresponds to the minimum pressure drop point. The minimum pressure drop curve can be obtained by connecting these corresponding c points at different solid mass flow rates.

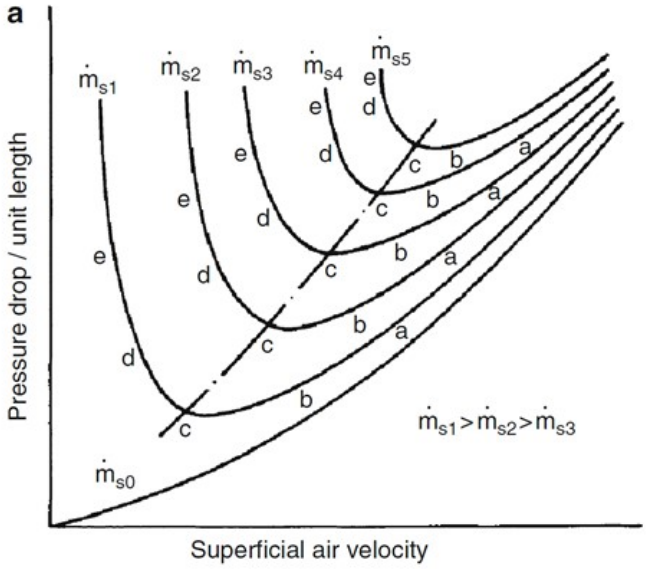

Figure 2.4: State diagram for horizontal pneumatic conveying [35]

The region of ***a-c*** represents dilute phase conveying (fully suspended). As the air velocity is decreasing from a to c, the solid loading ratio($\eta = \frac{\dot{m}_s}{\dot{m}_g}$) is increasing. At a particular point, when the air flow rate is not sufficient to suspend all the solid particles, the particles begin to separate from the gas-solid mixture and start forming beds on the bottom of the conveying line. The air velocity at this point is denoted as the saltation velocity. For fine particles, this occurs before the minimum pressure point and for the coarse particles this occurs at the minimum pressure point [35]. Generally, the saltation point has to be decided by visual observations or by using techniques such as electrical capacitance tomography (ECT).

2.2.1 Theoretical background

The pressure drop in a pneumatic conveying system represents the amount of power required to convey the gas-solid mixture. The total pressure drop in pneumatic conveying consists of the pressure drop due to the air only flow, pressure drop due to the acceleration of solids, pressure drop due to the friction and impact of particles, pressure drop due to the raising and suspending of particles and the pressure drop due to pipe bends.

The most common approach to study the pressure drop in pneumatic conveying is to consider the total pressure drop as a linear summation of the pressure drops due to the gas only flow (ΔP_g) and pressure drop due to the solid flow (ΔP_s) [35].

$$\Delta P = \Delta P_g + \Delta P_s \tag{2.17}$$

Gas phase pressure drop

It is assumed that the pressure drop due to gas flow is independent of the presence of solids. Based on Darcy-Weisbach model, the pressure drop due to gas flow is commonly expressed as follows[36],

$$\Delta P_g = \frac{f_D}{2} \frac{\rho_g u_g^2 \Delta L}{D} \tag{2.18}$$

Where f_D is the Darcy friction factor. According to the Blasius equation, the friction factor is a function of the Reynolds number (Re) and for smooth pipes it can be expressed as [37],

$$f_D = \frac{0.3164}{Re^{0.25}} \tag{2.19}$$

The Equation 2.19 is valid for the range of $4000 < Re < 80\ 000$. The friction factor can also be estimated by using the Moody diagram for both smooth and rough pipes. There are other semi-empirical correlations developed by different researchers under different flow conditions. Klinzing [35] has proposed the following relationship for the compressed air in straight pipes.

$$\Delta P_g = 1.6 \times 10^3 \dot{V}^{1.85} \frac{L}{D^5 P_i} \tag{2.20}$$

Where $\dot{V}$ is the volumetric air flow rate and P_i is the initial pressure.

Another empirical correlation has been present by Wypych and Arnold as follows,

$$\Delta P_g = 0.5\left[(101^2 + 0.004567 m_g^{1.85} L D^{-5})^{0.5} - 101\right] \tag{2.21}$$

Solid flow pressure drop in dilute phase

Many research work has been conducted with regarding the pneumatic conveying for more than a century, but still no universal mathematical model has been developed to express the pressure drop in pneumatic conveying. The models acknowledged by professional books deviate from one another as they have been developed for different systems with different operating conditions. The approaches followed by the researchers to model the pressure drop in pneumatic conveying can be classified into two groups as [36],

- **Particles' friction approach-** The interactions of particles with the wall in a gas-solid mixture is represented by a friction factor similar to the fluid friction model for single phase flow.
- **Force balance approach-** The presence of particles in a gas flow is considered to be a disturbance to the motion of the gas. This is represented by an additional gas pressure drop which is obtained through force balance.

Particles' friction approach

Similar to the Equation 2.18 pressure drop due to the impact and frictional forces in solid flow can be expressed as,

$$\Delta P_s = \lambda_p \eta \frac{\rho_g}{2} \frac{u_c^2 \Delta L}{D} \tag{2.22}$$

Where λ_p is the additional pressure drop factor and η is the solid loading ratio which is defined as,

$$\eta = \frac{\dot{m}_s}{\dot{m}_g} \tag{2.23}$$

The additional pressure drop factor (λ_p) can be expressed as a function of the Frode number based on the pipe diameter (Fr_D). The Frode number based on pipe diameter is defined as,

$$Fr_D = \frac{u}{\sqrt{gD}} \tag{2.24}$$

Some previous correlations developed to express the additional pressure drop factor is presented by Naveh et al. [36] as.

$$\lambda_p = 0.005 \frac{1 - Fr_D^{-1}}{1 + 0.00125(Fr_{D,\infty})^2} \tag{2.25}$$

Where, $Fr_{D,\infty}$ is the pipe Frode number based on the terminal velocity of the particles . For spherical particle conveying following model can be used.

$$\lambda_p = 0.012\eta^{-0.1} \frac{1}{\sqrt{Fr_D}} \left(\frac{d_p}{D}\right)^{-0.9} \tag{2.26}$$

Konno and Saito [38] have obtained a correlation for the additional pressure drop factor as,

$$\lambda_p = 0.114 \sqrt{\frac{D}{u_s g}} \tag{2.27}$$

The Equation 2.27 has been derived based on the experimental results on pneumatic conveying of glass beads, copper spheres, millet and grass seed with a particle diameter in the range of 0.1 - 1 mm.

The model developed by Naveh et al. [36] is given by,

$$\lambda_p = 2D \frac{\rho_g g d_p}{\mu} \frac{a}{u_{mp}} \tag{2.28}$$

Where u_{mp} is the air velocity corresponding to the minimum pressure drop in pneumatic conveying. In situations where u_{mp} cannot be determined experimentally, it can be estimated by using mathematical models presented by Rabinovich and Kalman [39].

Instead of expressing the pressure drop due to solid flow separately, some models represent the total pressure drop using a global friction factor (λ_t) as follows,

$$\Delta P_t = \lambda_t \eta \frac{\rho_g}{2} \frac{u_c^2 \Delta L}{D} \tag{2.29}$$

The global friction factor can be written as a function of several dimensionless parameters as follows [40],

$$\lambda_t = x_1 \eta^{x_2} Fr^{\,x_3} \left(\frac{d_p}{D}\right)^{x_4} \left(\frac{\rho_g}{\rho_s}\right)^{x_5} \tag{2.30}$$

The parameters (x_i) have to be determined by fitting the experimental data. Several researchers have developed models based on this approach but the parameters in the Equation 2.30 significantly depend on the type of material and conveying conditions.

Force balance approach

In this approach the pressure drop due to solid flow is expressed using the impact and friction coefficient (f_p). The model format is similar to the Fanning equaiton and it can be expressed as [36],

$$\Delta P_s = f_p(1-\varepsilon)\frac{\rho_s u_p^2 L}{2D} \tag{2.31}$$

The Equation 2.31 can be obtained by substituting for the η in Equation 2.22 and the friction coefficient can be correlated to the additional pressure drop factor as,

$$\lambda_p = f_p\left(\frac{u_p}{u_c}\right) \tag{2.32}$$

Based on Yang's unified theory, Wei et al. [41] have developed a model for dilute phase conveying by taking the particle shape into consideration. According to Wei et al. [41] the particle friction factor is given by,

$$f_p = 1.98\frac{(1-\varepsilon)^{-0.057}}{\varepsilon^3}\left(\frac{Re_\infty}{Re_p}\right)^{-0.902}\left(\frac{u_g}{\sqrt{gD}}\right)^{-1.95} \tag{2.33}$$

And the particle velocity to solve the Equation 2.31 is given by,

$$u_p = u_g - \sqrt{\frac{4(\rho_s-\rho_g)gd_p}{3\rho_g C_d}}\sqrt{\frac{f_p u_p^2}{2gDf(\varepsilon)}} \tag{2.34}$$

Where $f(\varepsilon)$ is voidage function used to calculate the drag coefficient in multiparticle systems.

Raheman and Jindal [42] have developed a model analogous to the Equation 2.31 to express the pressure drop of solid flow as,

$$\Delta P_s = 2f_p(1-\varepsilon)\frac{\rho_s u_p^2 L}{9.81D} \tag{2.35}$$

And the friction factor is given by,

$$f_p = 3.35\left(\frac{u_\infty}{u_p}\right)\left(\frac{u_\infty^2}{gD}\right)^{-0.95}\left(\frac{d_p}{D}\right)^{0.7} + 3.3\times10^{-4}\eta^{1.5} + 0.53\left(\frac{u_g^2}{gD}\right)^{-0.7} + 3.4\times10^{-7}\left(\frac{\rho_g u_r d_p}{\mu}\right)^{0.9} - 0.006 \tag{2.36}$$

Based on the principles of power balance,Naveh et al. [36] have presented a model to express the behaviour of pressure drop as,

$$\frac{\Delta P_s}{\Delta P_g} = \frac{6}{\pi}\frac{\dot{m}_s}{\rho_s}\frac{1}{Dd_p}\frac{C_{d,HC}}{f_d}\frac{1}{u_s}\left(\frac{1}{\varepsilon} - \frac{u_p}{u_c}\right)^2 \tag{2.37}$$

Where $C_{d,HC}$ is the effective drag coefficient for dilute horizontal conveying and it can be related to the standard drag curve as,

$$C_{d,HC} = C_d f(Ar, Re_D, Fr_p) \tag{2.38}$$

An empirical function $f(Ar, Re_D, Fr_p)$ based on curve fitting for experimental data has been presented by the authors to evaluate $C_{d,HC}$.

2.2.2 Pneumatic conveying of wet materials

Traditionally pneumatic conveying is considered to be capable of conveying mostly dry materials. When it comes to wet material, pneumatic conveying becomes challenging due to the possible blockages and excessive energy consumption. It is impossible to have dry drill cuttings on the rig. Hence this challenge has to be overcome when applying powder conveying principles in designing a drill cutting transfer system.

Experimental studies conducted by Cai et.al. [43][44] to investigate the effect of the moisture content on conveying characterisitics of pulverized coal show that the mass flow rate decreases with the increasing moisture content in pulverized coal. These expeiments have been conducted for coal particles with a median size of 31 -36 μm and with a particle density of 1350 -1400 kgm^{-3}. The study shows that when the moisture content is greater than 6% - 8% (wt.) the pneumatic conveying becomes difficult. In the pneumatic conveying state diagram, it was observed that for the same superficial air velocity, the pressure drop decreases with increasing moisture content. At low moisture concentrations (3%. wt) the friction coefficient between the particles are less and as a result higher solid mass flow rate can be obtained. High mass flow rate results a higher pressure drop.

In a series of experiments conducted by Sheer [45] to develop models to predict the flow regimes of wet ice with air flow have come out with significant findings with regarding pneumatic conveying of wet material. Slush ice having ice content of 70-75% was unable to move in dilute phase using acceptable air velocities. But they were able to convey dispersed dense phase mixtures in small agglomerating using air velocities up to 25 m/s. When the ice content was reduced down to 65% the nature of the ice was completely changed into a semi-fluid. Then the flow regime was changed into slow moving longer slugs or full plugs due to low wall resistance. This shows that the liquid content has a major impact towards the flow regime.

2.3 Flow properties of bulk solid

The ability of a granular bulk solid or a powder to flow is known as its flowability. The flowability of a bulk solid depends not only on its material properties but also on the environmental conditions and the material handling and storage equipment. The most influential parameters on the flowability of a bulk solid is the moisture content, particle size, particle shape, humidity, temperature and pressure [46].

According to Jenike [47] two flow patterns can be observed in hoppers, namely mass flow and funnel flow. In the funnel flow hoppers, the solid elements move towards the outlet of the hopper in a channel and the solid elements outside the channel are stationary. In mass flow hoppers this channel overlaps with the wall of the hopper, leaving no stationary solid elements within the hopper . In funnel flow hoppers the flow can stop due to the formation of stable arches or due to piping (rat-holing) where the bulk solid directly above the outlet falls out. In funnel flow hoppers, arches can collapse and large stresses can be exerted on the lower part of the hopper which can even tear off the section. If the stored bulk material is easily aeratable, there is a risk of flooding when arches collapse in funnel flow hoppers. As there are dead zones in funnel flow hoppers, there is a possibility that the initially fed material remain within the hopper even after a long period of time. Free flowing material can be segregated in funnel flow.

In mass flow hoppers, no stable arches or piping can occur and hence the flow will not be interrupted. Steady bulk density and flow rate can be obtained when discharging from a mass flow hopper. Material tends to come out in the order that they are fed into the hopper. The main advantage of using mass flow hoppers for cohesive material is that material flow interruptions are minimized. For non-cohesive materials the main advantage is the minimization of particle segregation based on size. However, if the particle segregation is not an issue there is no significant advantage of using a mass flow hopper to store free flowing materials. The main disadvantage of a mass flow hopper is that, a conical mass flow hopper will be taller than a funnel flow hopper with the same capacity. Particle degradation and wall erosion can occur in mass flow hoppers as the

particles move along the walls. Very high but predictable stresses occur in the area of the beginning of the converging section of the mass flow hopper [48]. In Chapter 1, it is described that the conventional drill cuttings storage devices such as skips have to be replaced by hoppers when pneumatic conveying principals are applied in conveying drill cuttings. It is a known fact that poorly designed storage bins and hoppers are unreliable in having a continuous discharge.

2.3.1 Theoretical background on bulk solid flow

An arbitrary solid element which moves from the top of the hopper to the outlet is subjected to a major principal stress (σ_1) and a minor principal stress (σ_2). When the solid element lies on the top surface of the bulk solid in the hopper, no stresses are acting on it. As the solid element moves downwards in the silo, it gets covered with layers of solid elements and the stresses acting on the considered solid element increase. It is assumed and experimentally justified that a radial stress field occurs in the conical section of the hopper. In a radial stress field, the major principal stress in the conical section is directly proportional to the local diameter of the hopper. Therefore, the major principal stress tends to reach zero at the virtual hopper apex. Hence the stresses acting on the considered solid element increase and reach a maximum at the beginning of the conical section and reduces towards zero at the virtual apex of the silo. When the stresses acting on the solid element changes, the particles in the element slide on one another and change the shape and volume of the element. Therefore, the density of the solid element changes during the flow of the element through the channel. This density depends on the last stresses acted on the element and those stresses are known as consolidating stresses. The strength of a bulk solid (ability to withstand shear failure) depends on the consolidation level that the bulk solid has been subjected to. Generally, the bulk solid material gain higher strength when subjected to a higher consolidation stresses and the flowability of the material reduces. The fundamental principle of designing a mass flow hopper is that, the strength of a bulk solid in a hopper should not be adequate to support any form (arches) of obstruction to flow. Therefore, the stress – strength relationship of a bulk solid material lays the foundation for the designing of a mass flow hopper [47] [49].

The shear stress (τ) - normal stress (σ) relationship of a bulk solid element can be illustrated by a Mohr semi-circle which is shown in the Figure 2.5. A shear tester is used to determine this relationship for the considering bulk solid material. The experimental procedure is described in the Section 3.4

A bulk solid element which has been initially consolidated under a particular normal stress (σ), can be sheared to failure at different shear stresses ($\tau_{t1}, \tau_{t2}, \tau_{t3}$) by changing the applied normal stress (less than the consolidating stress). The resulting shear stress and normal stress pairs at failure gives the yield locus of the bulk material for the given consolidating stress. A Mohr semi-circle representing the stresses acting on the bulk solid

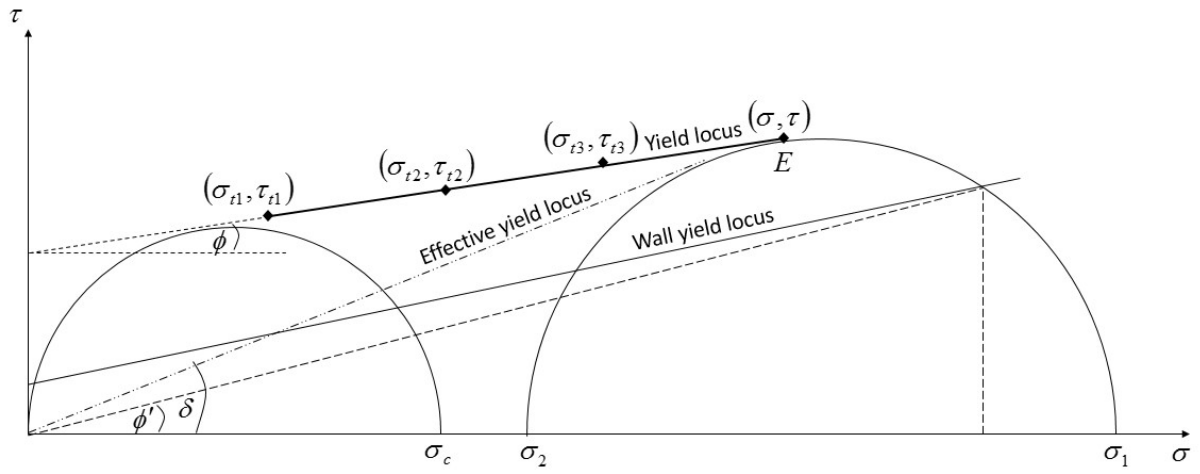

Figure 2.5: Shear stress - normal stress diagram and the Mohr semi-circle for a bulk solid element

element at failure will be tangent to the yield locus. The major and minor consolidating stresses acting on the bulk solid element are represented by the two intersections of the Mohr semi-circle at the x-axis. The yield locus terminates at point $\boldsymbol{E}$ where the applied normal stress equals to the initial consolidation stress. The angle between the yield locus and the horizontal axis (normal stress axis) is the kinematic angle of internal friction and it is denoted by $\boldsymbol{\phi}$. A different yield locus can be obtained by changing the initial consolidation stress. Higher the consolidation stress, higher the yield locus will be [49].

Effective yield locus

The straight line which goes through the origin of the $\boldsymbol{\sigma - \tau}$ plot and which is tangent to the steady flow Mohr semi-circle is the Effective yield stress and the angle between the effective yield stress and the x-axis is the effective angle of internal friction which is denoted by $\boldsymbol{\delta}$. This is a measurement of the resistance to flow when the material is in flowing conditions. Larger $\boldsymbol{\delta}$ implies a lower flowability and normally $\boldsymbol{\delta}$ decreases with decreasing consolidation stress. Different yield loci corresponding to different consolidation stresses will have the same effective yield locus and effective angle of internal friction [49].

Unconfined yield strength

When an arch is formed, there exists a free surface. The normal force acting on the free surface is zero. Therefor the minor principal stress acting on solid elements on the arch is zero. This can be represented by a Mohr semi-circle which intersects the x-axis at the origin of the $\boldsymbol{\sigma - \tau}$ plot. When the arch is about to fail and collapse this Mohr semi-circle should be tangent to the yield locus. The major principal stress corresponding

to this Mohr semi-circle is σ_c and it is the largest stress that the material can withstand at a free surface. This is also known as the unconfined yield strength (f_c) and this lies tangent to the surface of the arch. For a particular initial consolidation stress, there exists a corresponding unconfined yield strength and it is directly proportional to the initial consolidation stress [49].

Wall yield locus

Solid elements in a hopper, flow along the slip lines that are formed at the boundaries between the dynamic and static solid elements or between the dynamic solid elements and the wall. The stresses along the boundary between the moving and stationary solid elements are represented by the yield locus. Similarly, the stresses along the boundary between the moving solid elements and hopper wall can be represented by a wall yield locus. A straight line going through the origin of the $\sigma - \tau$ plot and the intersection of the wall yield stress and the considered Mohr semi-circle is used to determine ϕ' which is the static angle of surface friction [49].

Flow function (FF)

The concept of flow function was introduced by Jenike [47] and it is also known as the failure function. The flowability of a bulk solid material is governed by the strength of the material. The strength of the material is developed as a result of the consolidating stresses which the bulk solid material is subjected to. The unconfined yield strength (f_c) can be used to represent the strength of the material. As described previously different unconfined yield strengths can be obtained by changing the initial consolidation stress. The flow function of a bulk material can be obtained by plotting f_c *vs.* σ_1 [49].

Flow-no-flow condition

The most important parameters in designing a mass flow silo are the maximum allowable hopper angle (θ) and the minimum required area at the outlet to ensure a continuous discharge from the silo.

As mentioned previously, the major principal stress (σ_1) is proportional to the local diameter of the in the conical section of the hopper due to the radial stress field. When a stable arch is formed in the hopper, a force due to the weight of the bulk solid is transferred to the wall of the hopper. The major stress that is required to support the arch (σ_1') is given by [49],

$$\sigma_1' = \frac{2r \sin\theta g \rho_b}{1+m} \tag{2.39}$$

Where $m = 0$ for wedged shaped hoppers and $m = 1$ for conical shaped hoppers. The term $2r\sin\theta$ describes the geometry of the considered hopper. The arch will be stable if the unconfined yield strength is large enough to support it ($\sigma_c > \sigma_1'$). The behaviour of these stress are illustrated in Figure 2.6. The vertical location corresponding to the position where $\sigma_c = \sigma_1'$ gives the critical area of the hopper outlet. Any location above the critical height gives a larger area and the corresponding unconfined yield strength will not be sufficient enough to support an arch. The critical area gives the minimum area which will avoid stable arch formation. The critical area can be calculated according to [49],

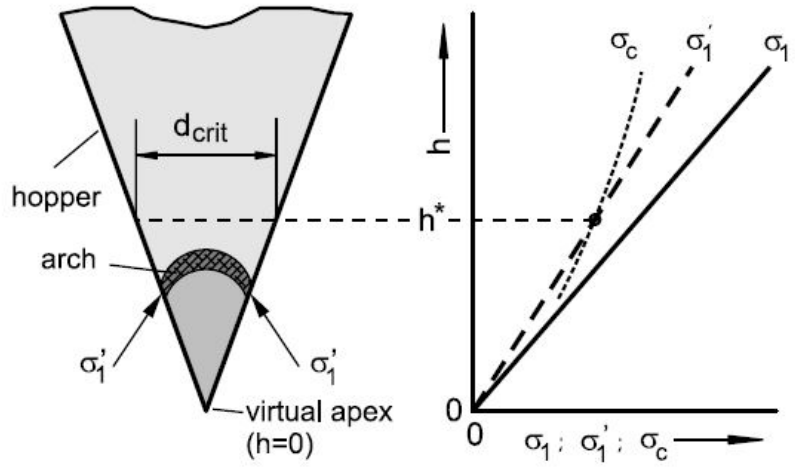

Figure 2.6: Behaviour of stress at the lower section of the hopper

$$B = H(\theta)\frac{\sigma_c}{g\rho_b} \tag{2.40}$$

Where B is the minor dimension of the outlet of the hopper (B = diameter for a circular shaped outlet). $H(\theta)$ is a function of the hopper geometry and it has been calculated and presented as a graph for different shapes by Jenike [47].

The major principal stress (σ_1) in the hopper acts as the consolidation stress and the corresponding σ_c is given by the flow function (FF) (σ_c vs. σ_1). The relationship between σ_1' and σ_1 is given by the flow factor (ff), which is defined as,

$$ff = \frac{\sigma_1}{\sigma_1'} \tag{2.41}$$

The flow factor (ff) will be increased and the flowability of the bulk solid will be reduced by increasing the consolidation stress (represented by σ_1). The flowability of the bulk

solid will also be reduced if the major stress required to support the formed arch (σ_1') is lowered and the corresponding ff will be increased. Therefore, a lower ff implies a better flow of bulk solid.

The flow factor for a given hopper geometry and a bulk material can be calculated based on the hopper angle (θ), kinematic angle of wall friction (ϕ) and effective angle of internal friction (δ). Jenike [47] has calculated the values of flow factors covering the most common range of the parameters mentioned above and the results are presented in forms of graphs. Using these graphs, for a particular combination of δ and ϕ which represent material properties, the critical hopper angle, θ that transforms the mass flow into funnel flow region can be estimated. 3^0 to 5^0 should be reduced from this critical hopper angle which lies in the boundary of the mass and funnel flow to ensure a mass flow hopper design. The flow factor corresponding to the selected hopper angle can be estimated by using the same graph. Once the flow factor is estimated, σ_c vs. σ_1 and σ_1' vs. σ_1 can be plotted in the same graph and the critical unconfined yield strength ($\sigma_{c,crit}$) at $\sigma_c = \sigma_1'$ can be calculated. By substituting the $\sigma_{c,crit}$ in equation 2.40 the critical area of the outlet of the hopper can be calculated.

Time consolidation

Most of the bulk solid materials tend to increase their strength when they are stored at rest for a period of time. The stresses acting on a flowing bulk solid element will prevail even if the flow of the hopper is stopped. These prevailing stresses cause the bulk solid element to be consolidated and increase its strength. This phenomenon is know as the time consolidation or caking. The yield locus of a bulk solid which has been subjected to time consolidation will be increased compared to the instantaneous yield locus of the same material. The unconfined yield strength, flow factor corresponding to time consolidation will be also increased.

2.3.2 Flowability of wet bulk solids

Inter-particle adhesive forces highly influence the flowability of bulk solid. Van der Waals forces, electrostatic forces and liquid bridges are the most influential adhesive forces in fine grained bulk solid material. Liquid bridges will be present in bulk solid with liquids that have a viscosity sufficiently low enough to form liquid bridges. The magnitude of these adhesive forces depend on the distance between the particles. The Van der Waals forces will be dominant when the particles are in contact. The influence of Van der Waals forces will be rapidly reduced at distances larger than 1 μm. Then the liquid bridges will be the dominant adhesive force in short distances. The liquid bridges will diminish when the distance is increased further and only the electrostatic forces will prevail. The amount of liquid present in the bulk solid affect the magnitude of the liquid bridges. The influence

of distance is significant when there is small amount of liquid present, ie. when there is small amount of liquid present, the liquid bridges will diminish at longer distances. When there is large amount of liquid present in the bulk solid, the variation of the magnitude of the adhesive forces along the distance is less significant. Liquid bridges and Van der Waals forces are the dominant forces among smaller particles with a diameter less than 100 μm. The impact of the weight of the particle rapidly increase for larger particles as the weight is proportional to the third power of the particle diameter.Therefore,the flowability of smaller particles are less compared to the larger particles as the adhesive forces are more significant [49].

The moisture content can affect the frictional properties of the bulk solid and the hopper. Generally it is expected that as the moisture content is increased the angle of internal friction, unconfined yield strength and compressibility of bulk solid can be increased significantly [46]. However, it was found that for rapeseed at higher normal stresses and water saturation level higher than 10% (weight) , yield locus tends to reduce with the increasing moisture content. Therefore,at higher moisture levels, it is possible to have a thin layer of water existing on the surface of the particles and it can act as a lubricating agent to reduce the inter-particle frictional forces. This lubricating effect can be significant in large and hard particles with approximately spherical shape [50]. According to Çağli [51], at low shear stresses the flow function of sand tends to increase with increasing moisture content but at higher shear stresses the behaviour of the flow functions depend on the moisture level of sand. That is, at higher shear stresses and low moisture levels (1% wt.), the flow function tends to increase with increasing moisture content and at higher shear stresses and high moisture levels (14% wt.) the flow function tends to decrease with increasing moisture content.

The experimental measurement of yield loci of bulk solid is time consuming and the accuracy is operator dependent. Pierrat [52] has proposed a fundamental relationship between the yield locus of a dry free flowing material, tensile strength of the wet material and the yield locus of the wet material based on theory of shift. The yield locus of a free flowing dry material is horizontally shifted left when moisture is added. The magnitude of the horizontal displacement depends on the tensile strength of the wet material and the angle of internal friction. The horizontal displacement of the yield locus (isostatic tensile strength) is given by,

$$\Delta\sigma = \Delta T \frac{1+\sin\phi}{2\sin\phi} \tag{2.42}$$

Where ΔT is the difference of the tensile strengths of the wet and dry material.

3 Experimental setup, instruments and procedure

3.1 Material selection

The most critical challenge in conducting experiments was to obtain a representative sample of drill cuttings and their affiliated fluids in adequate amounts. The major challenges in obtaining drill cuttings were,

- The physical properties of the drill cuttings tend to change with time
- The physical properties of drill cuttings are highly influenced by the type of drilling fluid used for drilling and the composition of the rock layers. Hence obtaining drill cuttings with constant physical properties was a challenge.
- Legal, economical and safety constrains of both transporting and handling drill cuttings.

Therefore, it was decided to use an alternative material to represent drill cuttings in pneumatic conveying, fluidization and bulk solid shear tests.

3.1.1 Alternative material for drill cuttings

A thermally treated drill cutting sample was obtained from CUBILITY AS to analyse the basic properties of the drill cuttings. The average particle density was 2598.25 kgm^{-3} which was measured by using a gas pycnometer. The offshore drill cuttings can have a size larger than 30 mm, but generally the largest size would be around 20 mm (Appendix A). The particle size distribution of the drill cutting sample was obtained through sieving and the particle size distribution of the sample is shown in Figure 3.1. The major portion of the particles less than 100 μm in the drill cuttings sample is barite and other additives present in the drilling fluid. Therefore, for the experimental purposes particle size distribution larger than 100 μm was considered.

The particle size distribution of the considered treated drill cutting sample is compared with the particle size of the commonly available granular material in order to select an

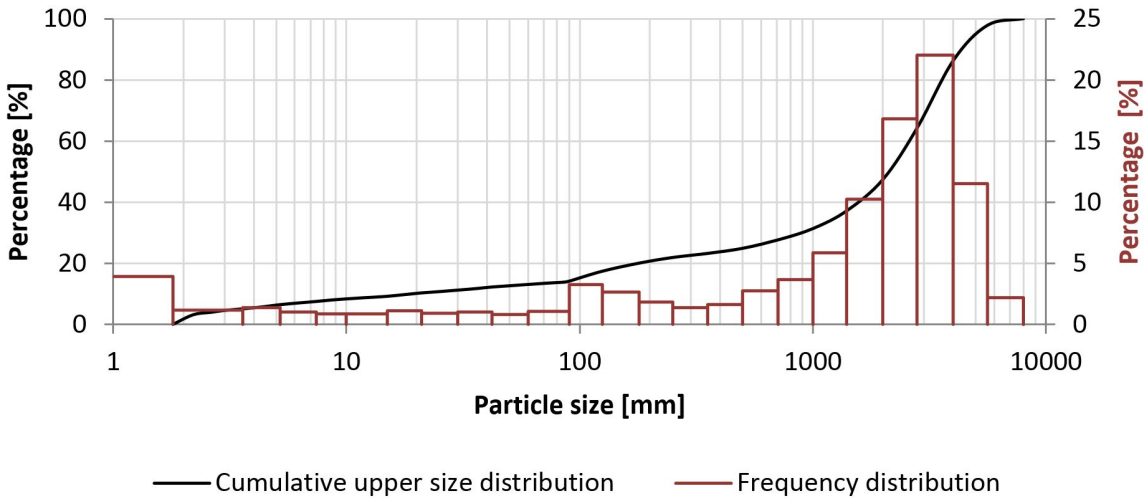

Figure 3.1: Particle size distribution of the drill cuttings sample

alternative representative material. According to the Figure 3.2, sand has a particle size in the range of 74 - 2000 μm and gravel have a particle size larger than 2000 μm, which indicate that the sand and gravel can be used to develop a mixture having a particle size distribution equivalent to the treated drill cutting sample. The average particle density of the sand and gravel are measured to be 2718.5 kgm^{-3} which is close to the particle density of the drill cuttings. Adequate amounts of sand and gravel with constant properties can be obtained easily and there are no special safety risks in handling and transporting sand. Sand and gravel were categorized into five groups depending on the range of the particle size distribution. These different particle size distributions were selected based on the drill cuttings samples obtained from CUBILITY AS. These sand and gravel groups are named as **B,C,D,E** and **F** and hereafter they are mentioned as *sand groups*. Particle size distributions of the five sand groups are shown in Figure 3.3.

This basic five sand groups were mixed together as described in the Table 3.1 to get differnt particle size distributions. The ratio between the five basic sand groups is $B : C : D : E : F = 1 : 1.6 : 2.4 : 2.5 : 2.5$ and it was selected to approximately represent the particle size distribution of the drill cuttings which is shown in Figure 3.1.

The particle size distributions plots of these sand mixtures are given in the Appendix C.

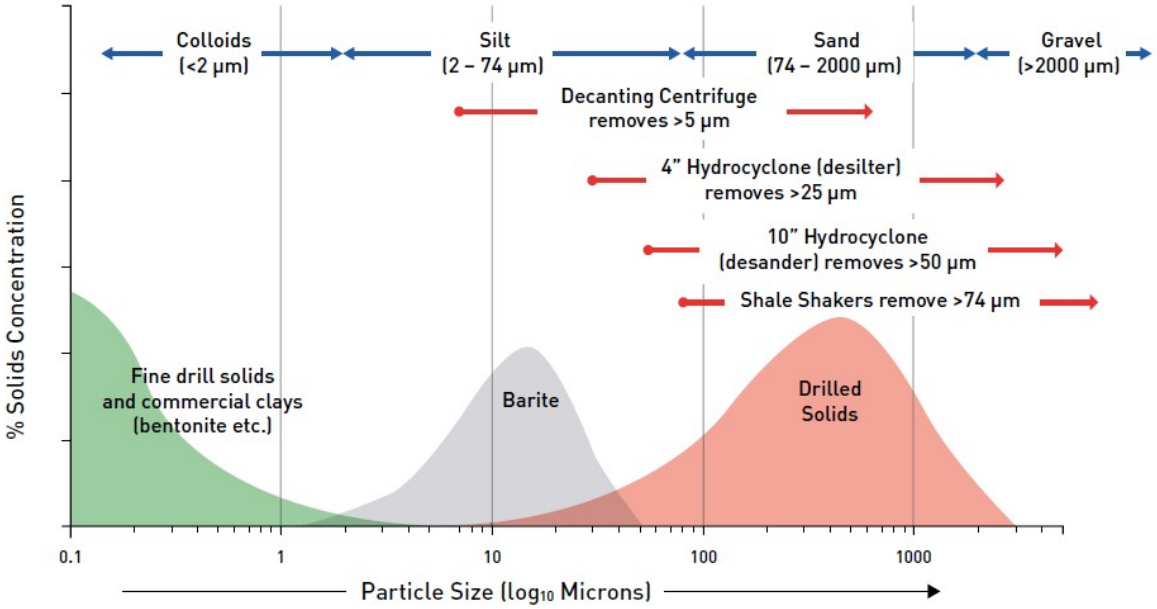

Figure 3.2: Particle size and solid removal equipment [4]

Table 3.1: Properties of sand samples

Sample	**Composition [%]**					**D90**	**D75**	**D50**	**D25**	**D10**
	B	*C*	*D*	*E*	*F*	*[mm]*	*[mm]*	*[mm]*	*[mm]*	*[mm]*
B	100	-	-	-	-	0.44	0.36	0.29	0.23	0.17
C	-	100	-	-	-	0.91	0.83	0.69	0.59	0.52
D	-	-	100	-	-	1.97	1.79	1.57	1.32	1.14
E	-	-	-	100	-	5.4	4.9	4.1	3.4	3.0
F	-	-	-	-	100	10.27	8.2	5.67		
BC	38.5	61.5	-	-	-	0.87	0.74	0.56	0.32	0.23
CD	-	40	60	-	-	1.84	1.62	1.22	0.80	0.60
BCD	20	32	48	-	-	1.82	1.55	0.95	0.55	0.29
BCDE	13.3	21.3	32	33.3	-	4.7	3.4	1.5	0.7	0.35
BCDEF	10	16	24	25	25	8.8	5.6	2.8	1.0	0.5
CDEF	-	17.8	26.7	27.8	27.8	9.0	6.0	3.3	1.4	0.7
DEF	-	-	32.4	33.8	33.8	9.4	6.8	4.0	1.8	1.4
EF	-	-	-	50	50	9.8	8.1	5.6	4.1	3.4

3.1.2 Drilling fluid

EDC 95/11 which is a base oil used for drilling and a premix based on the same base oil were used for the experiments in this research work. These drilling fluids were supplied

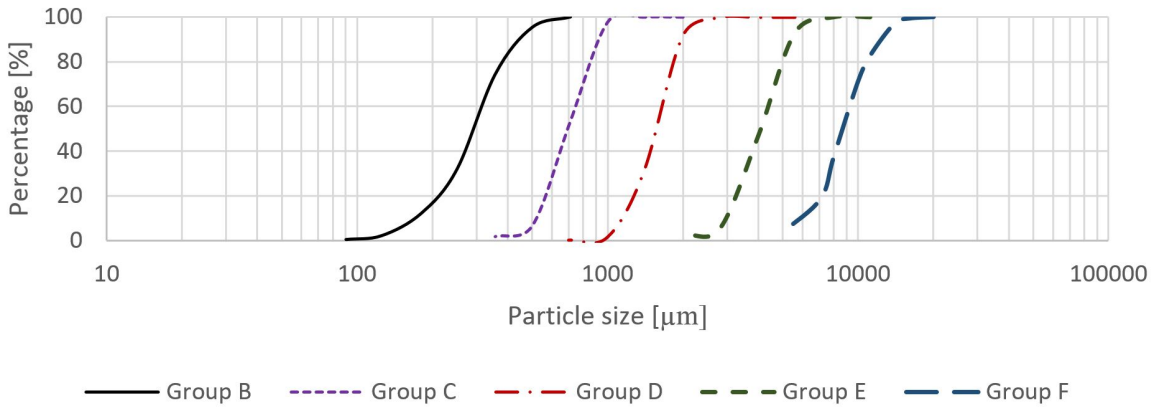

Figure 3.3: Particle size distribution of the sand groups

by MI SWACO. According to the manufacturer, the premix consists of,

- Base oil EDC 95/11
- Fresh water
- Calcium Chloride (1% - 5%)
- Lime (Calcium hydroxide) (1% - 3%)
- Organophilic clay
- Emulsifiers

According to the material safety data sheets provided by the manufacturer, the densities of the base oil and premix are, 800 kgm^{-3} and 1300 kgm^{-3} respectively at 20^0C. These values were verified by the laboratory tests. The viscosity profile of the two fluids were measured at the laboratory and are shown in Figure 3.4.

3.2 Pneumatic conveying tests

The pneumatic conveying tests were carried out at the powder research laboratory of the research group of Powder Science and TEChnology (POSTEC) of the department of SINTEF-Tel-Tek (formerly Tel-Tek).

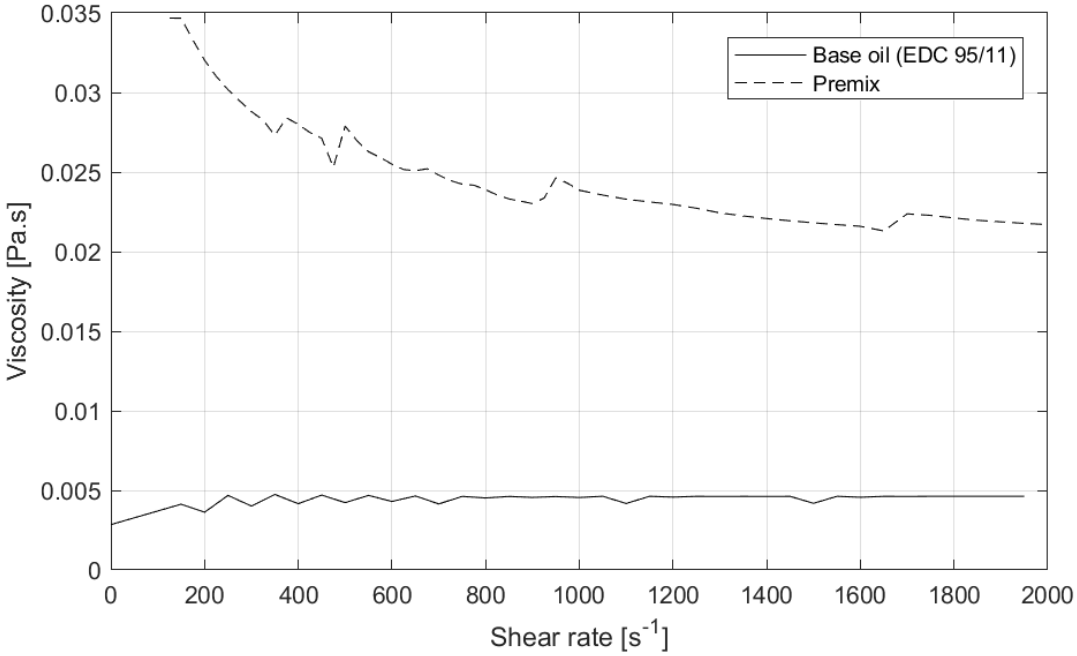

Figure 3.4: Viscosity of the drilling fluids

3.2.1 Pneumatic conveying test facilities

The pilot-scale pneumatic conveying rig consists of a storage tank, rotary feeder, air-solid mixing chamber and a receiving tank. A schematic diagram of the rig is shown in Figure 3.5. The material conveying pipelines are made from stainless steel and they have an inner diameter of 81.2 mm. The test rig has a closed loop flow path for solid material. The outlet of the receiving tank is connected to the inlet of the storage tank which has a capacity of 2.5 m^3 and the layout of the receiving tank and the storage tank is shown in Figure 3.6. The rotary feeder is used to control the material feed rate into the conveying line. The solid flow rate in the conveying line depends not only on the rotary feeder speed but also on the air flow rate and the type of the material. The motor speed of the rotary feeder can be controlled manually. The mixing chamber is located just beneath the rotary feeder where the solid particles will be mixed with compressed air before initiating to be conveyed. A pneumatically controlled sample taker is installed just before the receiving tank. Air stream separated from the receiving tank is sent to an air filter to separate fine particles before discharging air into the environment. The pressure drop in the horizontal section PT 8 - PT 9 with a length of 11.5m was considered in this research work as it demonstrated best experimental data agreement with the theoretical models for air only flow.

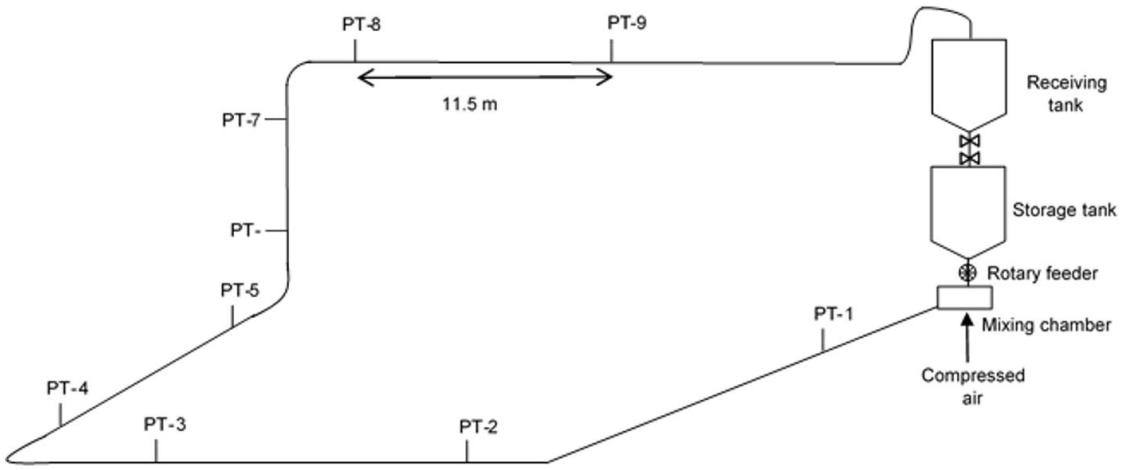

Figure 3.5: Schematic diagram of the pneumatic conveying rig

Air flow meter

There are two air flow meters installed to measure the inlet and outlet air flow rates of the pneumatic conveying rig. The technical specifications of the air flow meters are given below.

Manufacturer	: Yokogawa Electric
Model	: YF 108
Capacity	: 1000 Nm^3/h
Supply ovltage	: 24 V DC
Electrical output	: 4 to 20 mA
Accuracy category	: $\pm 1.0\%$ for velocity $\leq 35 ms^{-1}$
	$\pm 1.5\%$ for $35 ms^{-1}$ < velocity $\leq 80 ms^{-1}$

Pressure transducers

There are several pressure transducers installed in the pipelines of the pneumatic conveying rig. In the Figure 3.5 the locations of the pressure transducers installed on the pipeline are illustrated. The type of the pressure transducers installed is UNIK 5000 series pressure transducer manufactured by the General Electric. The technical specifications of the pressure transducers are given below.

1 : Receiving tank
2 : Storage tank
3 : Rotary feeder
4 : Mixing chamber
5 : Air filter
6 : Air inlet valve
7 : Air inlet to mixing chamber
8 : Receiving tank discharge valve
9 : Storage tank inlet valve

Figure 3.6: Storage and receving tanks of the conveying rig

Model	: PTX5072-TC-A1-CA-H0-PA
Material	: 25mm Stainless Steel Industrial
Pressure range	: 0 to 2.5 bar, Gauge
Electrical connection	: DIN 43650 Demountable
Electrical output	: 4 to 20 mA 2-wire (PTX)
Temperature range	: -40 to +80 ^{0}C (-40 to +176 ^{0}F)
Accuracy category	: Industrial
Calibration	: Zero/span data
Pressure connector	: G1/4 Female

3.2.2 Pneumatic conveying experimental procedure

The material which is to be conveyed is fed into the storage tank through the opening on the top. Approximately 100 kg of the conveying material is required to achieve steady

state conveying. Once the material is filled into the storage tank, the top opening is closed and the pipe connecting the bottom opening of the receiving tank and the top opening of the storage tank is installed. It must be make sure that both outlet valve of the receiving tank and the inlet valve of the storage tank are closed. Then the pneumatic conveying rig is ready to initiate the conveying tests. Each conveying test is conducted under predetermined air flow rate and a solid loading ratio.

As the first step, the air inlet valve is opened until the desired air flow rate is achieved. Once the air flow becomes steady, the solid particles are introduced into the mixing chamber through the rotary feeder. The air flow rate tends to decrease as the solid particles are introduced into the conveying pipe line. Hence the air flow rate is maintained within an acceptable range of the desired flow rate by controlling the air inlet valve manually. The pressure readings from the pressure transducers, air flow rate and the accumulated weight of the receiving tank is recorded continuously through a LabVIEW program. When the pressure values of the pressure transducers of the conveying line reach steady state, it is assumed that the solid conveying has also reached steady state conditions. It is desired to have a steady state flow at least for 20 seconds before the test is terminated. Since the real time solid flow rate cannot be monitored through the data acquisition system, saved data are analysed by a simple MATLAB script to calculate the solid flow rate and the respective solid loading ratio. If the desired solid loading ratio has not been achieved, a new conveying test has to be conducted with modified rotary feeder speed accordingly.

Once adequate amount of data is recorded under steady state conditions, the conveying test is terminated by stopping the rotary feeder. Then the data acquisition is also stopped. Then the air flow rate is increased up to 400-450 Nm^3/hr and maintained for about 30 seconds to make sure that the conveying pipeline is cleaned before the next conveying test. The material collected in the receiving tank is fed into the storage tank by opening the two valves and when the receiving tank is emptied these valves are closed again. Then the pneumatic conveying rig is ready to conduct another conveying test under different flow conditions. Likewise, pneumatic conveying tests are conducted at all the desired air flowrates at all the desired solid loading ratios that are required to complete the state diagram. Then the conveying material is discharged from the experimental rig and a new conveying material is fed into the storage tank.

Pneumatic conveying tests were conducted for both dry and oily samples and the details of the test samples are given in the Table 3.2.

For each of these samples pneumatic conveying tests were conducted under superficial air velocities of 250 Nm^3hr^{-1}, 300 Nm^3hr^{-1}, 350 Nm^3hr^{-1} and 400 Nm^3hr^{-1} with solid flow rates of 0.2 kgs^{-1}, 0.25 kgs^{-1}, 0.3 kgs^{-1}, 0.35 kgs^{-1} and 0.4 kgs^{-1} . For some samples with coarse particles such as the sample **D**, solid loading ratio of 0.2 was difficult to achieve as the rotary feeder tends to get blocked due to large the presence of large particles. On the other hand for samples with fine particles such as the sample **B**, high solid loading

Table 3.2: Pneumatic conveying samples

Sample	**Premix concentration** [*%wt.*]			
B	0	-	-	-
C	0	-	-	-
D	0	-	-	-
BC	0	1.5	-	-
CD	0	1.5	6.3	10
BCD	0	1.5	6.3	-
BCDE	0	1.5	6.3	-

ratios were difficult to be achieved as the discharge rate from the storage tank was not adequate to maintain a steady state flow.

3.3 Fluidization tests

Fluidization tests were conducted to study the impact of the amount of drilling fluid present and the particle size distribution towards the fluidization behaviour of the model drill cuttings and the experiments were carried out at the 'Process hall' of the Univerisity of South-Eastern Norway (USN).

3.3.1 Fluidization test facilities

The lab-scale fluidization test rig is composed of a cylindrical pipe made from Lexan plastic with a diameter of 84 mm and a height of 140 cm. A schematic diagram of the test apparatus is shown in Figure 3.7. The compressed air is supplied via a compressor and an air distributor is installed at the bottom of the cylinder between the first and the second pressure transducers. There are 10 pressure transducers installed on the cylinder with a distance of 0.1 m.

The compressor used in this experiment is manufactured by Nessco and it has a pressure range of 7.5 bar. A Sierra mass flow controller is used to control the air flow rate into the fluidization rig and the technical details of the mass flow controller is given below.

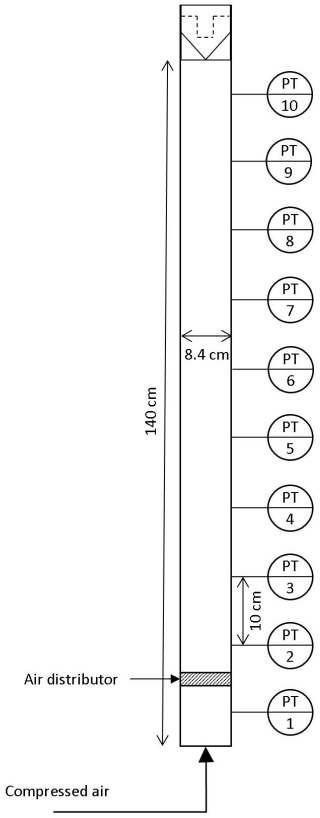

Figure 3.7: Schematic diagram of the fluidization rig

Model	: C100H2-DD-17-OV1-SV1-PV2-V1-S4-C3-CC
Flow range	: 0 to 1000 SLPM at 21^0C and 760 mmHg
Output signal	: 0 - 5 VDC/ 4-20 mA
Set signal	: 4 -20 mA
Inlet pressure	: 4.5 bar g
Outlet pressure	: 0.5 bar g
Maximum pressure	: 500 psi g
Temperature range	: 20^0C - 50^0C

3.3.2 Fluidization experimental procedure

A sand mixture sample of 2 kg was poured into the fluidization cylinder from the top opening using a funnel. The sample forms a bed on the air distribution plate. A paper bag filter is installed at the outlet of the pipe to minimize health and safety issues that may arise due to dust and drilling fluid vapour. A relatively large air flow pulse is given to the bed to obtain a uniformly distributed bed. The height of the bed before and after

the air flow pulse was measured. The fluidization test was initiated by introducing the compressed air flow from the bottom of the fluidization cylinder. The desired air flow rate is set at the air flow controller and when the air flow rate and the pressure readings from the pressure transmitters reach a steady state, air flow rate and the pressure reading values are saved by using the LabVIEW interface. Then the air flow is increased to a higher value and the air flow rate and pressure readings at steady conditions are saved. Likewise, the air flow rate is increased step wise and corresponding data are saved. This procedure is continued until either the bed is fully fluidized or the maximum allowable air flow rate through the air flow controller is reached. 2-3 replicate tests were conducted for each sample and a new material with the same particle size distribution and oil concentration was used for the replicate tests. After completing a fluidization test for each test sample, the fluidization cylinder was thoroughly cleaned before introducing a new sample.

Fluidization tests were conducted for both dry and oil samples and the details of the test samples are given in the Table 3.3.

Table 3.3: Fluidization test samples

Sample	**Premix concentration** [*%wt.*]				**Base oil concentration** [*%wt.*]		
B	0	-	-	-	-	-	-
C	0	1.5	6.3	10	1.5	4	6.3
D	0	1.5	6.3	10	1.5	4	6.3
E	0	-	-	-	-	-	-
BC	0	1.5	6.3	10	1.5	6.3	10
CD	0	1.5	6.3	10	1.5	6.3	8
BCD	0	1.5	6.3	10	1.5	6.3	10
BCDE	0	1.5	6.3	10	1.5	6.3	10
BCDEF	0	-	-	-	-	-	-
CDEF	0	-	-	-	-	-	-
DEF	0	-	-	-	-	-	-
EF	0	-	-	-	-	-	-
Treated Drill cuttings	0	1.5	6.3	10	1.5	6.3	10

3.4 Bulk solid shear tests

Bulk solid shear tests were conducted to study the influence of drilling fluid towards the flowability of the model drill cuttings and the shear tests were conducted at the Powder Science and TEChnology (POSTEC) of the department of SINTEF-Tel-Tek.

3.4.1 Shear test apparatus

Different shear testers such as Jenike shear tester, torsional shear tester and ring shear tester can be used for the reliable measurement of flowability of bulk solid. Among those shear testers, Jenike shear tester was selected as it has been used for a long period of time and a well established testing procedure is available.

The experiments were conducted in accordance with the standard shear testing technique presented by the Institution of Chemical Engineers [53] with the standard Jenike shear cell. A schematic diagram of the Jenike shear cell is shown in Figure 3.8.

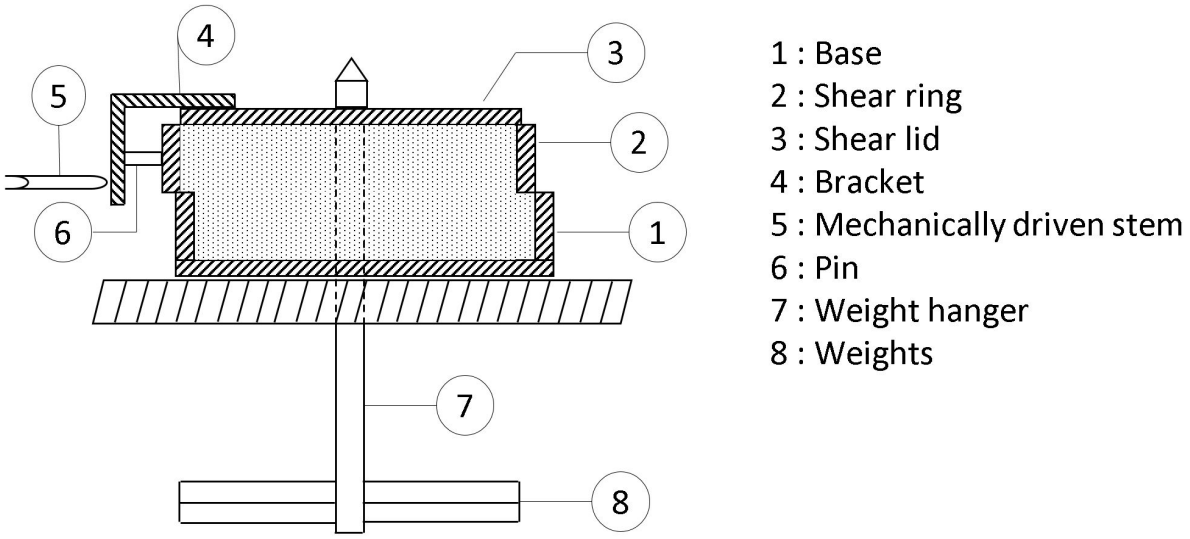

Figure 3.8: Schematic diagram of the Jenike shear cell

The dimensions of the shear cell used for the experiments is equivalent to the dimensions of the standard Jenike cell where the diameter of the shear ring is 95.25 mm, height of the shear ring is 15.875 mm and the inner height of the base is 12.7 mm. The shear cell is made from stainless steel.

In Figure 3.8 the shear ring is located at the initial off-set position. A vertical force is applied to the particulate material in the Jenike cell by using weights which are connected to the shear lid. A mechanically driven stem is used to apply the horizontal force to the particulate material in the cell. It is driven at a steady speed of approximately 1-3 mm/min. The shear ring will be moved horizontally due to the applied horizontal force and the maximum horizontal distance that it will be moved is twice the thickness of the wall of the base. The horizontal force acting on the shear ring is recorded against time and since the stem is driven at a steady speed, this can be transformed into shear force-shear strain plot.

3.4.2 Shear test experimental procedure

Shear testing using Jenike shear cell is carried out in two steps. The first step is the sample preparation and the second one is the actual shear stress measurement. In order to measure the shear stress correctly, the samples have to be prepared in a special manner. The experiments were conducted for the sand sample **CD** and samples containing 10 % (vol.), 20%, 30% and 40% of premix and base oil were tested separately. Another shear test was performed for the dry sample as well. For all the samples both instantaneous and 7 day time consolidation shear tests were conducted.

Sample preparation

A mould ring which is similar to the shear ring but having a height of 9.525 mm is placed on top of the shear ring (the shear lid is removed) before filling the particulate material into the shear cell. The material has to be filled in small uniform horizontal layers by using a spoon until it is filled slightly above the mould ring. When filling the material, it has to be make sure that no force is applied to the surface of the material. The excess material has to be scraped in small quantities by using a blade and the surface of the material should be levelled. The blade should be used in a zig-zag motion without disturbing the position of the shear ring on the base.

After the material is filled into the cell correctly, it has to be preconsolidated before conducting the actual shear tests. A twisting lid (consolidation lid) is placed on top of the levelled surface and a vertical force is applied to the material though a mass of $m_{w_{tw}}$ hanging in the weight hanger. This weight should impose a normal shear stress on the material that is approximately equal to the preshearing normal stress (σ_p). It has to be kept for a short period of time to let the air in material to scape and then the weights, hanger and the twisting lid are removed carefully. If there is space above the compressed material, it has to be refilled and compressed again following the same procedure. After having the shear cell filled with compressed material, the twisting lid is placed on the surface of the material and once again a mass of $m_{w_{tw}}$ is mounted on the weight hanger to apply the vertical force on the material. Then the sample is twisted with about by 20 cycles by using a twisting device. Rotation of the lid for 90^0 and reverse is considered as a twist cycle. When twisting, no vertical force should be applied on the material and the mould and shear ring should be allowed to rotate freely and independently of each other. After finishing twisting, the weight and the weight hanger should be removed. The mould is also carefully removed while keeping the twisting lid by placing a finger on it without applying a pressure on it. Then the twisting lid is removed by sliding it off gently in the direction towards the stem. After twisting the compressed material must be evenly distributed above the shear ring and the excess material should be scraped as described above.

Then the shear lid is placed on the surface of the material and the apparatus is completed as shown in Figure 3.8. The weight in the weight hanger should imposes a normal shear stress of σ_p on the material. The horizontal force is applied on the shear ring until it moves complete shear distance and the corresponding force vs. time data are recorded. The shear stress - shear strain plot obtained from those data is used to determine the consolidation status of the sample. A typical shear stress - shear strain plot is shown in figure which shows the different behaviour under different consolidation conditions.

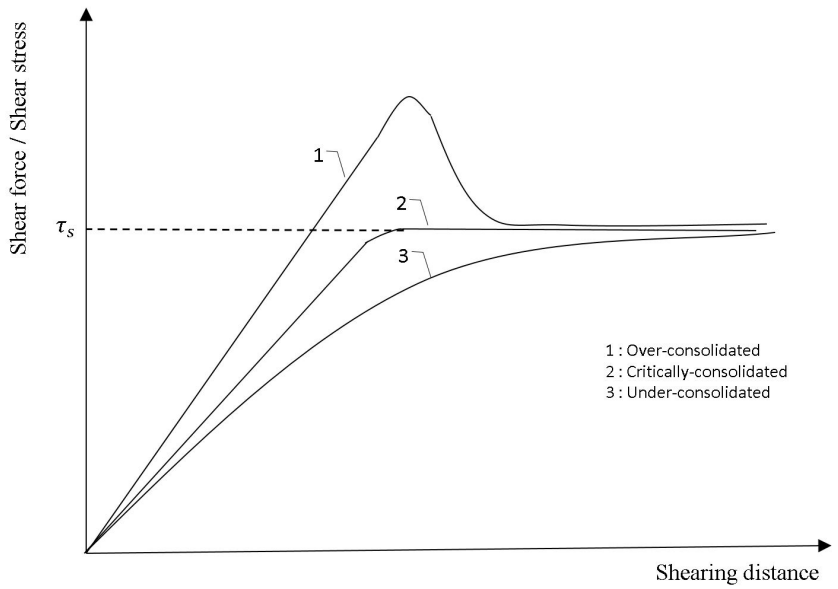

Figure 3.9: Shear stress - strain diagram

For the shear tests, it is desired to have critically consolidated samples. If the sample is overconsolidated, the number of twisting cycles used in the twisting stage has to be reduced systematically until the critical consolidation is achieved and if the sample is underconsolidated, the number of twisting cycles has to be increased gradually until the critical consolidation is achieved. For each preshearing stress level the corresponding number of twist cycles to achieve critical consolidation should be determined by following this procedure.

Shear tests

A sample which is in critically consolidated conditions corresponding to the considered preshearing normal stress is placed in the shear tester according to the apparatus in Figure 3.8. Weight corresponding to preshear normal stress σ_p is connected through the weight hanger. The horizontal force is applied on the ring until the shear stress increases and reach the steady state value of τ_p. This steady state shear stress has to

be achieved within 3/4 of the total shear distance available. After achieving the steady state value, the forward moving stem is stopped and disconnected from the bracket. Then the weights corresponding to the preshear normal stress is reduced down to the weight corresponding to the desired shear normal stress and the horizontal force is applied again. The monitored shear stress will rise upto a maximum value of τ_s and decreased. The shear stress τ_s is the stress at failure which is also known as shear point corresponding to the considered shear normal stress and preshear normal stress. In order to develop a yield locus corresponding to the considered preshear normal stress at least three shear tests must be conducted under different shear normal stresses. In order to develop the material flow function, several yield loci are obtained by conducting the shear tests under different preshear normal stresses.

Shear testing for time consolidation

Similar to the instantaneous shear test procedure described above, a critically consolidated sample is presheared until the steady state shear stress τ_p is reached. Then the stem and the weight hanger is carefully removed and the shear cell is transformed to the consolidation bench which is shown in Figure 3.10.

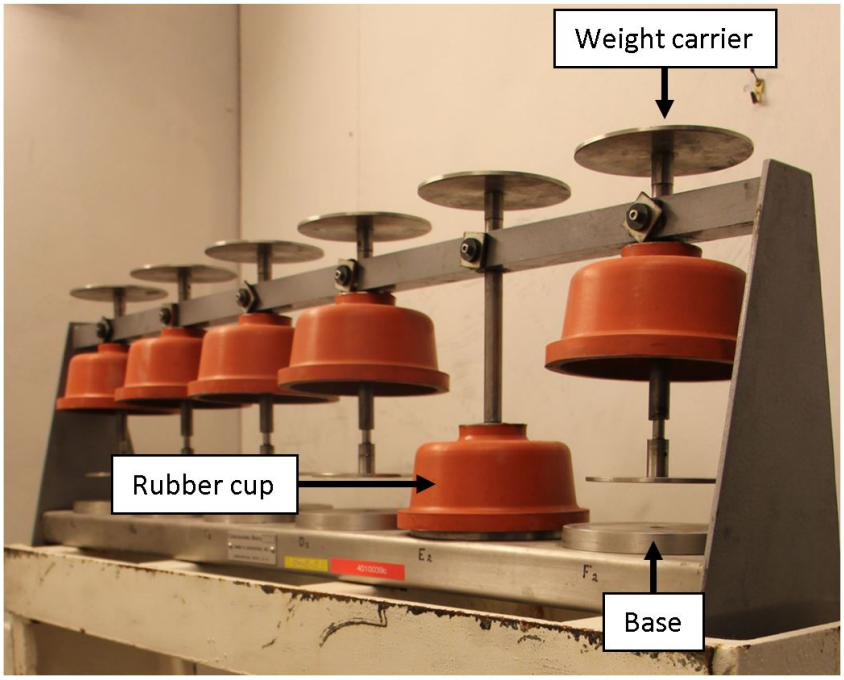

Figure 3.10: The consolidation bench

The shear cell should be mounted in manner so that the weight carrier acts centrally on the shear lid. The rubber cover is lowered to cover the shear cell and a weight of m_{W_t}

is placed on the weight carrier. The samples were kept in the consolidation bench for 7 days. After that the weights are removed from the weight carrier and the shear cell is transformed back to the shear tester. Then the shear is performed on the sample according to the same procedure for instantaneous shear test. For time consolidation shear test at least two experimental replicates must be conducted.

Wall friction test

The sample wall material corresponding to the standard Jenike shear cell must have a dimension of 120 × 120 mm. It must be washed and dried before the test. The wall material sample should be fixed on the shear tester in a manner such that the top surface of the wall material sample lays on the horizontal plane of the force measuring stem. The shear ring is placed on the edge of the wall material sample covering only the inner wall of the ring. This ensures that the shear ring can be moved the maximum distance during the test.

A mould ring is mounted on the shear ring and the particulate material is filled in layers similar to the sample preparation procedure in the shear test. Then the twisting lid is placed on the surface of the particulate material and the weight hanger is connected. Generally, six wall friction normal stresses are considered and the weight corresponding to the maximum normal stress is mounted on the weight hanger. Then the sample is twisted carefully without applying any vertical force on the particulate material and making sure that the mould and shear rings are allowed to rotate freely. After twisting is completed, the weights are removed, the mould ring is removed while holding the twisting lid gently. The twisting lid is removed by sliding it carefully in the direction of the stem. The excess material above the shear ring is scraped carefully and the shear lid is placed on the levelled material surface.

The selected wall friction normal stresses in the wall friction test is denoted by $\sigma_{w1}, ..., \sigma_{w6}$ and the corresponding weights mounted on the weight hanger is denoted by $m_1, ..., m_6$. The weights on the hanger should be mounted in a manner such that by removing a weight, the corresponding wall friction normal stress should be lowered by one level. Initially the highest wall friction shear stress is applied by mounting a weight of m_{w1} Then the horizontal force is applied and shear starts. The shear stress will increase and reach a constant value τ_{w6}. If the shear stress passes through a maximum value when reaching the constant value, the maximum value corresponds to the static wall friction while the constant value corresponds to the kinematic wall friction. While the horizontal force is applied, a weight is removed to achieve the wall friction normal strss of σ_{w5}. Then the shear stress will reach a new constant value of τ_{w5} and that value is recorded. Likewise, different wall friction normal stresses are applied by removing weights and the corresponding constant shear stress values are recorded. Once the test is completed the

weight of the sample is measured. The recorded constant values of shear stresses are used to obtain the kinematic angle of wall friction.

A similar test is conducted to obtain the static angle of wall friction. In this test, the horizontal force is removed when the maximum shear stress is reached. Then a weight is removed to reach a lower wall friction normal stress and then the horizontal force is applied again. Then the shear stress will reach another maximum value and it will be recorded. Likewise, the horizontal force is stopped at the maximum shear stress and a weight is removed to reach a different wall friction normal stress. The recorded maximum values of shear stresses are used to obtain the static angle of wall friction. Generally, 2-3 replicate experiments must be conducted in wall friction tests. Since it is known that the operator might have an influence over the shear tests, special consideration was taken when conducting the tests to achieve the best repeatability.

4 Fluidization and pneumatic conveying behaviour

4.1 Fluidization

4.1.1 Fluidization behaviour of dry particles

Fluidization tests were conducted for the **B,C,D,E** sand groups (sample **B** has the smallest particle diameter and the sample **E** has the largest particle diameter) and their mixtures such as **BC,BCD,BCDE** and **CD**. A complete list of the sand mixtures that were considered in the fluidization tests are presented in the Table 3.3. The particle size distribution of the considered sand mixtures are significantly different from each other and it is important to select a parameter to represent the particle size distribution of these sand mixtures. The parameters obtained from the particle size distribution are, D90 (particle diameter at the 90% of the cumulative distribution), D75, D50, D25, D10, mean diameter, span, relative span, and quartile ratio. The values of the parameters of all the considered sand mixtures are given in the Appendix C. A basic multivariate analysis was conducted to identify the influential parameters of the particle size distribution towards the minimum fluidization velocity of the dry sand samples. The loadings plot corresponding to the principle component analysis (PCA) is shown in the Figure 4.1.

The loadings plot shows that the minimum fluidization velocity of a dry sand sample is closely related to the mean particle diameter and to the particle diameters at the 25% and at the 10% of the cumulative distribution (D25 and D10). In Figure 4.2 the variation of the minimum fluidization velocity of the dry sand samples are plotted against the the D25, D10 and the mean diameters of the different sand mixtures. Since D25 is more correlated to the minimum fluidization velocities of the samples, D25 was taken as the parameter to represent the particle size in further analysis of the fluidization behaviour of the particles under dry and wet (mixed with drilling fluid) conditions.

Based on the D25 diameter of the particles, the relative positions of the sand samples in the Geldart's diagram is shown in Figure 4.3. The particle density of the sand samples are represented by an average value which is equal to 2718.5 kgm^{-3}.

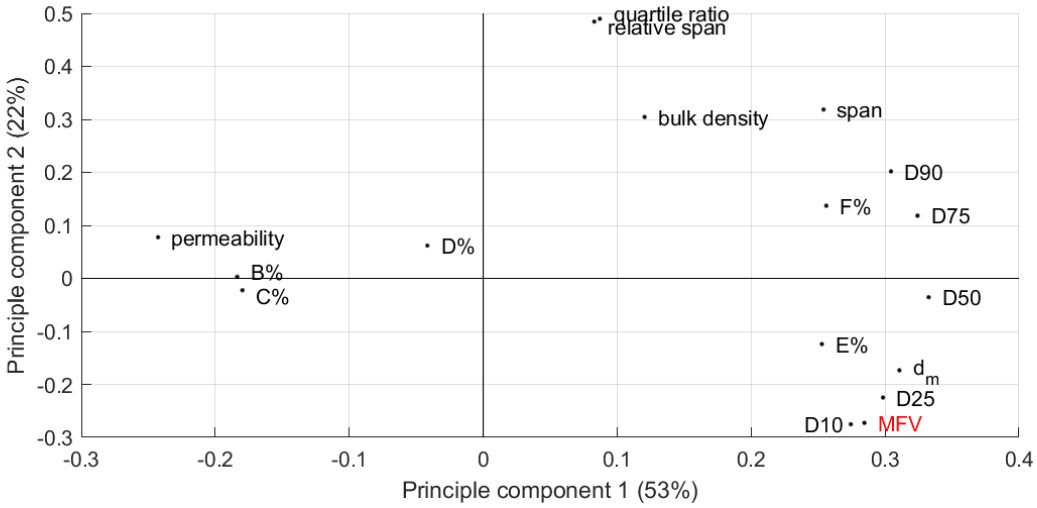

Figure 4.1: Loadings plot from the PCA of the fluidization and particle size distribution parameters of the dry sand samples

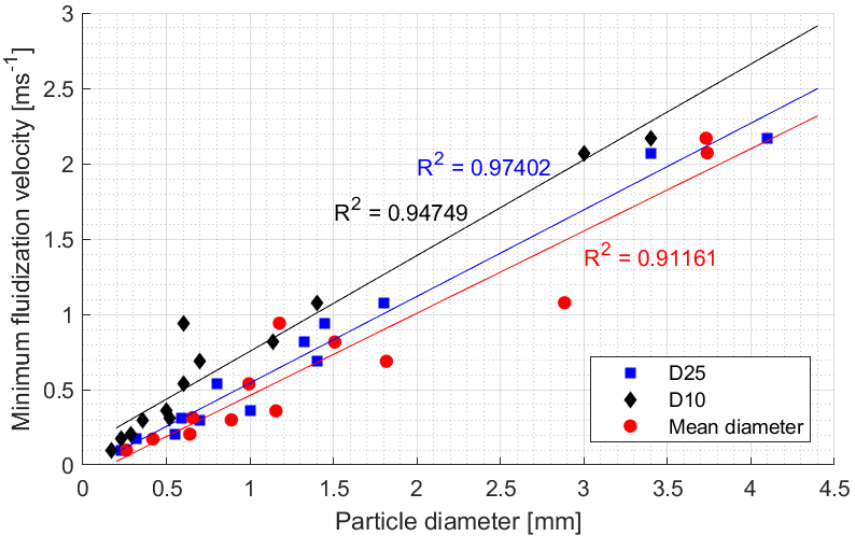

Figure 4.2: Minimum fluidization velocity vs. particle diameter of dry sand samples

According to the Figure 4.3, the sand mixtures of **B,BC,BCD** and **C** belong to the Geldart's *Group B* while all the other sand mixtures can be classified into the Geldart's *Group D*. However, the sand mixtures of **C,BCD,BCDE** and **CD** lie in the boundary between *Group B* and *Groupd D*. The treated drill cuttings sample can be also classified into the *Group D* and it lies close to the samples of **D,CDEF** and **DEF** . According to Shaul et al. [54], the Archimedes number (Ar) which is defined in Equation 2.12, has a value between 80 and 3000 for the Geldart's *Group B* materials while the *Group D*

materials have an Archimedes number greater than 3000. The boundaries corresponding to the values of $Ar = 80$ and $Ar = 3000$ for sand particles are also plotted in Figure 4.3 and it agrees with the classification of the sand samples based on the classical Geldart's diagram. Based on the Equation 2.12, the Ar number for the treated drill cuttings sample is calculated to be 1.43E+05 which lies in the Geldart's *Group D* region. Therefore, for the considered dry sand samples and the treated drill cuttings samples, both Geldart's diagram and the Ar number can be used to categorize the materials according to their fluidization behaviour.

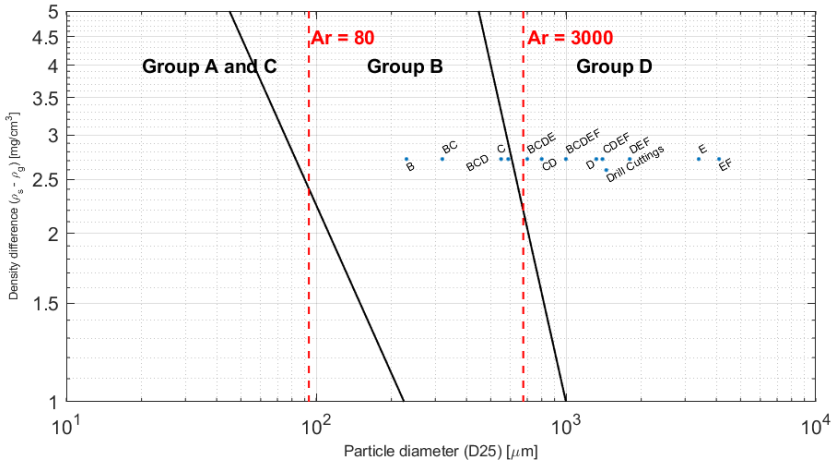

Figure 4.3: Geldart's classification for dry sand mixtures

The classification of the sand mixtures based on the empirical models have to be confirmed through the fluidization experiments. Based on the observations of the experiments it can be stated that the fluidization tests also support the classification in Figure 4.3 as the samples **B,C,BCD** and **BC** does not expand the bed at minimum fluidization state and reach the bubbling conditions as soon as reaching the minimum fluidization condition which is similar to a *Group B* material. For the samples **E,EF** and **DEF** the spouting behaviour was clearly visible which is an inherent property of the *Group D* materials.

The pressure gradient vs. superficial air velocity curves which is also known as the fluidization curves obtained from the fluidization tests for all the considered dry samples are given in the Figure 4.4. The fluidization curves for the dry sand samples and the minimum fluidization velocities corresponding to each sample is given in the Appendix D. The fluidization curves are grouped into 3 groups in the Figure 4.4 to present the data more clearly. The fluidization curve corresponding to the treated drill cuttings sample is plotted in all three groups to compare its fluidization behaviour with all the sand mixtures.

The pressure gradient across the fluidization bed in the packed bed state shows a parabolic behaviour for the mixtures of **E** and **EF** which is a characteristic property of the Geldart's *Group D* material. **B** and **BC** samples show a linear pressure gradient characteristic in

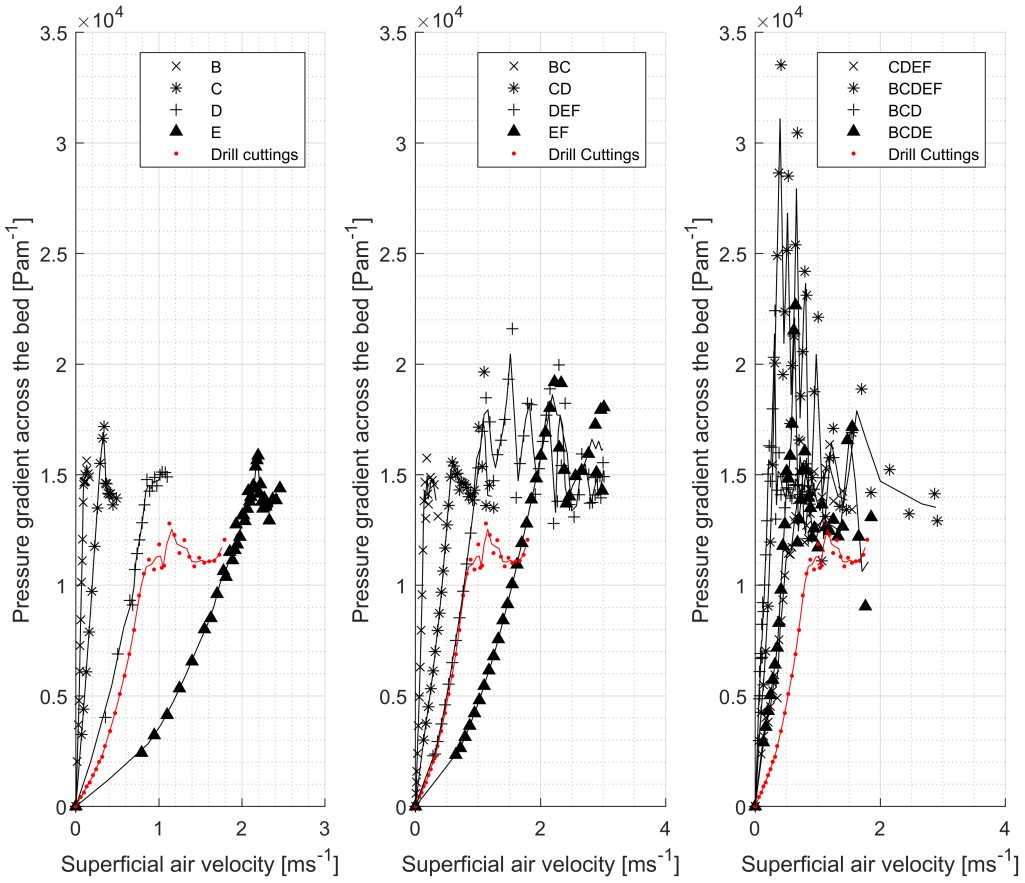

Figure 4.4: Fluidization curves for dry sand samples

the packed bed state implying that they belong to the Geldart's *Group B*. All the other samples show a slightly parabolic pressure gradient curves. It is also interesting to observe that the fluidization curve for the treated drill cuttings sample follows a similar path to the sand mixtures, specially to the sand mixtures of **D** and **DEF**. The similar fluidization behaviour of the drill cuttings and the sand samples can be considered as a justification for the selection of sand to represent drill cuttings in the considered research work.

Before analysing the impact of the presence of drilling fluid towards the fluidization behaviour of the dry samples, it is important to validate the experimental results of the fluidization behaviour of the the dry samples based on available fluidization models. The voidage at the minimum fluidization state and the sphericity of the particles could not be measured due to the time and instrumentation limitations during the experiments. Therefore, the minimum fluidization velocity for each sample was estimated based on the Equation 2.9 and using the constants presented in the Table 2.1. The obtained results are compared in the Figure 4.5.

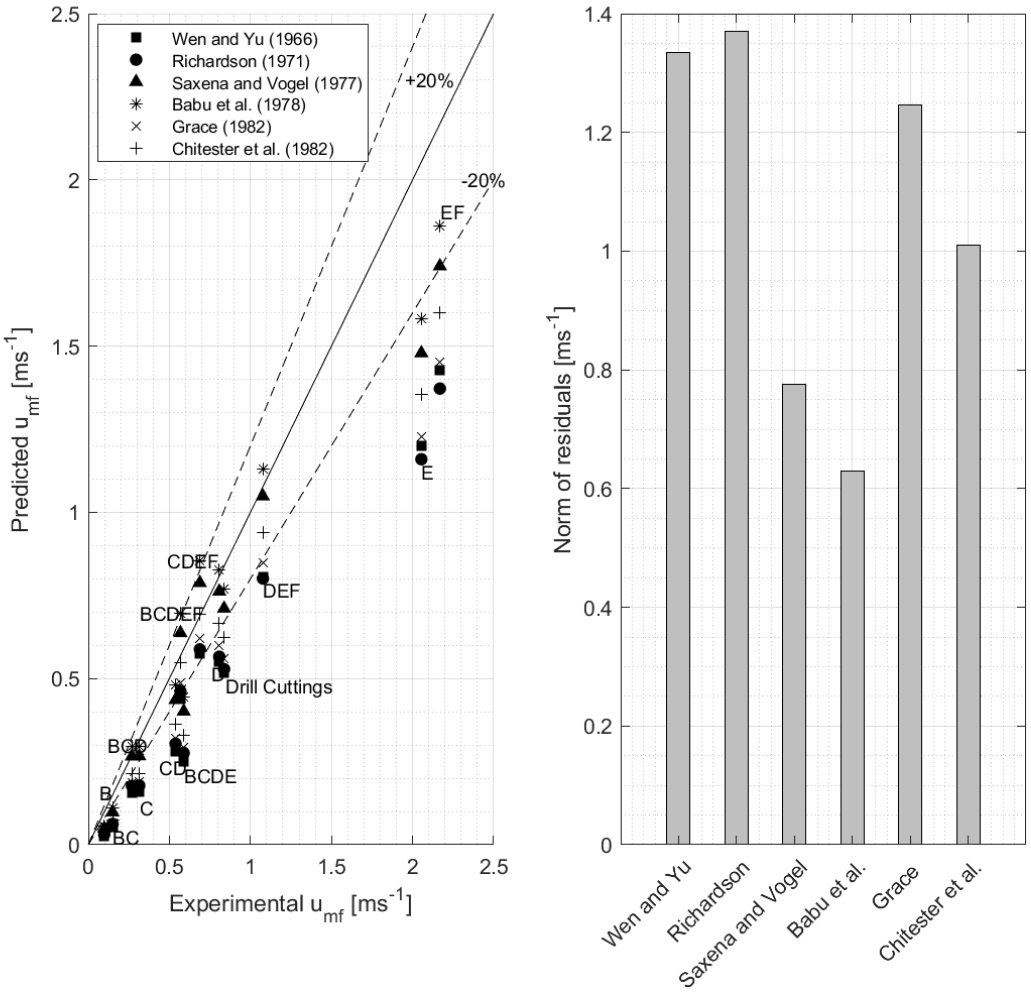

Figure 4.5: Comparison of the models to predict the minimum fluidization velocities

The calculations were performed based on the D25 diameter of the samples as it gave the best results compared to the the mean particle diameter corresponding to the same sample. The norm of the residuals which is calculated according to the Equation 4.1 of the 6 models considered are also compared in the Figure 4.5. Based on the results it can be concluded that the model present by Babu et.al. [22] which has a value of K_1 = 15.4 and K_2= 779.24 can be used to calculate the minimum fluidization velocity with an error less than 20%. The model is highly deviated for the samples of **E** and **EF** which have relatively larger particles. Since the experimental results can be predicted based on an available empirical model with an acceptable accuracy, it can be considered that the results obtained from the tests are physically acceptable.

$$Norm\ of\ residuals = \sqrt{\sum (Value_{measured} - Value_{predicted})^2} \tag{4.1}$$

4.1.2 Impact of drilling fluids towards the fluidization behaviour

An initial set of experiments were conducted with the sand mixtures of **C,D** and **CD** to get an overview of the impact of drilling fluid towards the fluidization behaviour of the particles. The fluidization curves corresponding to the sample **C** - Premix mixtures are presented in Figure 4.6 and the fluidization curves corresponding to the samples of **D** and **CD** are presented in the Appendix E. The drilling fluid concentration is presented as weight percentage (wet basis).

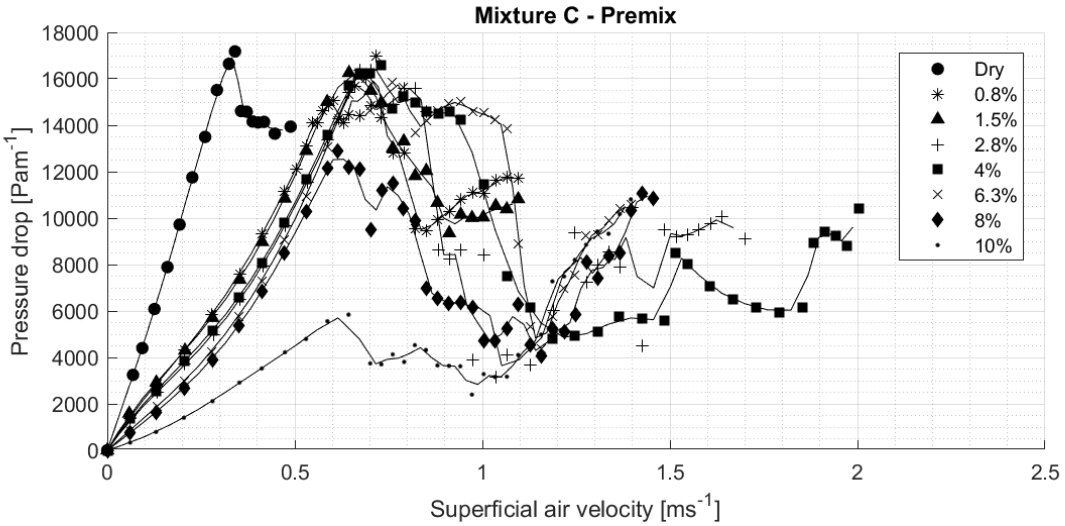

Figure 4.6: Fluidization curves for C - Premix mixture

According to the Figure 4.6 it can be observed that the fluidization curves corresponding to the sample **C**-Premix mixtures are clearly deviated from the fluidization curve of the dry condition. It is interesting to observe that the fluidization curves of the sample **C**-premix mixtures do not deviate much with respect to the drilling fluid concentration associated with the mixtures except for the concentration of 10% of the premix. A similar behaviour can be observed in the fluidization curves of the mixtures of **D** and **CD** as well. The variation of the minimum fluidization velocity with the drilling fluid concentration is given in the Figure 4.7 for the considered three sand mixtures. It can be seen that the minimum fluidization velocity is increased significantly with respect to the dry conditions by introducing a small amount of drilling fluid such as 0.8% by weight (for the mixtures of **C**-premix, **CD**-premix and **CD**-base oil). For the samples of **C** and **CD** it can be seen that the minimum fluidization velocity remains at a relatively constant value with further

increasement of the drilling fluid concentration. However, the sample **CD** displayed a sudden drop in the minimum fluidization velocity at the drilling fluid concentration of 10% and 8% for the premix and the base oil respectively. The sample **D** displayed a similar behaviour to the other two sample by increasing the minimum fluidization velocity when drilling fluid is introduced to the system but contrast to the other two samples, the minimum fluidization velocity was decreasing with the increasing drilling fluid concentration.

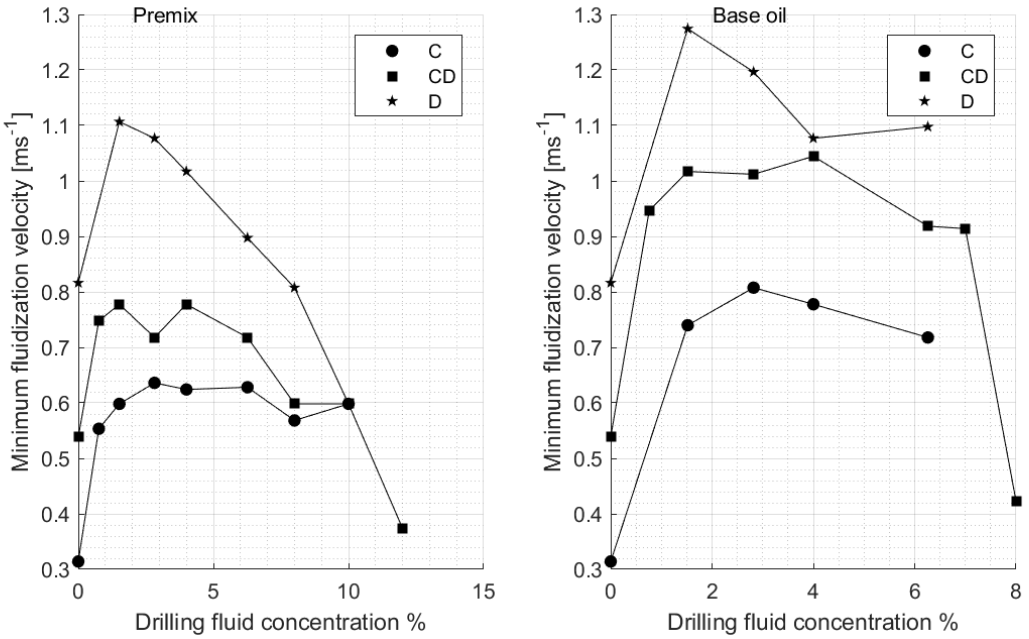

Figure 4.7: Minimum fluidization velocity vs. Drilling fluid concentration for the samples of **C,CD** and **D**

Based on these observations, fluidization tests were conducted for the mixtures of **BC, BCD, BCDE** and for a sample of treated dry drill cuttings with a drilling fluid concentrations of 1.5%, 6.3% and 10% of premix and base oil. The fluidization curves obtained from these experiments are presented in the Appendix E.

Basically, the fluidization curves of all the samples significantly deviates from the dry conditions when a drilling fluid is introduced. The linear pressure gradient in the packed bed state has transformed into a parabolic behaviour and the minimum fluidization velocity has been increased compared to the dry conditions. This phenomenon can be observed in all the samples which is given in the Appendix E. It is also observed that all the samples except sample **D**-premix mixture, display a relatively constant minimum fluidization velocities at the drilling fluid concentrations of 1.5% and 6.3% for both premix and the base oil. When the drilling fluid concentration is increased up to 10%, the fluidization curve

is shifted back towards the dry condition. For some samples such as **CD** and **BCDE** the fluidization curve corresponding to the concentration of 10% is shifted left side surpassing the fluidization curve at the dry conditions, resulting a lower minimum fluidization velocity compared to the dry state. Both in **CD** and **BCDE** - base oil 10% mixtures, it was observed during the fluidization tests, that the drilling fluid is separated from the sand-drilling fluid mixture and the drilling fluid reaches the top of the fluidization bed as shown in Figure 4.8. Almost all the samples started slugging with increment of air velocity beyond the minimum fluidization velocity.

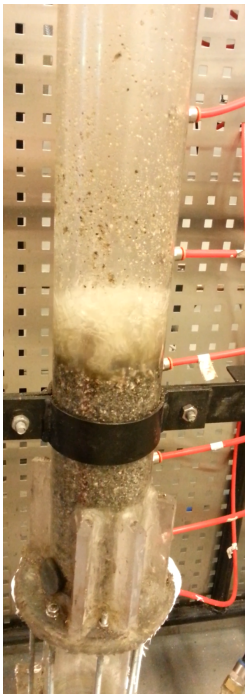

Figure 4.8: Separation of drilling fluid for the mixture of BCDE-Base oil at air velocity of 100 SLPM

The minimum fluidization velocities obtained from the experimental data are presented separately for both base oil and the premix in Figure 4.9. As discussed above, it can be seen that the minimum fluidization velocity is increased when drilling fluid is added to the dry sample. The most interesting observation is that there is no significant difference between the minimum fluidization velocities at the fluid concentrations of 1.5% and 6.3% for both drilling fluid samples. This phenomenon can be observed not only in sand samples but also in the treated drill cuttings sample as well. However, when the drilling fluid concentration is further increased up to 10%, the minimum fluidization velocity of all the samples tends to be lowered compared to the value at the drilling fluid concentration of 6.3%.

It was observed that in the treated drill cuttings mixture with 10% premix, the particles in the mixture stick together and forms a strong cake like material that tends to move

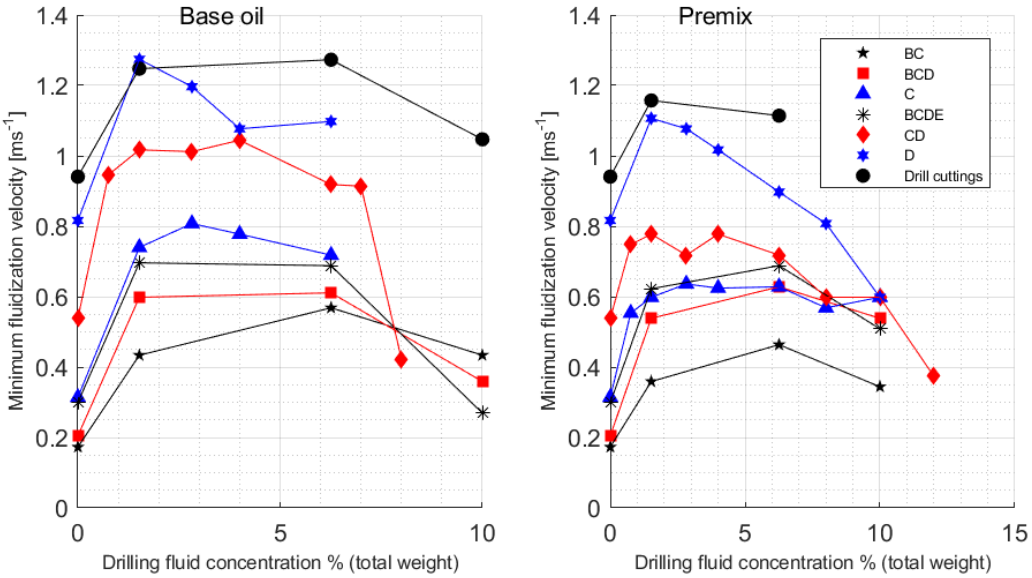

Figure 4.9: Minimum fluidization velocity vs. drilling fluid concentrations

as a plug at higher air velocities. As a result it was not possible to determine a clear fluidization velocity for the sample and it was considered as an outlier in further analysis of the samples. However, this behaviour must be taken into consideration as it indicates that sand might not be a suitable replicate material to represent drill cuttings at higher concentrations of drilling fluids.

Since the considered dry samples displayed a linear relationship between the minimum fluidization velocity and the D25 diameter of the particles, it is interesting to see the behaviour of the minimum fluidization velocity of the samples mixed with drilling fluids with respect to the D25 diameter of the mixture. The plots of minimum fluidization velocity vs. D25 diameter of the particles are plotted for the concentrations of 1.5%, 6.3% and 10% for both the premix and the base oil are presented in the Figure 4.10. The parameters of the linear regression correlation between the minimum fluidization velocity and the particle diameter are tabulated in the Table 4.1.

All the mixtures associated with drilling fluids tend to increase the minimum fluidization velocity as the particle diameter of the mixture increases. The linear regression models for the mixtures of 1.5% and 6.3% of both premix and the base oil have a similar gradient compared to the dry conditions. Only the 10% premix mixtures are highly deviated from this pattern. The Figure 4.10 clearly indicates that the variation of the drilling fluid concentration at low levels of drilling fluid concentrations (less than 6% of weight) has a negligible impact on the fluidization behaviour of the particles as the linear regression models for the mixtures of 1.5% and 6.3% of both premix and the base oil almost overlap on one another. The Figure 4.10 also shows that the presence of base oil in a certain

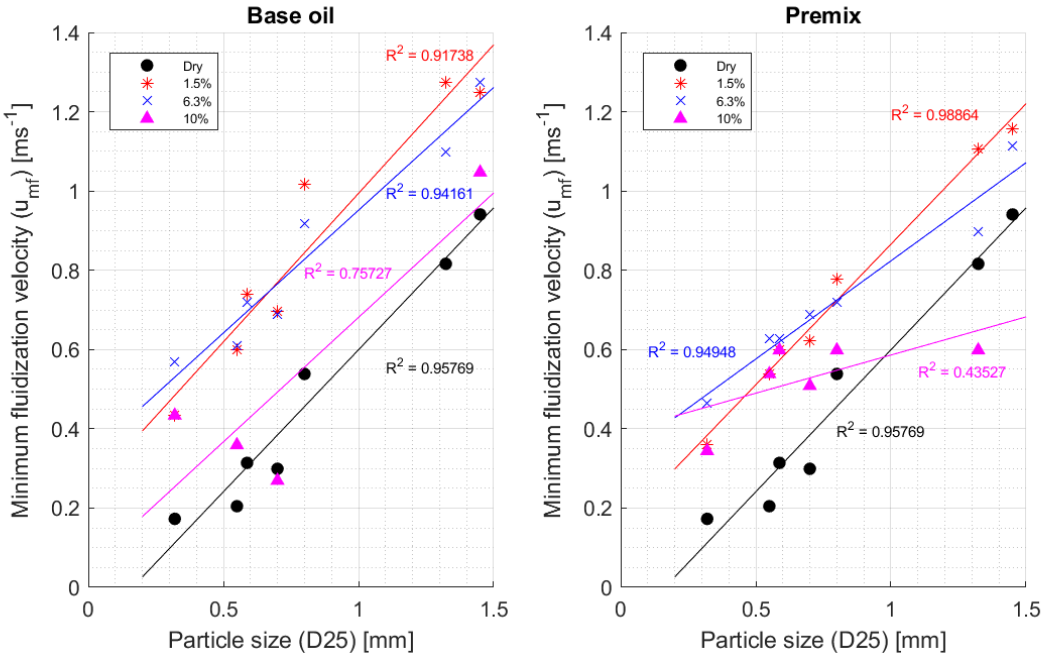

Figure 4.10: Minimum fluidization velocity at different drilling fluid concentrations vs. particle diameter

Table 4.1: Parameters of the linear regression correlation between the minimum fluidization velocity and the particle diameter

Mixture	Gradient	Intercept	Coefficient of determination	Norm of residuals
Dry	0.7166	-0.1172	0.9577	0.15372
Base oil - 1.5%	0.7496	0.2455	0.9174	0.22958
Base oil - 6.3%	0.6193	0.3321	0.9416	0.1574
Base oil - 10%	0.6281	0.0530	0.7573	0.30118
Premix- 1.5%	0.7091	0.1566	0.9886	0.077571
Premix - 6.3%	0.4952	0.3285	0.9495	0.11659
Premix - 10%	0.1925	0.3936	0.4353	0.16651

mixture cause a higher fluidization velocity compared to the presence of premix in the same mixture with the same concentration.

The deviation of the minimum fluidization velocity compared to the dry condition of different sand mixtures are presented in the Figure 4.11 for both base oil and the premix. Mixtures such as **BC** and **BCD** which have smaller D25 diameter tend to have a higher minimum fluidization velocity increment ratio compared to the mixtures with larger D25 diameters. This phenomenon is clearly presented by the Figure 4.12. According to the Figure 4.12 as the D25 diameter of the sample increases the increment ratio of the

minimum fluidization velocity decreases and the correlation between the two parameters display a parabolic behaviour.

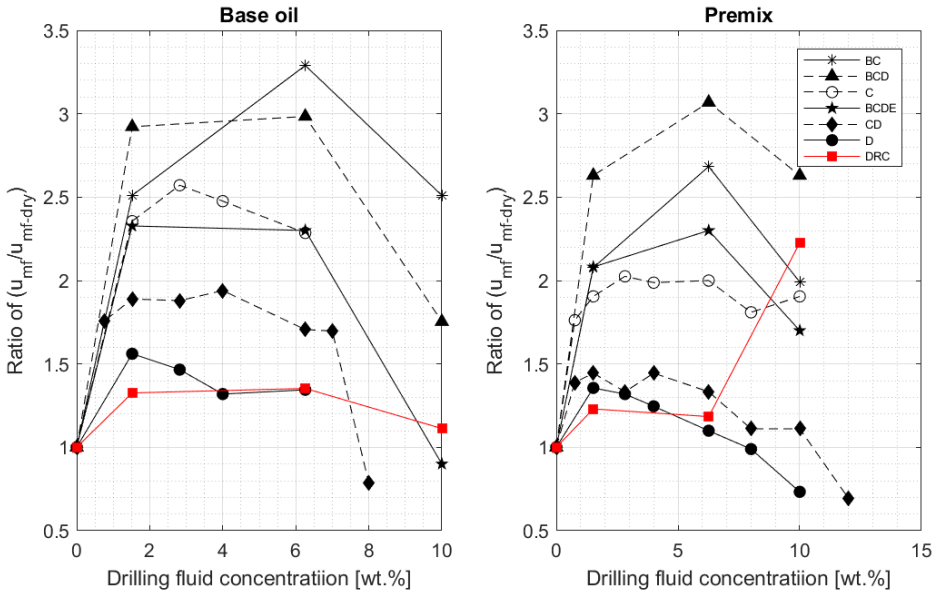

Figure 4.11: Increasement of minimum fluidization velocity compared to the dry conditions vs. drilling fluid concentration

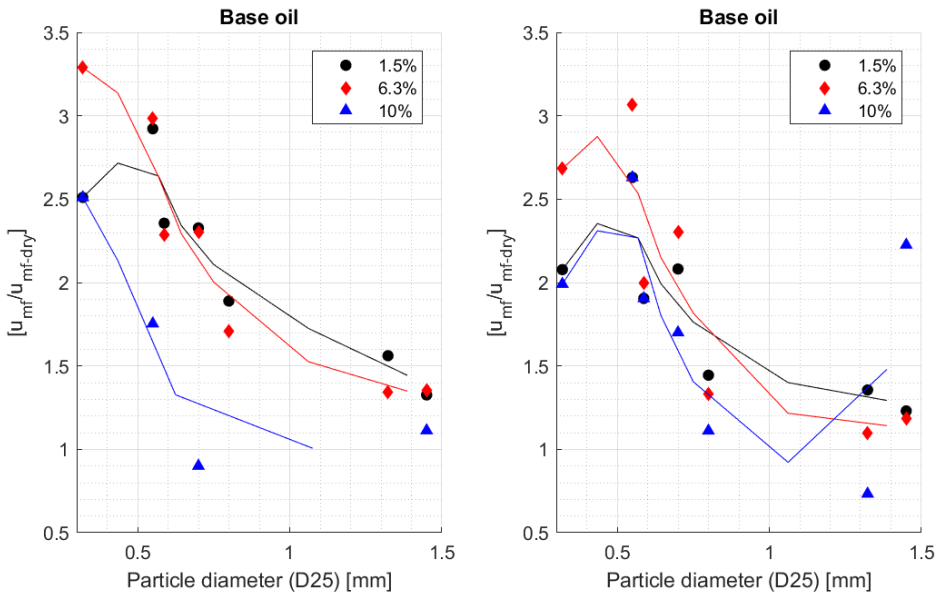

Figure 4.12: Increasement of minimum fluidization velocity compared to the dry conditions vs. particle diameter

According to the Figure 4.11 the behaviour of the treated drill cuttings sample and the

sand mixture **D** is relatively similar at low drilling fluid concentrations. This can be also seen in the Figures of the Appendix F where the fluidization curves of different sand mixtures are compared at a particular drilling fluid concentration. At the drilling fluid concentration of 1.5% for both premix and the base oil, the pressure gradient across the bed of the mixture **D** and the treated drill cuttings sample follow the same path in the packed bed condition. At the drilling fluid concentration of 6.3% both samples follow the same pressure gradient curve at very low superficial air velocities and starts to deviate after about 0.5 ms^{-1} of air flow.

When considering the fluidization curves presented in the Appendix E, it can be seen that the deviation of the minimum fluidization velocity of the oily samples occur as a result of the change of the pressure gradient across the bed in the packed bed conditions. The gradient in the fluidization curve in the packed bed state is proportional to the air-particle friction coefficient of the system and it is inversely proportional to the permeability of the bulk solid material. The variation of the air-particle friction coefficient with the drilling fluid concentration is presented in the Figure 4.13.

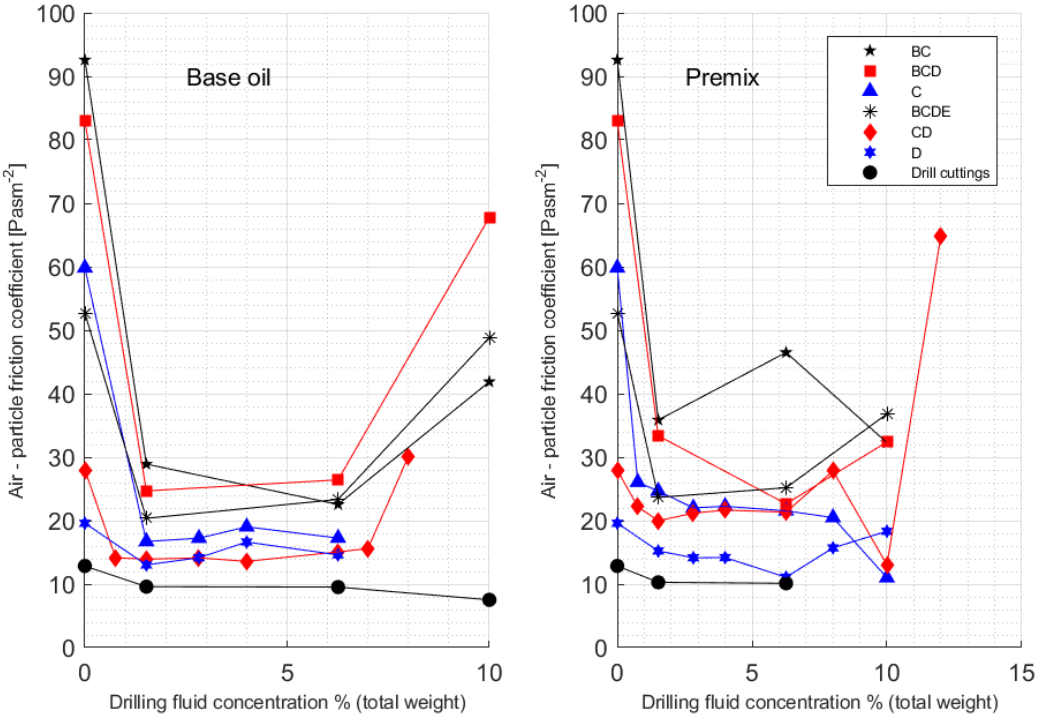

Figure 4.13: Air-particle friction coefficient vs. drilling fluid concentration

It can be seen that as a little amount of drilling fluid is mixed with the dry sand mixture, the air-particle friction coefficient reduces significantly for both premix and the base oil. The reduction of the air-particle friction coefficient is relatively significant for the sand

mixtures with smaller D25 particle diameters. The sand mixtures with premix tend to have a higher air-particle friction coefficient compared to the mixtures with base oil with the same drilling fluid concentration. The Figure 4.13 also shows that the air-particle friction coefficient is not affected by the increasing drilling fluid concentration up to around a concentration of 6% and beyond that the air-particle friction coefficient would be increased significantly. The variation of the air-particle friction coefficient with the particle diameter is present in the Figure 4.14.

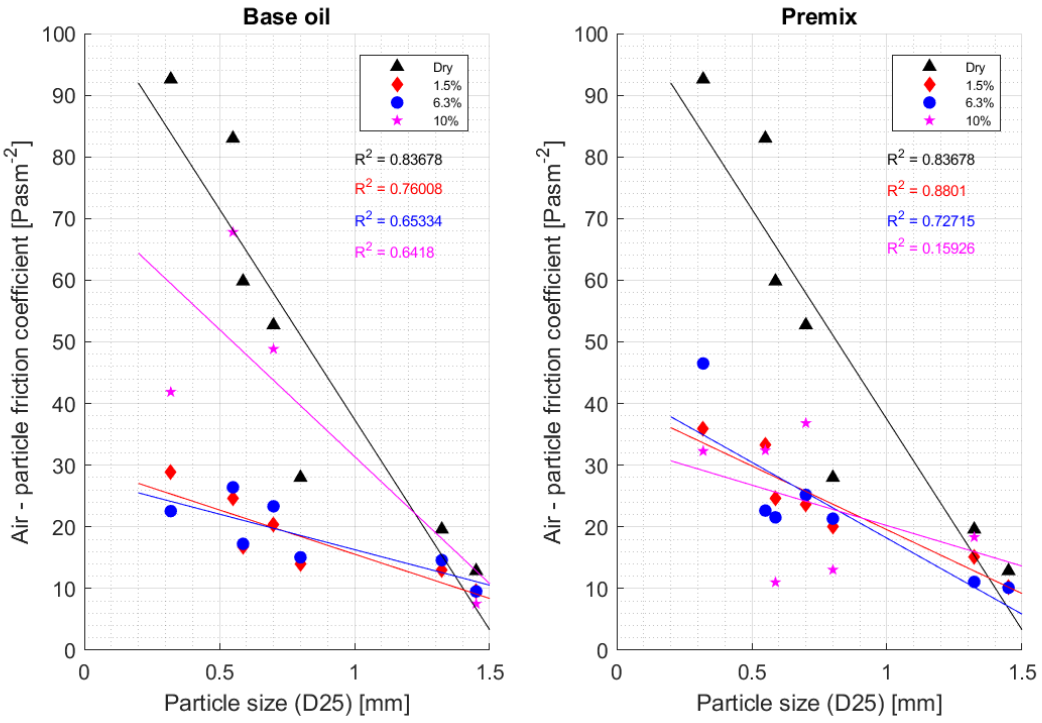

Figure 4.14: Air-particle friction coefficient vs. particle diameter

According to the Figure 4.14, it can be seen that the air-particle friction coefficient of the dry mixtures significantly depend on the particle diameter and as the D25 diameter of the sample increases the the air-particle friction coefficient decreases. The samples mixed with drilling fluid also have a reduced air-particle friction coefficient with increasing drilling fluid concentration but the dependency of the air-particle friction coefficient on the particle size is smaller compared to the dry conditions. The behaviour of the mixtures with 10% drilling fluid is significantly deviated from the rest of the samples and it can be expected as oil and solid particles tend to be separated in some of the samples with 10% of drilling fluid.

4.1.3 Summary

Based on the analysis of the fluidization tests it can be concluded that when a dry sample is mixed with a little amount of drilling fluid (even less than 1% of weight), the air-particle friction coefficient of the mixture will be reduced significantly compared to the dry condition. As a result the minimum fluidization velocity of the mixture is increased. With further increasement of the associated drilling fluid concentration (up to around 6% of weight) neither the air-particle friction coefficient nor the minimum fluidization velocity of the mixture change significantly. It can be observed that the fluidization curves follows the same path regardless of the increasing drilling fluid concentration. However, when the drilling fluid concentration exceed the value of 6-8%, drilling fluid tends to be separated from the packed bed with increasing air velocity and according to the fluidization curves, the air-particle friction coefficient is significantly enhanced while reducing the minimum fluidization velocity. The fluidization tests also show that the treated drill cuttings sample display a similar behaviour to the mixture **D** at low levels of drilling fluid concentrations.

The fluidization tests display that the minimum fluidization velocity increase with the increasing D25 diameter of the mixtures while the air-particle friction coefficient reduces. The mixtures with smaller D25 diameter tend to have a higher increasement of the minimum fluidization velocity compared to the dry condition while the increasement of the mixtures with larger D25 diameters are relatively low.

4.2 Pneumatic conveying

Pneumatic conveying tests were conducted for the dry mixtures of the **B,C,D,BC,CD, BCD** and **BCDE** mixtures (**B** has the smallest particle diameter and **E** has the largest particle diameter). The composition of the considered sand mixtures are presented in the Table 3.1. The state diagrams of those mixtures obtained for the horizontal section of PT 8 - PT 9 in the pneumatic conveying rig are presented in the Appendix G. Based on the state diagrams it can be seen that both the dry and oily mixtures were conveyed in the dilute phase and some mixtures such as **B**(dry) entered into the dense phase at low air flow rates.

4.2.1 Pnematic conveying of dry mixtures

The state diagrams of the pneumatic conveying of the dry mixtures of **B,C,D,BC,CD, BCD** and **BCDE** are presented in the Appendix G by the figures of G.1, G.3, G.5, G.2, G.4, G.6 and G.7 respectively. Based on those state diagrams, the pressure drop for different sand mixtures at different solid flow rates are compared at different air flow rates and it is presented by the Figure 4.15.

The pneumatic conveying state diagrams of the considered mixtures display the flow pattern similar to a general state diagram which is described in the Section 2.2 under the Figure 2.4. At a particular air flow rate, all the mixtures display a higher pressure drop at a higher solid flow rate. The pressure drop at a particular solid flow rate increases with the air flow rate for all the considered mixtures. However, some mixtures such as **B** and C tend to reach a minimum pressure drop in the region of 12-15 ms^{-1} of air velocity and tend to increase the pressure drop with decreasing air velocity. It is considered that this behaviour occurs when the conveying mode is transformed from the dilute phase into the dense phase. The mixtures displaying an increasing pressure drop with decreasing air flow rate are marked as 'Dense' in the Figure 4.15.

The sand mixtures in the Figure 4.15 are sorted according to the span of the particle size distribution, where the mixture **B** has the lowest span and the mixture **BCDE** has the largest span. According to the Figure 4.15, there is a general trend to have a decreasing pressure drop with decreasing span of the particle size distribution of the mixtures in the dilute phase flow conditions. When transformed into the dense phase region the samples with low span and low particle diameter, tend to have a higher pressure drop compared to the other mixtures.

An initial analysis of the pneumatic conveying of sample **B,C** and **D** shows that the all three samples would reach theit minimum pressure drop in pneumatic conveying when the superficial air velocity is in the region of 15-18 ms^{-1}. It was also observed that the impact of the particle size towards the pressure drop of the three samples are minimum in this flow region. CFD simulations based on multiphase particle-in-cell method were used to predict the horizontal pressure drop of the considered samples and the simulated results had a a good agreement with the experimental results. Detailed description of this study is presented in the Appendix B.

Correlation between pressure drop and material properties

In order to study the impact of the presence of drilling fluid towards the pneumatic conveying behaviour of the particles, it is important to establish a correlation between the pneumatic conveying pressure drop and the material properties of the dry particles. Since the particle conveying velocity and the voidage of the conveying material cannot be estimated in the pneumatic conveying experimental rig, a correlation was developed for the total pressure drop across the horizontal section of PT 8 - PT 9 based on the Equation 2.29 and the Equation 2.30. In order to suit the experimental system the Equation 2.30 is slightly modified as follows,

- The particle density (ρ_p) in the Equation 2.30 is replaced by the bulk density of the mixture as the particle density is same for all the considered text mixtures.
- Based on a basic multivariate data analysis it was observed that the span of the particle size distribution of the considered test mixtures are more closely related to

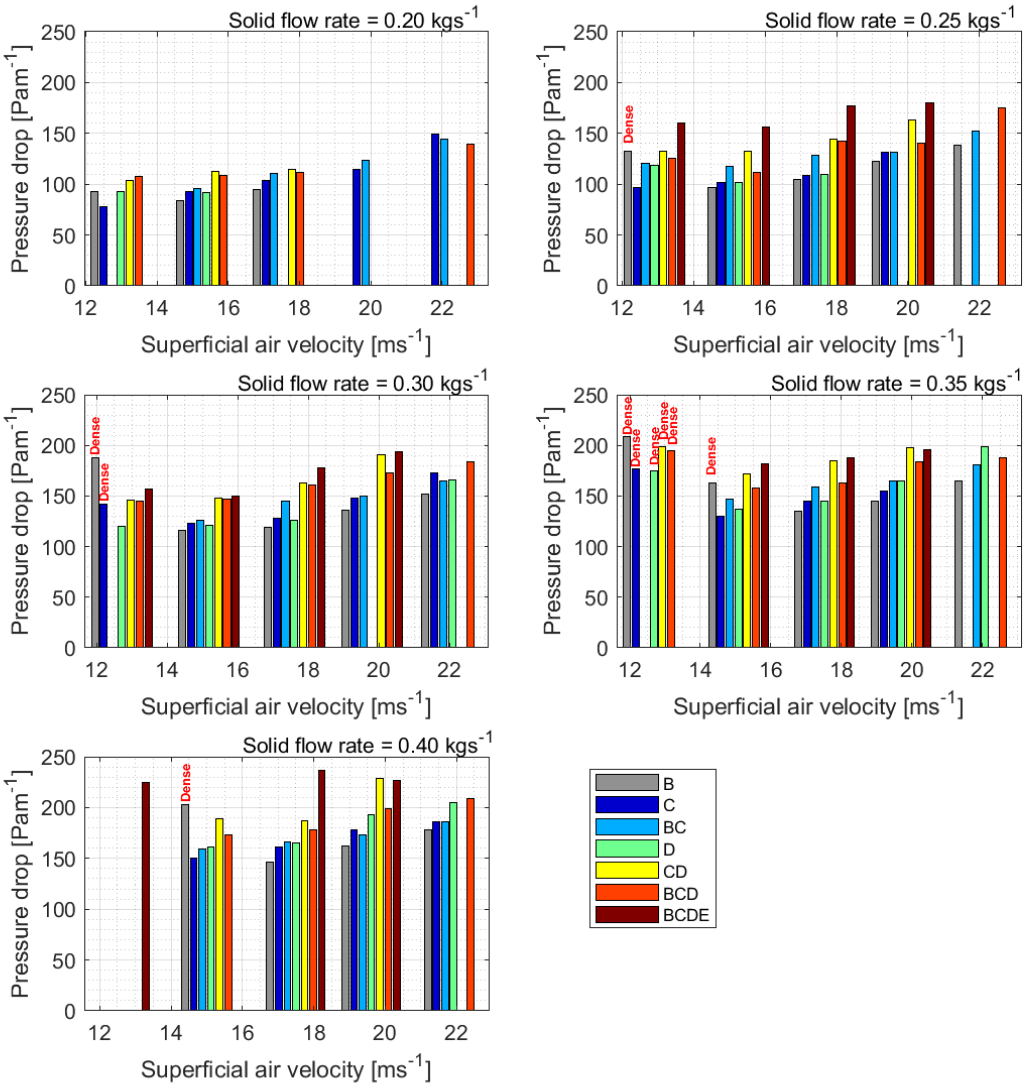

Figure 4.15: Pressure drop in the horizontal section of PT 8 - PT 9 vs. air velocity for pneumatic conveying of dry sand mixtures at different solid flow rates

the pressure drop than the particle diameter. Hence the particle diameter(d_p) is replaced by the span of the text mixtures.

The modified Equation 2.30 can be expressed as,

$$\lambda_t = x_1 \eta^{x_2} Fr^{x_3} \left(\frac{d_{span}}{D}\right)^{x_4} \left(\frac{\rho_g}{\rho_{bulk}}\right)^{x_5} \tag{4.2}$$

The coefficients (x_i) of the Equation 4.2 must be estimated based on the experimental data. The mixtures of **B,CD** and **D** were selected for the calibration of the model coefficients since those mixtures cover a wide range of particle diameter and span. The coefficients were determined by using the MATLAB function *fitlm* which is used to create linear regression models. The determined coefficients of the Equation 4.2 are tabulated in the Table 4.2.

Table 4.2: Coefficients of the Equation 4.2

Coefficient	**Value**
x_1	1.5524E+13
x_2	-0.34094
x_3	-1.1847
x_4	0.32806
x_5	4.0252

The Figure 4.16 gives the experimental vs. calculated pressure drop for the mixtures of **B,CD** and **D** for the considered section of the experimental rig. The mean absolute percentage error (MAPE) of the predicted pressure drop is 6.4% and the adjusted coefficient of determination (R^2) is 0.8.

In the Figure 4.16 it can be seen that the some data points corresponding to the mixture **B** is significantly under predicted compared to the rest of the data points. When considering the solid flow rate and the air flow rate corresponding to those experimental points it can be seen that the the model is unable to predict the pressure drop of mixture **B** at dense phase where the solid flow rate is high and the air flow rate is low. Therefore, it can be considered that the model developed for the horizontal pneumatic conveying of dry sand mixtures is suitable for the dilute phase conveying.

Based on this model, the pressure drop for the mixtures of **C,BC,BCD** and **BCDE** were predicted and the experimental vs. calculated pressure pressure drop in the horizontal section of PT 8 - PT 9 is presented in the Figure 4.17. It can be seen that the calibrated model can predict the pressure drop for the mixtures of **C,BC,BCD** and **BCDE** with an absolute mean percentage error of 8.9%. The R^2 value for the predicted pressure drop is 0.82. According to the Figure 4.17, the model slightly over predicts for the **C** mixture which has a relatively low span. A data point corresponding to the **BCD** mixture which is in dense phase conveying mode (solid flow of 0.4 kgs^{-1}, air flow rate of 13 ms^{-1}) is also under predicted. The accuracy of predicting the pressure drop corresponding to the **BCDE** which has the largest span is relatively low but is within the acceptable limits.

The results presented in the Figure 4.17 show that the calibrated model can be successfully used to estimate the pressure drop corresponding to dry mixtures with the same material but with different size distributions, with the solid flow rate in the region of 0.2 - 0.4 kgs^{-1} and with the air flow rate in the region of 13 - 22 ms^{-1}.

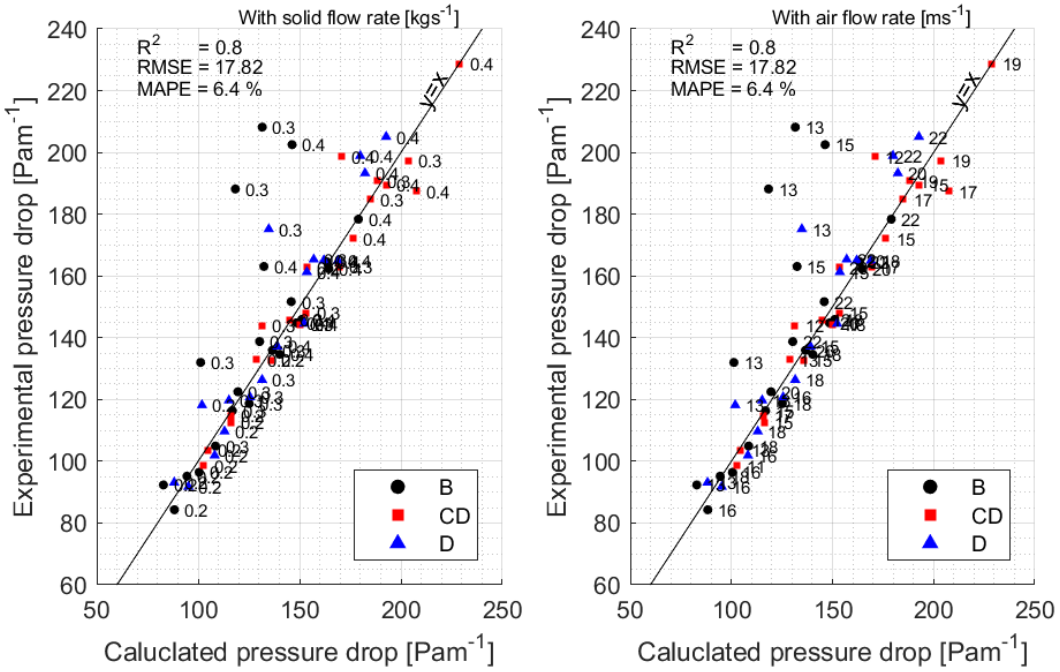

Figure 4.16: Experimental vs. calculated pressure pressure drop in the horizontal section of PT 8 - PT 9 (calibration)

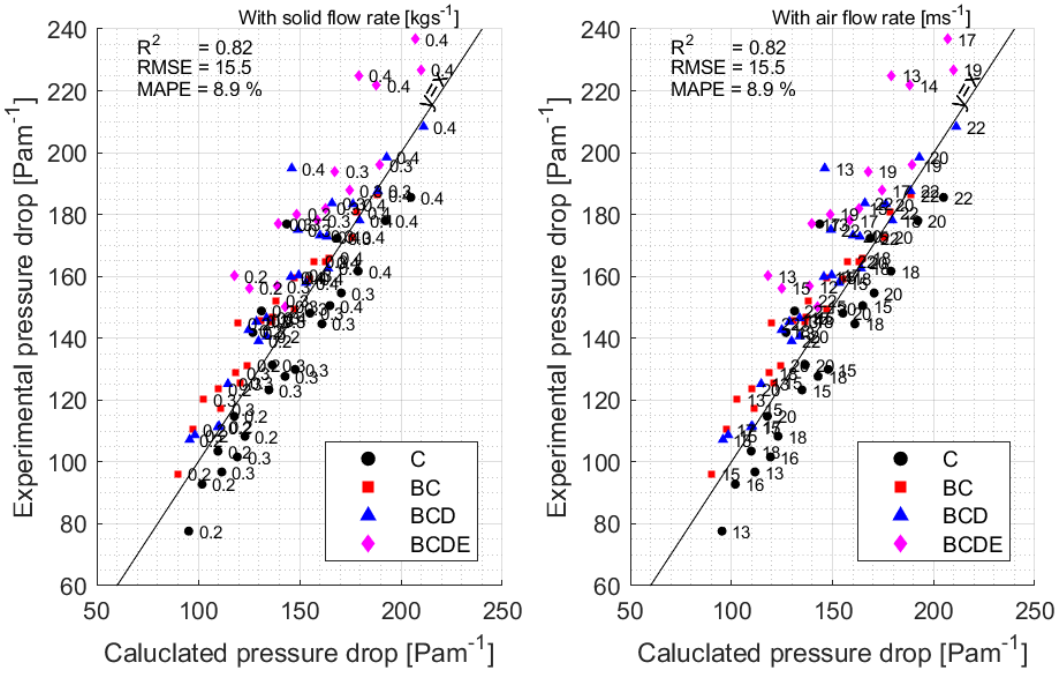

Figure 4.17: Experimental vs. calculated pressure pressure drop in the horizontal section of PT 8 - PT 9

4.2.2 Impact of drilling fluid towards the pneumatic conveying behaviour

When sand samples mixed with drilling fluid (premix) were pneumatically conveyed, they displayed a different pressure drop compared to the dry condition at a particular air and solid flow rate. The pneumatic conveying state diagrams of the sand mixture **CD** at different premix concentrations are compared in the Figure 4.18. The pneumatic conveying state diagrams corresponding to other sand mixtures are given in the Appendix G.

According to the Figure 4.18, it can be clearly seen that when a drilling fluid is mixed with the dry particles there is a considerable reduction in the pressure drop at a particular air flow rate and a solid flow rate compared to the dry conditions. However, there is no significant difference between the pressure drop at the drilling fluid concentrations of 1.5% and 6.3%. When the drilling fluid concentration is increased upto 10%, the pressure drop increases compared to the pressure drop at the drilling fluid concentration of 6.3%. A similar behaviour can be observed for the other sand mixtures for the drilling fluid concentrations of 1.5% and 6.3%. It can be also seen that the shape of the state diagrams are not affected by the presence of drilling fluid at the drilling fluid concentrations of 1.5% and 6.3% and the state diagrams suggest that the sand-drilling fluid mixtures are conveyed in the dilute phase under the considered air and solid flow rates.

The impact of the drilling fluid towards the horizontal pneumatic conveying pressure drop displays a behaviour similar to the change of minimum fluidization velocity with drilling fluid concentration. Therefore, it is interesting to compare the pressure drop ratio, minimum fluidization velocity ratio and the bulk density ratio of a particular solid-drilling fluid mixture with the same drilling fluid concentration at a particular air and solid flow rate. The pressure drop ratio, bulk density ratio and the minimum fluidization velocity (MFV) ratio are defined as follows,

$$Pressure\ drop\ ratio = \frac{Pressure\ drop\ of\ a\ sand + drilling\ fluid\ mixture}{Pressure\ drop\ of\ the\ same\ sand\ mixture\ at\ dry\ conditions} \tag{4.3}$$

$$Bulk\ density\ ratio = \frac{Bulk\ density\ of\ a\ sand + drilling\ fluid\ mixture}{Bulk\ density\ of\ the\ same\ sand\ mixture\ at\ dry\ conditions} \tag{4.4}$$

$$MFV\ \ ratio = \frac{MFV\ of\ a\ sand + drilling\ fluid\ mixture}{MFV\ of\ the\ same\ sand\ mixture\ at\ dry\ conditions} \tag{4.5}$$

The Figure 4.19 compares the variation of actual pressure drop at air flow rate of 400 Nm^3hr^{-1} at different solid flow rates and drilling fluids concentrations for the sand mixture of **CD**. The same figure compares the pressure drop ratio, minimum fluidization ratio and the bulk density ratio for the same sand-drilling fluid mixture.

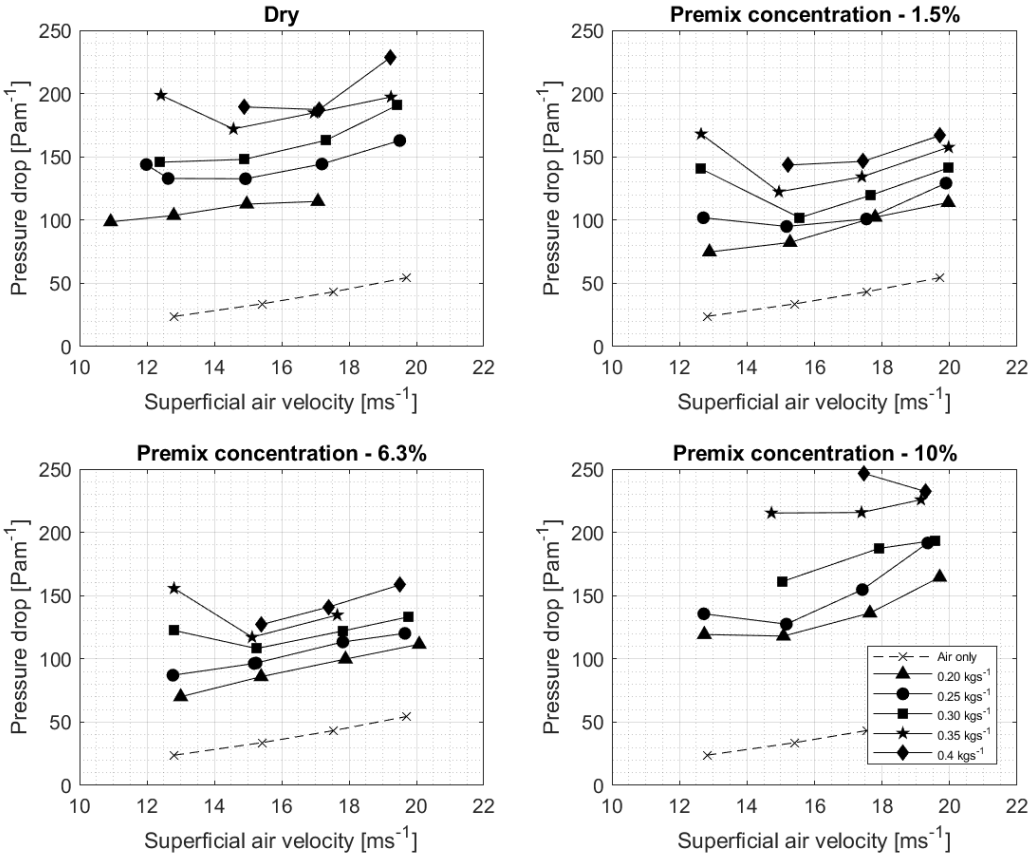

Figure 4.18: Pneumatic conveying state diagrams for **CD** for the section of PT 8 - PT -9 at different drilling fluid concentrations

The actual pressure drop for the other sand-drilling fluid mixtures at different air flow rates and solid flow rates are presented in the Figures from H.1 to H.15 (for the horizontal section of PT 8 - PT 9) in the Appendix H. The pressure drop ratio, minimum fluidization velocity ratio and the bulk density ratio of a particular solid-drilling fluid mixture at a certain air and solid flow rate are also compared in these figures.

The Figures from H.1 to H.15 show that both dry and wet samples have a higher pressure drop at higher air flow rates and at higher solid flow rates. All the considered mixtures with 1.5% of drilling fluid (premix) display a reduced pressure drop compared to the dry conditions. When thd drilling fluid concentration is increased up to 6.3%, **BCD** mixtures display a slight increasement in the pressure drop and the **BCDE** mixtures display a higher increasement in the pressure drop while the **CD** mixtures display a slightly reduced pressure drop. However, for all the sand mixtures the pressure drop at the drilling fluid concentration of 6.3% is less than the pressure drop corresponding to dry conditions. Pneumatic conveying tests for 10% of drilling fluid were conducted for the

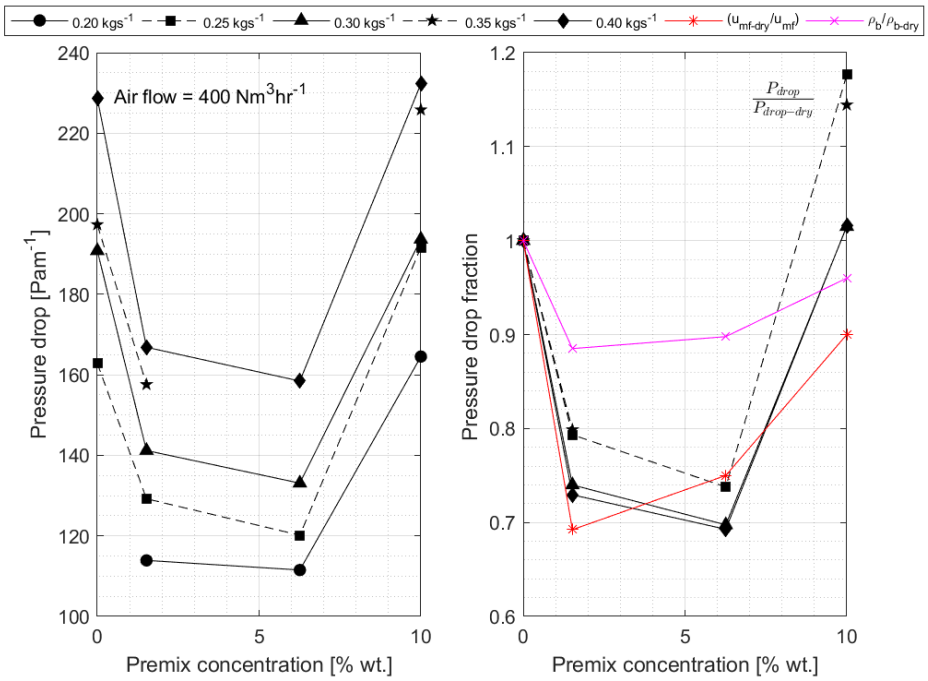

Figure 4.19: Pressure drop vs. drilling fluid concentration for the mixture **CD** at air flow of 400 Nm^3hr^{-1}

CD mixture and it displayed a significant increasement of the pressure drop compared to the pressure drop at 6.3% of drilling fluid and for most of samples with 10% drilling fluid display a pressure drop higher than the dry conditions.

Based on the Figures from H.1 to H.15 it can be observed that the pressure drop ratio of a particular sand-drilling fluid mixture at a certain drilling fluid concentration remains relatively at a constant value with changing air and solid flow rates. When comparing the pressure drop ratio with the bulk density ratio and the minimum fluidization velocity ratio it can be observed that the pressure drop ratio in the **BC** and **BCD** mixtures are closely related to the bulk density ratio except for the **BCD** mixtures at air flow rate of 250 Nm^3hr^{-1}. On the other hand the pressure drop ratio of the mixtures of **CD** and **BCDE** display a close relationship with the reciprocal of the minimum fluidization velocity ratio.

4.2.3 Correlation to predict the pneumatic conveying pressure drop of the sand-drilling fluid mixtures

Based on the results it can be seen that the deviation of the pressure drop of a particular sand-drilling fluid mixture with respect to its dry condition is closely related to either bulk density ratio or the minimum fluidization velocity ratio. The model presented by

the Equation 4.2 and the Table 4.2 can be used to estimate the pressure drop of the horizontal pneumatic conveying dry material. Therefore, it is interesting to incorporate the bulk density and the minimum fluidization velocity ratios in the model to predict the pressure drop of the pneumatic conveying of sand-drilling fluid mixtures. Initially the prediction capability of the proposed model is studied without any modification as the bulk density of the mixture is already a parameter in the Equation 4.2. The experimental vs. the calculated pressure drop value based on the model for the sand-drilling fluid mixtures are presented in the Figure 4.20.

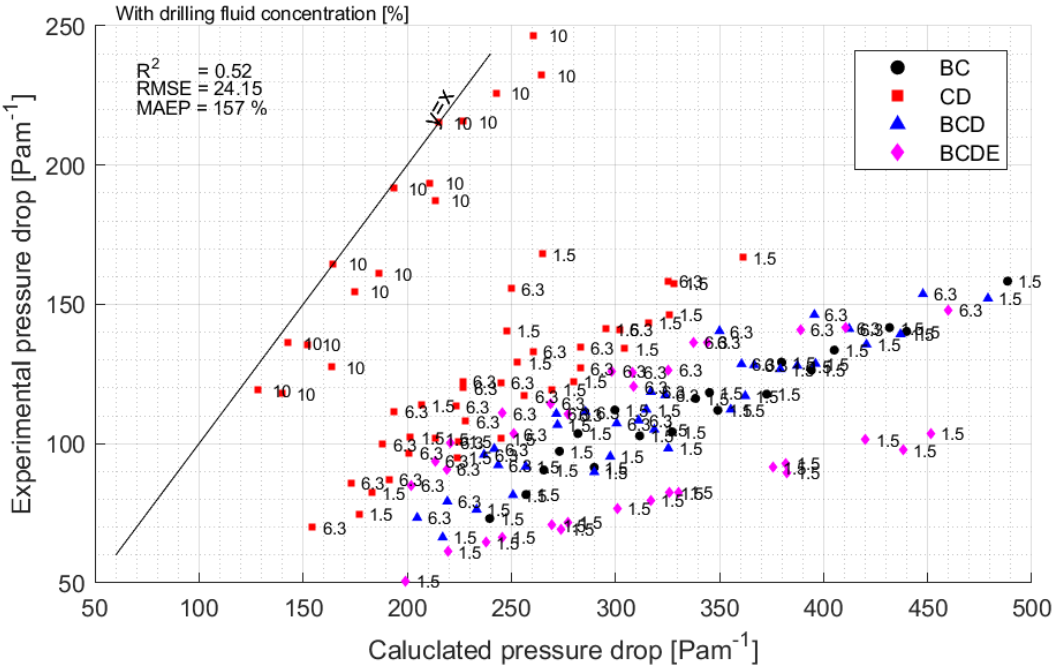

Figure 4.20: Pressure drop vs. drilling fluid concentration for the mixture **BC** at air flow of 250 Nm^3hr^{-1}

According to the Figure 4.20, it can be seen that except for the **CD** mixtures with 10% drilling fluid all the pressure drop for all the other mixtures are over predicted by the model. Since the dry mixture of **CD** was used to calibrate the model and as the **CD** with 10% drilling fluid mixtures have a pressure drop closer to dry conditions, the pressure drop for those mixtures are estimated with a good accuracy. Therefore, the bulk density term in the Equation 4.2 is not adequate to estimate the pressure drop of the mixtures with drilling fluids and the model has to be adjusted to suit the pneumatic conveying of wet mixtures. Since the pressure drop reduction of the sand-drilling fluid mixtures are closely associated with the reciprocal of the minimum fluidization velocity ratio, the model can be modified as follows,

$$\lambda_t = (1.55 \times 10^{13}) \frac{u_{mf}}{u_{mf,dry}} \eta^{-0.34} Fr^{-1.18} \left(\frac{d_{span}}{D}\right)^{0.328} \left(\frac{\rho_g}{\rho_{bulk}}\right)^{4.025} \tag{4.6}$$

The experimental vs. the calculated pressure drop based on the Equation 4.6 are presented in the Figure 4.21. The model can be further improved by raising the minimum fluidization velocity ratio by a factor which has to be estimated by calibrating with experimental data. Since there are not enough data to calibrate and validate such a model, no further modification is done to the proposed model.

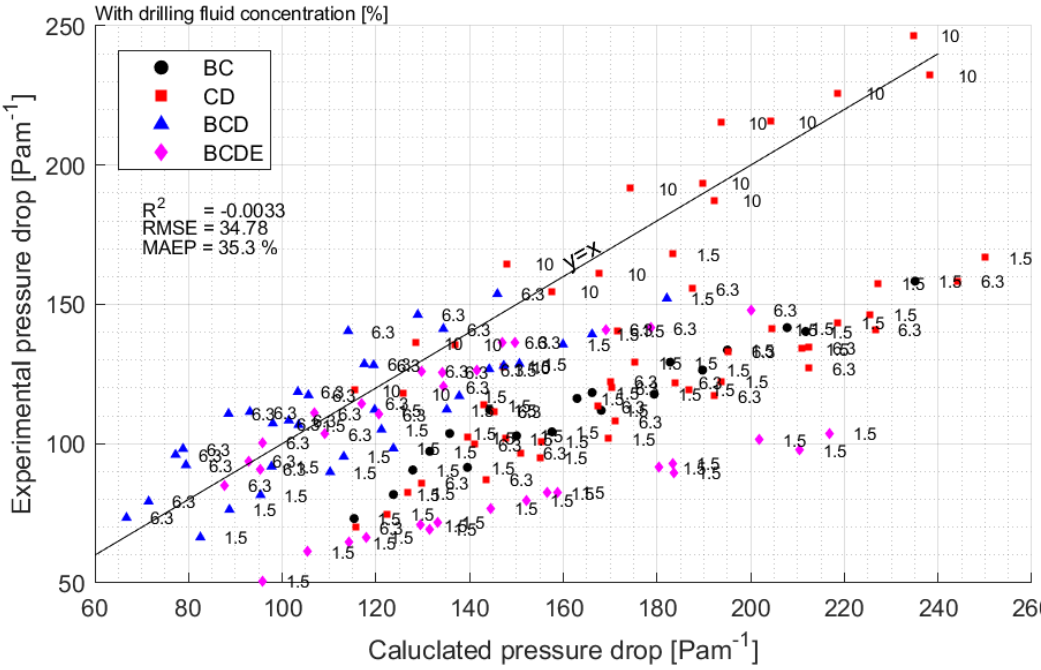

Figure 4.21: Pressure drop vs. drilling fluid concentration for the mixture **BC** at air flow of 250 Nm^3hr^{-1}

The comparison of the estimated values presented in the Figure 4.21 with the values in the Figure 4.20, it can be seen that the modified model has an improved prediction capability. The mean absolute error percentage has been reduced down to 35.3%

4.2.4 Summary

Under the considered regions of the superficial air velocities (10 - 22 ms^{-1}) and the solid flow rates (0.2 - 0.4 kgs^{-1}), dry sand mixtures were conveyed in dilute phase in the pneumatic conveying experimental rig where the pipe diameter is 8.12 cm. When a drilling fluid is mixed with the sand mixtures, the pneumatic conveying pressure drop reduces

relative to the pneumatic conveying pressure drop of the dry sand mixture. The deviation of pneumatic conveying pressure drop with the drilling fluid concentration display a similar behaviour as the deviation of the minimum fluidization velocity with the drilling fluid concentration. Therefore the change in the minimum fluidization velocity can be incorporated into a model to predict the pressure drop of pneumatic conveying of wet particles.

4.3 Discussion

Based on the fluidization and pneumatic conveying tests it can be concluded that the particles mixed with a drilling fluid exhibits a significantly deviated behaviour with respect to the dry particles. Basically the minimum fluidization velocity is increased and the pneumatic conveying pressure drop is decreased when drilling fluid is introduced to the dry particles. Since the drilling fluid has a lubricating effect, it lubricates the particle surface and the wall of the pipe. Then the friction between the air and particles and the friction between the wall and the particles reduce. As a result, in fluidization, air streams can penetrate through the bed more easily and hence higher air velocity is required to create a pressure drop equal to the weight of the bed. In pneumatic conveying, the pressure losses due to friction is reduces and as a result the pressure drop is reduced for mixtures with drilling fluid. However this phenomenon is valid only for low concentrations of drilling fluids, where the amount of drilling fluids are adequate to form a thin film of drilling fluid on the particles' surface. When the drilling fluid concentration is increased beyond a certain limit, drilling fluid tends to separate from the solids and accumulate in the voids. This was seen in the fluidization tests of 10% of drilling fluid. Under these conditions the behaviour of the sand-drilling fluid mixtures deviate from the low concentration mixtures. Since the voids are filled with drilling fluid, air cannot penetrate through the bed and as a result the minimum fluidization velocity will be reduced. At the same time as the mixture starts to behave more like a slurry, pneumatic conveying cause higher pressure drop.

According to Mills [55] wet or damped material can be conveyed pneumatically but the challenge is to feed them to the pipelines and to discharge from the hopper. If the material contains fine particles, wetness can be a challenge in pneumatically conveying systems as they tend to coat the pipeline and finally causing blockages. If the material is not so wet, hot air flow can be used to overcome the issue of wetness. Otherwise single plug blow tank systems have to be adopted in handling wet material. However, Hollier and Reddoch [56] claim that they have implemented a vacuum conveying system to convey the wet drill cuttings successfully.

When considering the drill cuttings, particle size distribution is a important parameter as it tends to differ from one location to another in the drilling well. The study shows that

conducting few pneumatic conveying tests of a dry sample with samples with same physical properties but with different particle size distributions, a reasonably good model can be developed to predict the pressure drop of horizontal pneumatic conveying under dilute phase for the mixtures with different particle size distributions. It was also observed that the pressured drop reduction in the pneumatic conveying and the minimum fluidization velocity reduction in the fluidization tests can be also correlated. Therefore, this study shows that a combination of pneumatic conveying of dry particles and the fluidization of particles mixed with drilling fluid can be used to develop a model to estimate the pressure drop in pneumatic conveying of particles mixed with drilling fluids.

5 Flow properties of sand - drilling fluid mixtures

In this chapter the flow properties of the sand - drilling fluid mixtures are analysed with varing drilling drilling fluid concentrations. According to the Section 3.4 , the shear tests were conducted for the **CD** sand mixture. The sand - fluid samples were prepared with premix, base oil, water and a soap mixture with concentrations of 10%, 20%, 30% and 40% (by volume). The analysis is conducted for both axial symmetric and plane symmetric silos and the basic geometrical shape of those two silos are given in the Figure 5.1.

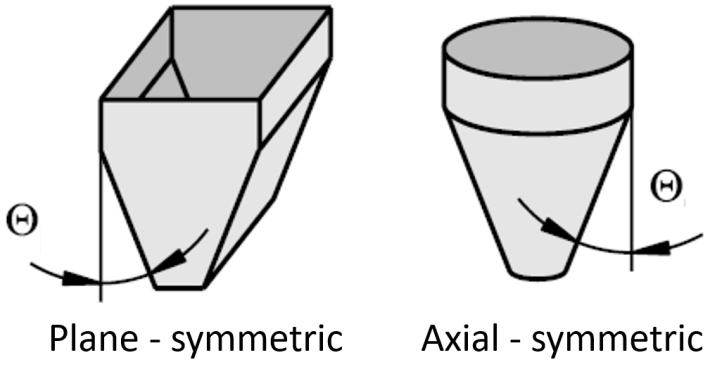

Figure 5.1: Plane and axial symmetric silos [49]

5.1 Wall friction and the hopper angle

The friction between the bulk solid and the hopper wall is represented by the wall friction angle. The wall friction angle between the experimental sand - fluid samples and the hopper wall are presented in the Figure 5.2 . The considered wall material is stainless steel.

Except for water, the other mixtures does not display a significant deviation from the dry conditions at low fluid concentrations (10% vol.). The wall friction angle of the premix

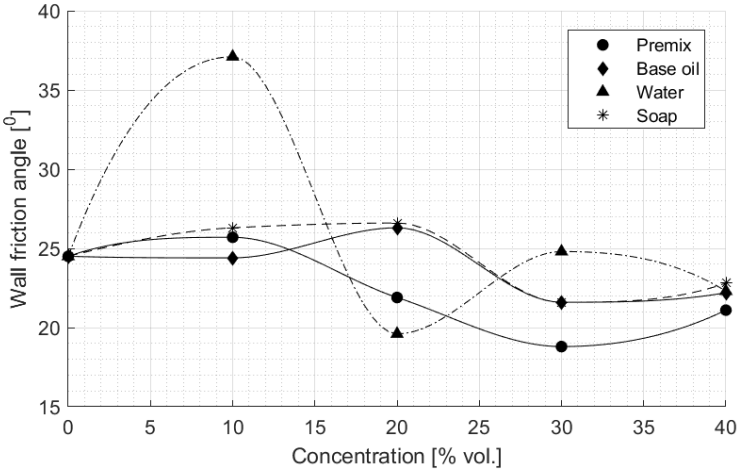

Figure 5.2: Wall friction angle vs. fluid concentration

samples reduces with increasing fluid concentration and reaches a minim at 30% of fluid. The wall friction angles of the base oil and soap mixtures start to reduce at 20% of fluid levels and reach a minimum at the concentration of 30% of fluid. Beyond 30% of fluid, the mixtures of premix, base oil and soap tend to have a increasing wall friction angle until a fluid concentration of 40%. The Figure 5.2 clearly shows that the behaviour of the sand-water mixtures are significantly different from the rest of the mixtures at low concentrations. The mixture with 10% of water has the highest wall friction angle and with increasing water concentration, the wall friction angle reduces dramatically and reaches a minimum at 20% of water. Beyond that the sand-water mixtures have a similar behaviour as rest of the mixtures.

The wall friction angle directly affects the hopper angle. The hopper angle of the considered mixtures are given for both axial and plane symmetric hoppers in the Figure 5.3.

The Figure 5.3 shows that the hopper angles of both silo types are inversely proportional to the wall friction angle. A large wall friction angle indicates a higher friction between the bulk solid and the hopper wall. Therefore, the flowability of the bulk solid decreases with increasing wall friction angle. A bulk solid with a high wall friction angle which indicates a low flowability requires a small hopper angle to ensure to have a massflow silo. Hence the sand mixtures of premix, base oil and soap have the highest flowability at 30% of fluid with the minimum wall friction angle and highest hopper angle. According to the the Figure 5.3 it can be seen that the hopper angle vs. fluid concentration profiles of the two silo types have the same shape but the hopper angle of a plane symmetric silo is larger than the hopper angle of an axial symmetric silo at a particular fluid concentration.

Based on the Figures of 5.2 and 5.3, it can be seen that at 10% fluid concentration, the sand-premix mixture has a slightly better flowability compared to the sand-base oil

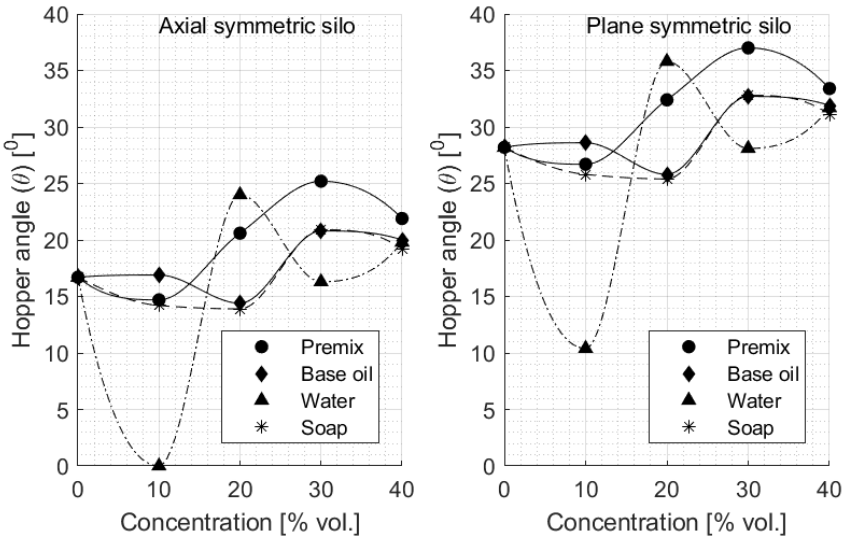

Figure 5.3: Hopper angle vs. fluid concentration

mixture. However, beyond the fluid concentration of 20% the sand-base oil mixtures have a better flowability compared to the sand-premix mixtures. It is also interesting observe that the behaviour of the sand-soap mixture is similar to the sand-base oil mixtures beyond the fluid concentration of 20%.

5.2 Effective angle of internal friction (δ)

The effective angle of internal friction (δ) which is described under the Figure 2.5 in the Section 2.3.1 is plotted for the considered mixtures in the Figure 5.4.

As described in the Section 2.3.1, the effective angle of internal friction represents the resistance to the flow when the bulk solid is in flowing conditions. The angle increases with decreasing flowability of the material. There is no significant difference between the internal friction angle of the base oil and soap mixtures at 10% of fluid when compared to the dry conditions. Both base oil and soap mixtures display a gradual increase of effective angle of internal friction until the 20% of fluid and start to decrease with further increasing fluid concentration and reach a minim angle at 30% of fluid. Similar to the wall friction and hopper angle plots, base oil and soap mixtures have a similar profile of effective angle of internal friction vs. fluid concentration. The sand-premix mixture display a significant reduction of the internal friction angle at 10% of fluid, with respect to the dry conditions and beyond that the effective angle of internal friction is decreasing with increasing drilling fluid concentration. The sand-water mixtures have the highest angle of internal friction at 10% of water and the minimum angle at 20% of water. With

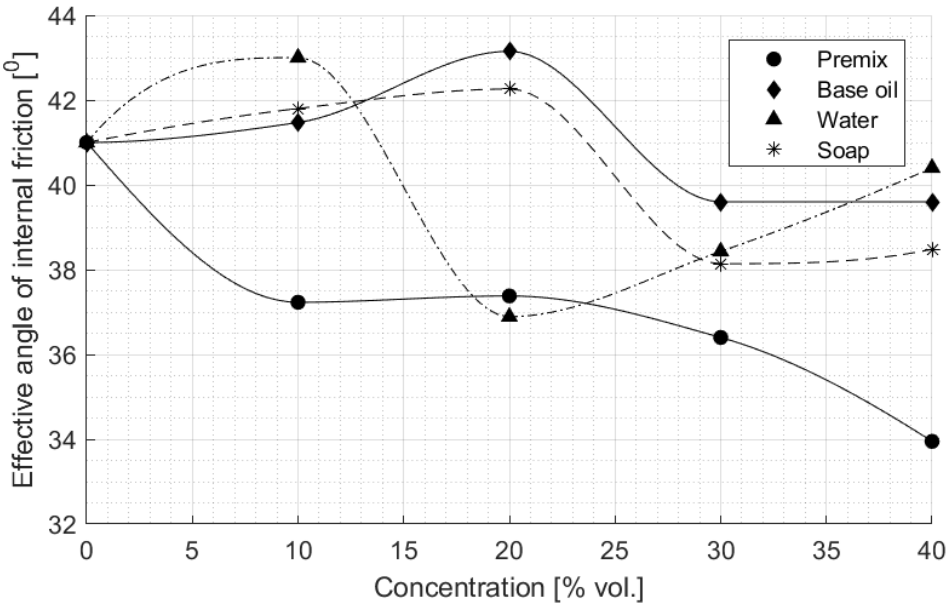

Figure 5.4: Effective angle of internal friction vs. fluid concentration

further increment of water concentration, the effective angle of internal friction tends to increase gradually.

5.3 Flow function and the flowability

The flow function (FF) which gives the relationship between the unconfined yield strength (f_c) and the major consolidation stress (σ_1) for the considered sand-fluid mixtures are given in the Figure 5.5.

Schulze[49] describe a numerical method to represent the flowability of a bulk solid mixture and it is given by,

$$flowability\ (ff_c) = \frac{\sigma_1}{f_c} \tag{5.1}$$

The lines of constant flowability are also plotted in the Figure 5.5. These constant flowability lines can be used to describe the boundaries of different flowing conditions [49].

- $ff_c < 1$: not flowing
- $1 < ff_c < 2$: very cohesive
- $2 < ff_c < 4$: cohesive

- $4 < ff_c < 10$: easy-flowing
- $10 < ff_c$: free-flowing

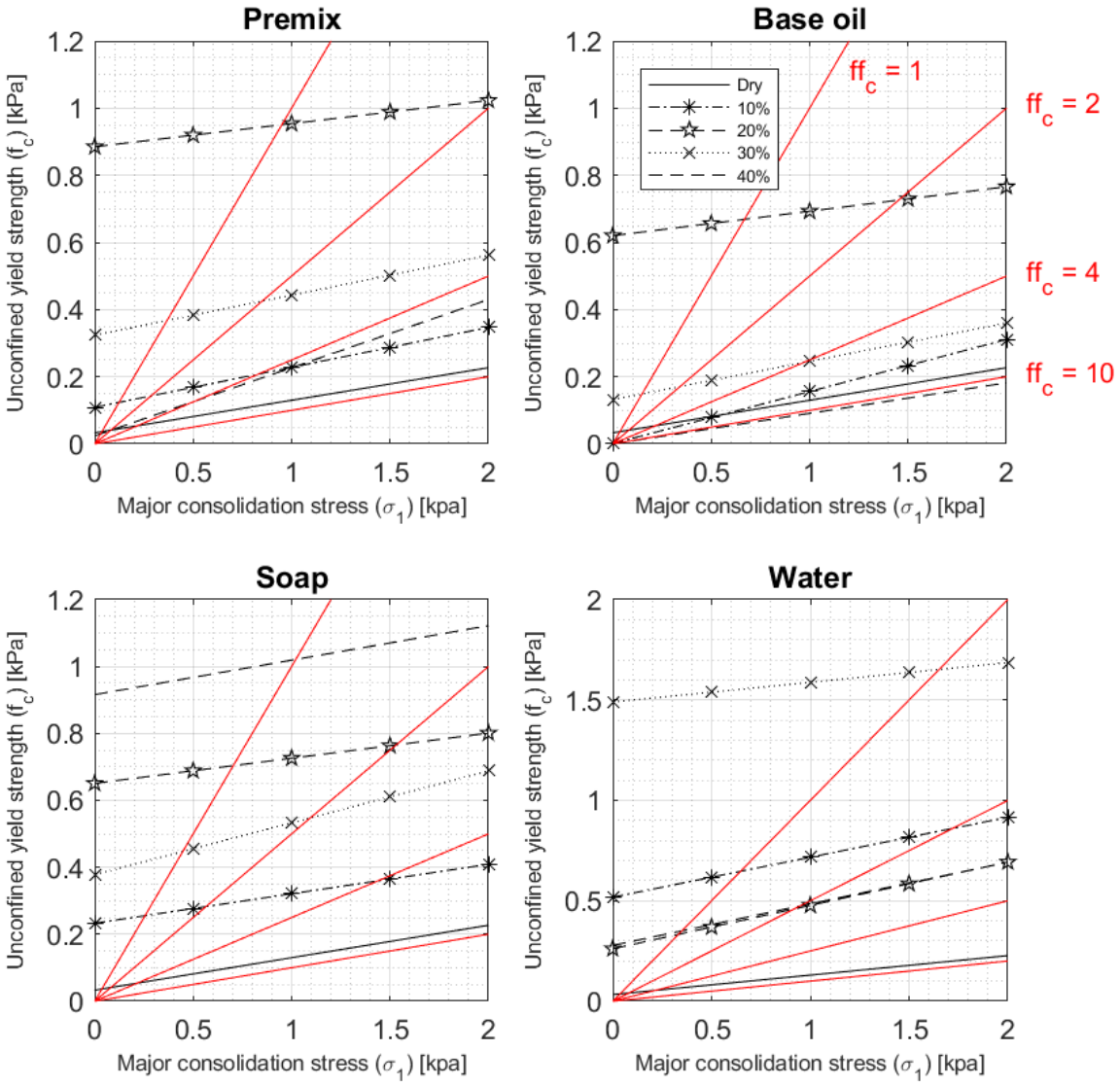

Figure 5.5: Instantaneous flow function vs. fluid concentration

According to this plot, the dry sand sample is a free flowing material as its flow function lies parallel to the $ff_c = 10$ line. All the sand-fluid mixtures except for the sand -base oil mixture at 40%, have a higher unconfined yield strength than the dry sample at a given major consolidation stress. The premix and the base oil mixtures with 10% of liquid display a slight reduction in the flow function with respect to the dry conditions.

The flow functions of the both drilling fluid mixtures significantly increase when the liquid concentration is increased up to 20%. However, the flow function of the mixtures decrease as the unconfined yield strength corresponding to 30% of fluid is reduced compared to the 20% of fluid. At 40% of concentrations both mixtures further decrease their flow functions. The plots also show that at a given fluid concentration, the sand-premix mixtures have a higher unconfined yield strength. The sand-soap mixture display a similar behaviour until the fluid concentration of 30%. Both the drilling fluid mixtures of 20% concentration lies in the no-flow/very cohesive flow region. The 10% and the 40% mixtures of both drill fluids lies in the region of easy-flowing region. The sand-premix mixture at 30% concentrations mainly display cohesive behaviour while the 30% of the base oil mixture display an easy-flowing/cohesive behaviour.

The flow function of the sand-soap mixture at 40% of fluid is significantly increased and when conducting the tests it was observed that some foam was formed at higher soap concentrations. The sand-water mixtures behave rather differently when compared to the other mixtures. It shows a high flow function at 10% of water and at 20% of water the flow function reduces. The experimental results show that sand-water mixtures have the highest flow function at 30% of water. The 30% of water mixture is basically in a no flow condition while the 10% mixture displays a high cohesive features.

5.4 Size of the hopper opening

Based on the results obtained from the Jenike shear test, the size of the hopper opening was calculated by using the silo designing software at SINTEF-Tel-Tek. The calculated hopper opening dimensions for both axial symmetric and plane symmetric hoppers are given in the Figure 5.6.

For both premix and base oil mixtures, the highest opening size is required at 20% of liquid concentration. The reason for this is that the both drilling fluid mixtures display the lowest flowability at the concentration of 20%. Similarly sand-water mixture which has the lowest flowability at 30% of water, requires the largest opening at 30% of water. Some mixtures such as 10% of base oil display a minimum opening of 0 cm which implies that at any opening size, a massflow discharge pattern can be obtained. However, as a rule of thumb the diameter of the opening should be 10 times the diameter of the largest particle in the bulk solid. Since the mixture **CD**'s largest particle size is 2.5 mm, the minimum required diameter of the opening is 2.5 cm. Therefore, if the calculation results a diameter less than 2.5 cm, the required hopper opening dimension should be taken as 2.5 cm.

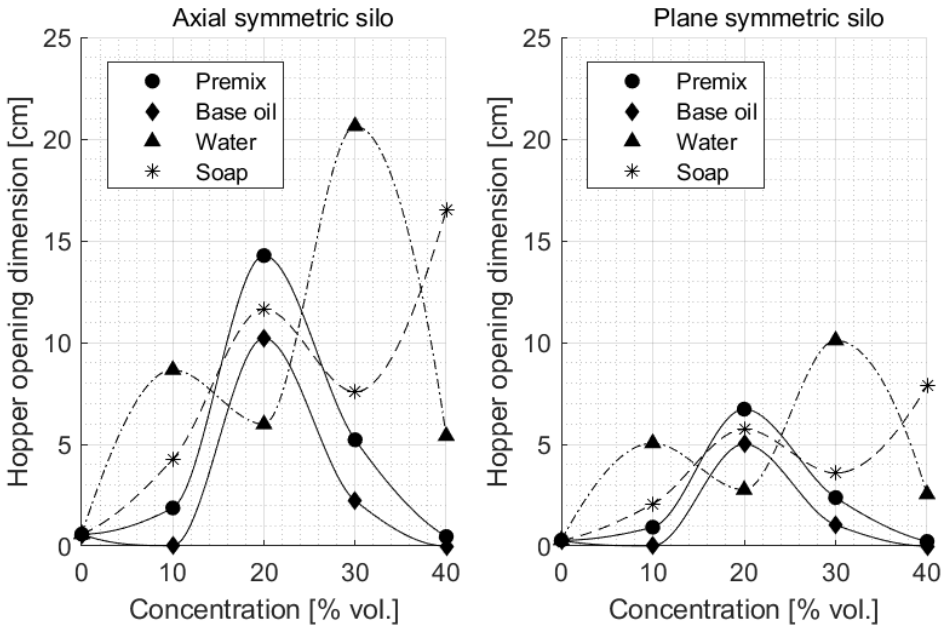

Figure 5.6: Hopper opening dimension [cm] vs. fluid concentration

5.5 Time consolidation

The flow functions obtained from the 7 days time consolidation tests are given in the Figure 5.7.

When compared to the Figure 5.5, which illustrate the instantaneous flow functions, it can be clearly seen that the flowability of all the mixtures have been reduced after 7 days of consolidation. No mixture lies in the regions of free flowing or easy-flowing. Almost all the mixtures display either no-flow or very cohesive flow features. For the sand-premix mixtures the lowest flowability is displayed at 20% of fluid while the sand-base oil and sand-water mixtures display the lowest flowability at 30% of liquid.

The hopper opening size of the considered samples after 7 days consolidation is given in the Figure 5.8.

It can be clearly seen that the required minimum opening size of the hopper after 7 days of consolidation has been increased compared to the required opening at instantaneous conditions. The sand-premix mixture requires the largest opening size at 20% of fluid concentration while the sand-base oil and sand -water mixtures require the highest opening size at 30% of fluid concentration. The sand-soap mixture displays significantly large opening size at 40% of fluid level but it displays a similar behaviour as sand-base oil mixtures in the region of fluid levels of 10% - 30%

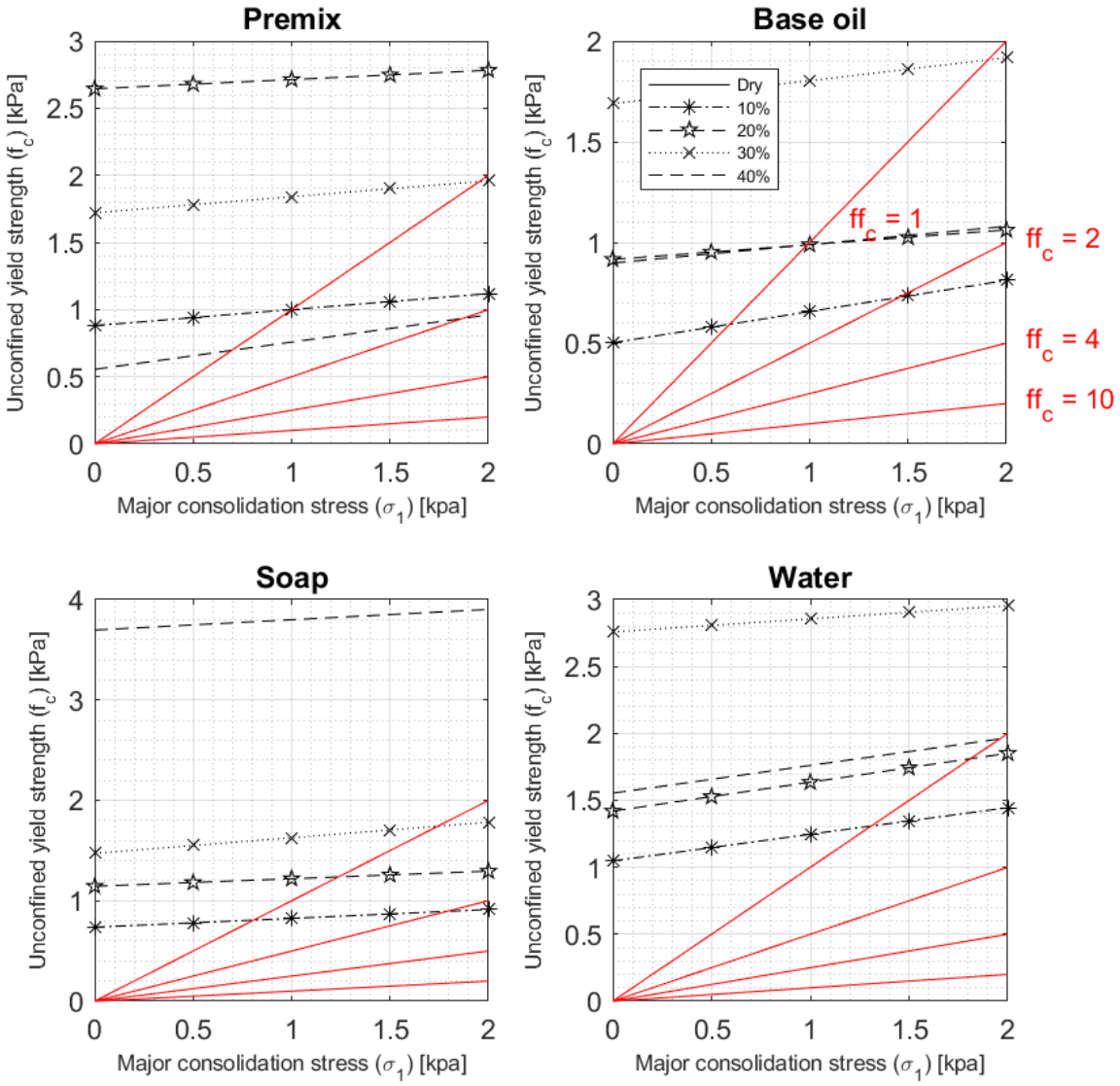

Figure 5.7: Instantaneous flow function vs. fluid concentration

5.6 Discussion

This study basically concerns about the impact of the drilling fluid towards the storage and the flowability of a bulk solid material. Based on the results, it can be clearly seen that the flowability of the considered sand mixture of **CD** is reduced with respect to its dry state when it is mixed with a liquid. The main reason for this phenomenon is the increase of inter-particle forces within the bulk solid due to the formation of liquid

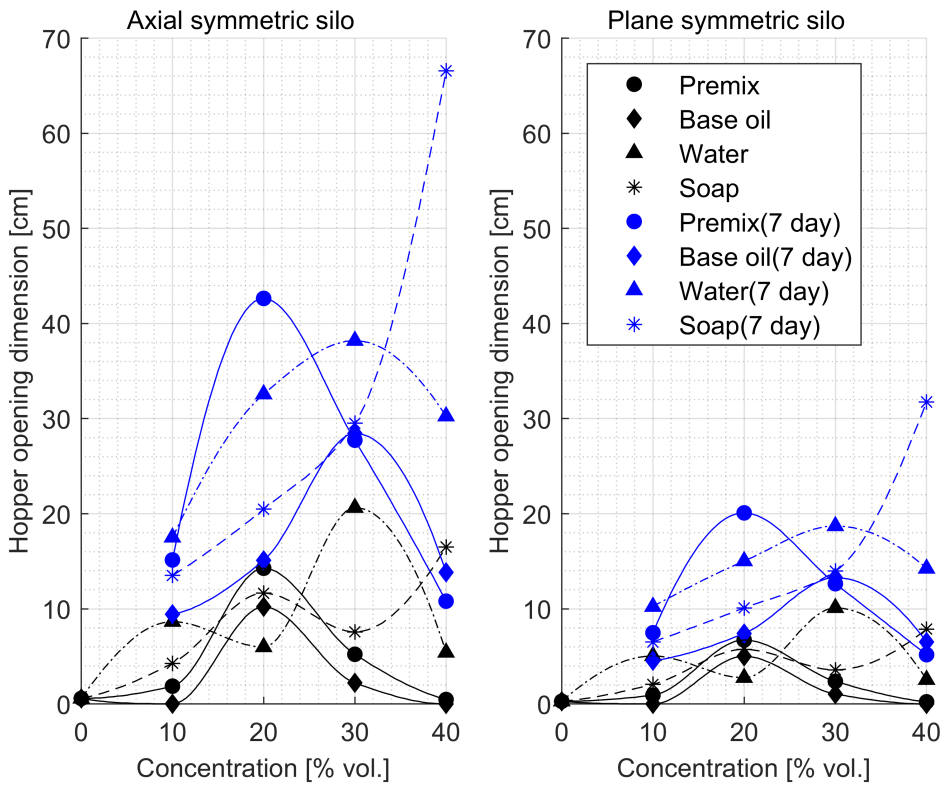

Figure 5.8: Hopper opening dimension [cm] (time consolidation) vs. fluid concentration

bridges. It is also observed that the level of flowability depends on the type of the fluid , fluid concentration and the time period which the bulk solid has been subjected to a consolidation stress.

Fluid concentration

The flowability of the sand-fluid mixtures are basically studied based on their flow functions. Under the instantaneous conditions the flowability is associated with the effective angle of internal friction. The lowest flowability is obtained at the fluid concentration where the effective angle of internal friction is the highest.

Both premix and base oil mixtures have the lowest flowability at 20% of fluid concentration at instantaneous conditions. After 7 days of consolidation, the sand-premix mixture has the lowest flowability at 20% of fluid and the sand-base oil mixture has the lowest flowability at 30% of fluid. The sand-soap mixture also has the lowest flowability at 40% fluid content under both instantaneous and 7 days time consolidation conditions. Since some foam was started to be formed beyond the soap concentration of 30%, the flowability at 40% of soap cannot be compared with the other mixtures. If the sand-soap mixture at 40% fluid content is considered as an outlier, the sand-soap mixtures have

the lowest flowability at 20% and 30% fluid concentrations under instantaneous and 7 days time consolidation conditions respectively. Contrary to these mixtures, sand-water mixtures display the largest effective angle of internal friction at 10% of water. When considering the flowability, the lowest flowability occurs at 30% of water but contrast to the other mixtures, sand-water mixture at 10% fluid content has a lower flowability than the sand-water mixture at 20% of water.

The fluctuation of the flowability with the fluid concentration can be described by the formation of liquid bridges. When a fluid is introduced in to a bulk solid, liquid bridges start to form and the inter-particle forces increase. With increasing fluid concentration, number of individual liquid bridges increase and the forces between the particles increase. As a result the flowability of the solid-liquid mixture is reduced. When the voidages starts to be filled with the fluid, the individual liquid bridges are diminished and a slurry is formed gradually. Beyond the liquid level where the individual liquid bridges start to diminish, the quantity of the inter-particle forces reduce. Therefore, the flowability will be increased beyond that fluid concentration.

Type of fluid

When comparing the sand-premix and sand-base oil mixtures, the sand-premix mixtures have a low flowability but the profile of the flow parameters with fluid concentration is similar under instantaneous conditions. The purpose of conducting tests with soap and water was to study the possibility of replacing the drilling fluid with a non-hazardous, easily available fluid to conduct laboratory test. It can be seen that sand-water mixtures significantly deviate from the sand-drilling fluid mixtures. The sand-water mixtures display a very low flowability when compared to the drilling fluid mixtures. This phenomenon justifies the reason for not adding sea water to drill cuttings when it get stuck in the screw conveyors. However in the fluid concentration level of 10% - 30%, the soap mixture display a similar behaviour as the sand - base oil mixture.

The flowability of the sand-water mixtures are significantly low compared to the other mixtures. The reason for that is water tends to form liquid bridges more easily. In a soap mixture, the surface tension is reduced and as a result there is a lubrication effect. This lubrication effect reduces the inter-particle friction forces. Therefore, drilling fluid and soap mixtures have a better flowability compared to the sand-water mixtures.

Time consolidation

The study shows that the time consolidation has reduced the flowability of the all the mixtures significantly. The mixtures having a easy-flowing or cohesive flowing under instantaneous conditions are transformed into cohesive or very cohesive flow after being subjected to time consolidation With time the inter-particle forces increase and as a result of that the flowability reduces. Therefore, the designing should be based on the results of time consolidation tests.

Wall friction angle

Even though the addition of drilling fluid has reduced the flowability of the sand mixture, the friction between the bulk solid and the silo wall has been reduced due to the presence of drilling fluid. The sand-drilling fluid mixtures display the lowest wall friction angle at 30% of fluid and under that condition the required hopper angle will be maximum. The reduction of the wall friction occurs due to lubrication effect of the fluids. A fluid layer formed on the wall of the silo reduces the friction forces between the bulk solid and the hopper wall. It can be also seen that the wall friction is significantly increased at 10% of water concentration. This increase of wall friction occurs due to the formation of liquid bridges but with increasing water content the individual liquid bridges diminish and the wall-particle forces reduce.

Size of the hopper opening

The required minimum opening size of the silos becomes larger as the flowability reduces. Therefore, both sand-drilling fluid mixtures have the largest opening size at the lowest flowability conditions. The study also shows that the time consolidation has reduced the flowability of the sand-drilling fluid mixtures significantly. Therefore, the designing should be based on the results of time consolidation tests.

Practical applications

When considering the practical applications it can be concluded that it will not be feasible to store sand-drilling fluid mixtures with fluid concentrations of 10%-30% (vol.). It is either better to have sand-drilling fluid mixtures with fluid concentration less than 10% or higher than 40%. The sand-drilling fluid mixtures with 40% of fluid display better flowability due to its slurry like nature and it will be difficult to be conveyed even though it can be discharged from the silo easily. Eventhough the mass flow design can over come the forming of arches and rat holing, the capacity of the silo is reduced due to the high angle conical bottom. Therefore, the potential of using silos with higher capacities (which are not mass flow silos) has to be considered as the space available for storage of drill cuttings in a drilling platform is a critical factor. These alternative silo designs should be assisted by mechanical systems such as internal agitators or screw type augers. It should be noted that such silos are more complex in design, expensive and have a potential for mechanical failure. A novel design with multiple outlets knwon as the 'Honey comb base tank' has been developed by Halliburton. In this design, compressed air is applied to the top of the silo to push the drill cuttings and another air stream is injected to the base of the tank to mechanically breakup and fluidize the cuttings. Therefore, no additional mechanical agitation system is required [57].

6 Conclusion

As discussed in Chapter 1, the objective of this research was to study the influence of drilling fluids towards the pneumatic conveying and storage of wet particles to illustrate offshore drill cutting handling. The basic findings of the study can be presented under fluidization and pneumatic conveying of wet particles and the storage of wet particles.

6.1 Fluidization and pneumatic conveying of wet particles

Based on the experiments, it can be concluded that the presence of drilling fluid has a significant impact towards the fluidization and pneumatic conveying behaviour of the considered sand mixtures. When a small amount of drilling fluid (about 1.5% by weight) is mixed with a sand mixture, both the minimum fluidization velocity and the pressure drop in pneumatic conveying is reduced when compared to the fluidization and pneumatic conveying behaviour of the dry mixtures. The reduction of the minimum fluidization velocity and the pneumatic conveying pressure drop suggest that the presence of drilling fluid in a sand mixture acts as a lubricating agent. As a thin layer of drilling fluid is formed on the surface of the particles, the air-particle, particle-particle and particle-wall frictions are reduced. However, it was also observed that the gradual increment of the drilling fluid concentration does not affect the change of either the minimum fluidization velocity or the pneumatic conveying pressure drop until reaching a certain drilling fluid concentration (approximately 6-10 % by weight). Beyond that concentration limit the drilling fluid tends to get separated from the sand mixtures.

The study shows that an empirical model can be developed to predict the pressure drop in horizontal pneumatic conveying under dilute phase for dry particles. It is also observed that the change of the minimum fluidization velocity, change of the bulk density and the change of the pneumatic conveying pressure drop due to the presence of drilling fluid are closely correlated. Hence by incorporating the change of minimum fluidization velocity factor to the pneumatic conveying pressure drop model, the pressure drop of the sand - drilling fluid mixtures could be predicted approximately. Therefore, it can be concluded that by conducting pneumatic conveying tests for dry mixtures and fluidization tests for particle - drilling fluid mixtures, a model can be developed to predict the pneumatic conveying pressure drop of the particle - drilling fluid mixtures.

6.2 Storage of wet particles

The study also shows that by conducting a proper bulk solid shear tests, both the impact of the drilling fluid towards the flow properties of the sand - mixtures and the design parameter for the storage silos can be estimated. It was observed that the presence of drilling fluid reduced the flowability of the bulk mixtures compared to the dry conditions. However, with increasing drilling fluid concentration flowability improves as the drilling fluid tends to lubricate the flow. The flowability depends on the fluid concentration, type of the fluid and the amount of time consolidation.

The Jenike shear test clearly shows that the consolidation for 7 days significantly reduces the flowability of the bulk solid compared to the instantaneous conditions. Therefore, when designing storage tanks the time period which the solids are to be stored in plays a vital role. The study also shows that, presence of water reduces flowability compared to the presence of drilling fluid. This shows the importance of not to add water to the drill cuttings during offshore handling. The use of soap mixture display a relatively similar behaviour as the drilling fluids which suggests that it is possible to use a soap mixture which is a non-hazardous solution to replicate drilling fluids in lab scale shear tests.

6.3 Recommendations

- This research study basically studies the impact of the drilling fluid concentration towards the pneumatic conveying and storage of particles relative to its dry conditions. The study can be further extended by conducting experiments with different drilling fluid types and different solid materials. It would be interesting to conduct pneumatic conveying tests for different drill cuttings samples. These test can be used to develop a more comprehensive model based on the findings of this study.
- It is also recommended to utilize the experimental data obtained from fluidization and pneumatic conveying tests in CFD simulations to predict the pressure drop and flow behaviour.
- It would be interesting to study the impact of the type and the amount of drilling fluids towards the interparticle forces.
- Process analytical technologies are recommended to be utilized for the online measurements of the particle size and the drilling fluid concentrations.

Bibliography

[1] U. S. E. I. Administration, Ed. (2016). Offshore production nearly 30% of global crude oil output in 2015, [Online]. Available: `https://www.eia.gov/todayinenergy/detail.php?id=28492`.

[2] J. Neff, "Fate and effects of water based drilling muds and cuttings in cold water environments", Houston (TX): Report to Shell Exploration and Production Company, 2010.

[3] M. Holmager, *Offshorebook: An Introduction to the Offshore Industry*. Offshore Center Danmark, 2010.

[4] IOGP, "Drilling waste management technology review, iogp report 557", International Association of Gas & Oil Producers, 2016.

[5] Norskolje&gass, "Environmental report 2016 - environmental work by the oil and gas industry facts and dvelopment trends", The Norwegian Oil and Gaas Association, 2017.

[6] J. Hartley, R. Trueman, S. Anderson, J. Neff, P. Dando and K. Fucik, "Drill cuttings initiative, food chain effects literature review", United Kingdom Offshore Operators Association (UKOOA), 2003.

[7] R. Caenn, H. Darley and G. R. Gray, "Drilling and drilling fluids waste management", in *Composition and Properties of Drilling and Completion Fluids (Sixth Edition)*. 2011.

[8] T. Svensen and K. Taugbol, "Drilling waste handling in challenging offshore operations", in *SPE Arctic and Extreme Environments Conference and Exhibition*, Society of Petroleum Engineers, 2011.

[9] F. J. Santarelli, F. Sanfilippo, R. W. James, H. H. Nielsen, M. Fidan, G. T. Aamodt *et al.*, "Injection in shale: Review of 15 years experience on the norwegian continental shelf (ncs) and implications for the stimulation of unconventional reservoirs", in *SPE Annual Technical Conference and Exhibition*, Society of Petroleum Engineers, 2014.

[10] A. Saasen, K. Jodestol and E. Furuholt, "CO_2 and NO_x emissions from cuttings handling operations", in *SPE Bergen One Day Seminar*, Society of Petroleum Engineers, 2014.

[11] S. Onwukwe and M. Nwakaudu, "Drilling wastes generation and management approach", *International Journal of Environmental Science and Development*, vol. 3, no. 3, p. 252, 2012.

[12] M. Mkpaoro, G. Okpokwasili, O. Joel *et al.*, "A review of drill-cuttings treatment and disposal methods in nigeria-the gaps and way forward", in *SPE Nigeria Annual International Conference and Exhibition*, Society of Petroleum Engineers, 2015.

[13] A. S. Ball, R. J. Stewart and K. Schliephake, "A review of the current options for the treatment and safe disposal of drill cuttings", *Waste Management & Research*, vol. 30, no. 5, pp. 457–473, 2012.

[14] D. Schonacher, J. Rojas, J. Gharst and B. Paiuk, "Meeting zero discharge requirements in the gulf of mexico using a unique cuttings transport system", in *SPE/EPA/DOE Exploration and Production Environmental Conference*, Society of Petroleum Engineers, 2003.

[15] A. Alba Rodriguez, F. E. Fragachan, A. Ovalle and T. A. Shokanov, "Environmentally safe waste disposal: The integration of cutting collection, transportation and re-injection", in *International Oil Conference and Exhibition in Mexico*, Society of Petroleum Engineers, 2007.

[16] D. Kunii and O. Levenspiel, *Fluidization engineering*. Elsevier, 2013.

[17] J. Richardson, J. Harker and J. Backhurst, "Fluidization", in *Coulson & Richardson's Chemical Engineering Vol 2*. Elsevier, 2008, ch. 6.

[18] D. Gidaspow, *Multiphase flow and fluidization: continuum and kinetic theory descriptions*. Academic press, 1994.

[19] C. Wen and Y. Yu, "A generalized method for predicting the minimum fluidization velocity", *AIChE Journal*, vol. 12, no. 3, pp. 610–612, 1966.

[20] J. Richardson, "Incipient fluidization and particulate systems", *Fluidization*, vol. 2, 1971.

[21] S. Saxena and G. Vogel, "The measurement of incipient fluidization velocities in a bed of coarse dolomite at temperature and pressure", *Trans. Inst. Chem. Eng*, vol. 55, no. 3, pp. 184–189, 1977.

[22] S. Babu, B. Shah and A. Talwalkar, "Fluidization correlations for coal gasification materials-minimum fluidization velocity and fluidized bed expansion ratio", in *AIChE Symp. Ser*, vol. 74, 1978, pp. 176–186.

[23] J. Grace, "Fluidized bed hydrodynamics", in *Handbook of Multiphase Flow*. Hemisphere, Washington, DC, 1982, ch. 8.1.

[24] D. C. Chitester, R. M. Kornosky, L.-S. Fan and J. P. Danko, "Characteristics of fluidization at high pressure", *Chemical Engineering Science*, vol. 39, no. 2, pp. 253–261, 1984.

[25] M. G. Jones and K. C. Williams, "Predicting the mode of flow in pneumatic conveying systems—a review", *Particuology*, vol. 6, no. 5, pp. 289–300, 2008.

[26] S. Shaul, E. Rabinovich and H. Kalman, "Typical fluidization characteristics for geldart's classification groups", *Particulate Science and Technology*, vol. 32, no. 2, pp. 197–205, 2014.

[27] O. Molerus, "Interpretation of geldart's type a, b, c and d powders by taking into account interparticle cohesion forces", *Powder technology*, vol. 33, no. 1, pp. 81–87, 1982.

[28] J. Seville and R. Clift, "The effect of thin liquid layers on fluidisation characteristics", *Powder Technology*, vol. 37, no. 1, pp. 117–129, 1984.

[29] L. J. McLaughlin and M. J. Rhodes, "Prediction of fluidized bed behaviour in the presence of liquid bridges", *Powder Technology*, vol. 114, no. 1, pp. 213–223, 2001.

[30] P. Wright and J. A. Raper, "Role of liquid bridge forces in cohesive fluidization", *Chemical Engineering Research and Design*, vol. 76, no. 6, pp. 753–760, 1998.

[31] M. Hartman, O. Trnka and M. Pohořelý, "M. hartman, o. trnka, and m. pohořelý: Fluidization behavior of oil-contaminated sand", vol. 61, pp. 236–236, Jun. 2007.

[32] O. Molerus, "Overview: Pneumatic transport of solids", *Powder technology*, vol. 88, no. 3, pp. 309–321, 1996.

[33] G. E. Klinzing, "Challenges in pneumatic conveying", *KONA Powder and Particle Journal*, vol. 18, pp. 81–87, 2000.

[34] D. Mills, *Pneumatic conveying design guide*. Butterworth-Heinemann, 2003.

[35] G. E. Klinzing, F. Rizk, R. Marcus and L. Leung, *Pneumatic conveying of solids: a theoretical and practical approach*. Springer Science & Business Media, 2011, vol. 8.

[36] R. Naveh, N. M. Tripathi and H. Kalman, "Experimental pressure drop analysis for horizontal dilute phase particle-fluid flows", *Powder Technology*, vol. 321, pp. 355–368, 2017.

[37] G. O. Brown, "The history of the darcy-weisbach equation for pipe flow resistance", in *Environmental and Water Resources History*, 2003, pp. 34–43.

[38] H. Konno and S. Saito, "Pneumatic conveying of solids through straight pipes", *Journal of Chemical Engineering of Japan*, vol. 2, no. 2, pp. 211–217, 1969.

[39] E. Rabinovich and H. Kalman, "Boundary saltation and minimum pressure velocities in particle–gas systems", *Powder Technology*, vol. 185, no. 1, pp. 67–79, 2008.

[40] G. Szikszay, "Friction factor for dilute phase pneumatic conveying", *Bulk Solids Handling*, vol. 8, no. 4, pp. 395–399, 1988.

[41] W. Wei, G. Qingliang, Z. Jiansheng and Y. Hairui, "A modified correlation to calculate solid friction factor for horizontal dilute phase pneumatic conveying", *Powder technology*, vol. 218, pp. 64–68, 2012.

[42] H. Raheman and V. Jindal, "Pressure drop gradient and solid friction factor in horizontal pneumatic conveying of agricultural grains", *Applied Engineering in Agriculture*, vol. 17, no. 5, p. 649, 2001.

[43] L. C., Z. C.-S., C. X.-P., P. W.-H., L. P. and F. C.-L., "Flow characteristics and shannon entropy analysis of dense-phase pneumatic conveying of pulverized coal with variable moisture content at high pressure", *Chemical Engineering & Technology*, vol. 30, no. 7, pp. 926–931, 2007.

[44] "Effect of moisture content on conveying characteristics of pulverized coal for pressurized entrained flow gasification", *Experimental Thermal and Fluid Science*, vol. 35, no. 6, pp. 1143–1150, 2011.

[45] T. Sheer, "Dense-phase pneumatic conveying of slush ice through plastic pipes", *Particulate Science and Technology*, vol. 26, no. 3, pp. 273–284, 2008.

[46] V. Ganesan, K. A. Rosentrater and K. Muthukumarappan, "Flowability and handling characteristics of bulk solids and powders–a review with implications for ddgs", *biosystems engineering*, vol. 101, no. 4, pp. 425–435, 2008.

[47] A. Jenike, "Storage and flow of solids. university of utah engineering experiment station", *Bulletin*, vol. 123, 1964.

[48] "Storage and flow of powders – hopper design", in *Introduction to Particle Technology*. John Wiley & Sons, 2008, ch. 10.

[49] D. Schulze, *Powders and bulk solids, Behaviour, Characterization, Storage and Flow. Springer*. Springer, 2008.

[50] I. Opaliński, M. Chutkowski and M. Stasiak, "Characterizing moist food-powder flowability using a jenike shear-tester", *Journal of food engineering*, vol. 108, no. 1, pp. 51–58, 2012.

[51] A. S. Çağli, B. N. Deveci, C. Okutan, D. Sirkeci and E. Teoman, "Flow property measurement using jenike shear cell for 7 different bulk solids", in *Proceedings of European Congress of Chemical Engineering (ECCE-6), Copenhagen*, 2007, pp. 16–20.

[52] P. Pierrat, D. K. Agrawal and H. S. Caram, "Effect of moisture on the yield locus of granular materials: Theory of shift", *Powder Technology*, vol. 99, no. 3, pp. 220–227, 1998.

[53] IChemE, "Standard shear testing technique for particulate solids using the jenike shear cell", The Institution of Chemical Engineers, 1989.

[54] S. Shaul, E. Rabinovich and H. Kalman, "Generalized flow regime diagram of fluidized beds based on the height to bed diameter ratio", *Powder technology*, vol. 228, pp. 264–271, 2012.

[55] D. Mills, M. G. Jones and V. K. Agarwal, *Handbook of pneumatic conveying engineering*. CRC Press, 2004.

[56] H. Hollier and J. Reddoch, "Successful optimization of advances in disposal and treatment technologies, to cost effectively meet new oil-based cuttings environmental regulations", in *AADE 2001 National drilling vonference, ¨Drilling Technology - The next 100 years¨*, 2001, pp. 27–29.

[57] R. Morris and S. Seaton, "Design and testing of bulk storage tanks for drill cuttings offers operators safer solution in zero discharge operations", in *AADE 2006 Fluids Conference*, 2006.

Appendix A

Powder conveying principles for efficient handling of offshore drill cuttings

This paper was published at the 8^{th} International conference for conveying and handling of particulate solids, Israel, May 2015.

The 8th International Conference for Conveying and Handling of Particulate Solids
Tel-Aviv, Israel, May 2015

POWDER CONVEYING PRINCIPLES FOR EFFICIENT HANDLING OF OFFSHORE DRILL CUTTINGS

A. Malagalage[1,2], C. Ratnayake[1,2] and A. Saasen[3,4]

1. Department of POSTEC, Tel-Tek
   Kjølnes ring 30, 3918 Porsgrunn, Norway
2. Telemark University College
   Postboks 203, N-3901 Porsgrunn, Norway
3. Det norske oljeselskap ASA
   Postboks 2070,Vika, 0125 Oslo, Norway
4. University of Stavanger
   4036 Stavanger, Norway

Abstract - Drill cuttings generated by offshore drilling operations are handled as a hazardous waste offshore. Its impact towards the marine environment has been concerned by different environmental regulatories. In sensitive marine environments, the concept of zero discharge of waste is implemented, which has emphasized the importance of having an advanced drill cutting treating system. A typical offshore well generates around 500-1000 tonnes of drill cuttings where its properties such as size, shape, composition and the type of the associated drilling fluid etc., change continuously and sometimes unpredictably. Hence transporting drill cuttings within the rig and from the rig to ships has become a challenge as no proper scientific procedure has been developed to design transportation and storage systems. Conventionally screw conveyors, manual forces along with the skip and ship methods have been utilized in transferring drill cuttings. As these methods are both lacking in efficiency and are associated with considerable health and safety issues, it has been focused on replacing those operations by vacuum and blowing systems. Powder technology principles have been successfully applied in transporting and storing bulk powders such as weighting materials and oil-well cement in offshore rigs. Therefore, it is a potential to implement the same fundamentals in designing drill cutting transportation and storage systems. Currently vacuum systems are used in several offshore rigs to convey drill cuttings from the shakers into the bulk storage tanks. From the bulk storage tanks, cuttings are blown into the transporting vessels. Due to the sticky nature of the cuttings, conveying and discharging from the tanks is a challenge. Several mechanically assisted tanks and pneumatic tanks with multiple discharge points have been developed to overcome this issue. However the

lack of understanding of the flow properties of the drill cuttings and their continuous changes of the properties, have caused these systems to face frequent operational failures. This ongoing research is focusing on characterizing the properties of the drill cuttings and relating them with their transport characteristics. It is necessary to control the flow behaviour of the drill cuttings along with the amount of associated fluids with it. Based on these relationships, it is proposed to develop a scientific method to convey the drill cuttings pneumatically. The need for this method is described in detail, and the basic principle of the method is outlined in the current article.

1.INTRODUCTION

Disposal of waste, generated from drilling and completion operations in offshore rigs has always been a challenge. These drilling wastes mainly consist of drill cuttings, drilling muds and completion fluids. During the drilling and completion operations these residual materials have to be transferred to the storage locations on the rig and then must be transferred to the treatment facilities via transport vessels. Conveying of drill cuttings is a challenging task due its sticky nature. Drill cuttings can be neither discharge into the marine environments directly nor can be stored on the rigs due to the space limitation. Hence a new scientific study is required to optimize the offshore drill cutting handling process.

1.1 Generation of the Drill Cuttings

Drill cuttings are the solid particles removed from the different rock layers which are being drilled through. Isolated grains and clusters are generated when the drill bit makes contact with the rock. These drill cuttings are carried to the surface with the drilling mud (drilling fluid) that is being used. Drilling muds are used in drilling operations to control the pressure within the wellbore, to cool down the drill bit and also to remove the drill cuttings from the wellbore. According to Caenn [1], three types of drilling muds are used which can be classified as, Water Based Muds (WBM), Oil Based Muds (OBM) and sometimes Synthetic Oil Based Muds (SBM). The size and the shape of the drill cuttings have a strong relationship with the type of the drill bit, rotation speed of the drill bit, lithology of the rock layer and the type of the drilling mud being used.

Since the drill cuttings are removed from the wellbore along with the drilling muds, they are contaminated with the solid and the liquid components associated with the adherent drilling mud. According to Neff [2] the size of the drill cuttings vary in the range of clay sized particles (~ 2μm) to coarse gravel particles (> 30mm). A sample of drill cuttings used by Saasen et al. (2012) [3] to measure the particle size distribution of a top-hole shale section is shown in **Fig.1**. This sample shows a significant variance of the size of the particles. The largest particle size was roughly around 2cm while the rest of the cuttings were larger than 100 μm.

Fig.1: A sample of cuttings used to measure the particle size distribution. (Distance between each line is 1 cm) (Saasen [3])

The volume of the drill cuttings generated from a particular well can be estimated by using Eq.(1)

$$V = \frac{\pi}{4} D^2 L(1-\varphi)(1+E) \qquad -(1)$$

An example well can be assumed to be drilled with 17 ½¨ section followed by a 12 ¼¨ section and then finally followed by a 8 ½¨ section hole. For the example, the lengths of the sections are assumed to be respectively 1700m, 1200m and 900m. It is calculated that the gauge hole cuttings volume of the well is 388m^3 while volume of the oil wet cuttings (including waste oil) is 873 m^3. As the densities of shale, sandstone and carbonates lie the range of 2200 kg/m^3 – 2700 kg/m^3, it can be roughly estimated that the considered example well has produced around 1000 tonnes of drill cuttings. The environmental impact assessment conducted by Irvine et al. [4] shows that 17 different wells drilled using both WBM and non-aqueous drilling fluids (NADF), have produced around 600 tonnes of drill cuttings on average. Hence depending on the length of the well and the properties of the rocks, a typical offshore well produces around 500-1000 tonnes of drill cuttings.

1.2 Chemical composition of the Drill Cuttings

The chemical and the mineral composition of the drill cuttings are closely associated with the compositions of the sedimentary layers that are being drilled through. Hence the composition and the properties of the cuttings differ from one location to another. Gerrard et al. [5] show that the cuttings generated in North sea are primarily composed of sandstone and shale while NRC (1983), cited in Neff [2] shows that the continental shelf cuttings contain 4 types of clay, quartz and natural minerals. When the size of the cuttings reduce, it becomes difficult to separate them from the drilling muds. Hence the amount of solid and liquid components of the drilling muds which are associated with the drill cuttings vary with the size of the cuttings. More importantly Wills [6] the drill cuttings are contaminated with heavy metals as well. Barium, zinc, chromium, nickel, vanadium and copper are commonly found in drill cuttings while trace amounts of arsenic, cadmium, mercury are silver are also found. According to Neff [2], the metal concentrations in the drill cuttings are similar to the concentrations in the drilling muds used in the drilling process. It can be seen that barium is a major component in barite used in drilling muds and as a result it has a significant concentration in the drilling muds as well. But for zinc the concentrations in the drilling muds are smaller than the concentrations in the cuttings. Neff [2] mentioned that the presence of zinc in drilling cuttings must be due to the erosion of the dope and not from the formation. Saasen et al. (2001) [7] illustrate the effect of low-toxic drilling muds such as nonaromatic base oils (NAOBM) and linear alphaolephine (LAO) based drilling

muds which are used in Norway. Due to the less toxicity cuttings associated with synthetic based muds are considered less harmful to the environment.

1.3 Discharge of drill cuttings into marine environments

According to Wills [6] until around year 2000, drill cuttings were freely discharged into offshore environments. Around 1.3 million cubic meters of drill cuttings and associated drilling wastes which have been discharged in the period of 1960-2000, are accumulated in the UK and Norwegian sectors of the North Sea. It is estimated that the cutting piles on the sea bed have a mass around 2 – 2.5 million tonnes. Other than that high concentration of heavy metals such as chromium, copper, nickel etc. are causing harmful environmental impacts. Practically it is not possible to completely remove the organic and inorganic traces from the drill cuttings by using separation and cleaning techniques. Hence different authorities have imposed various rules and regulations to control the discharge of drill cuttings. Some of the most influence offshore drilling regulations are presented by Neff [2].

1.3.1 United States of America

Discharge of drill cuttings in the territorial seas from the outer boundary of the state waters to the edge of the exclusive economic zone is regulated under the Outer Continental Shelf Lands Act (OCSLA). Under this act, reinjection of drill waste is approved to be carried out in suitable geological formations with necessary measurements to prevent any kind of leakages. It is recommended that discharging of drilling waste into offshore environment can be considered only if and only zero discharge techniques or reinjection are not feasible.

The Federal Water Pollution Control Act (CWA) regulates the discharge of drilling wastes and cuttings in the State and Federal waters. OBMs and cuttings associated with it are not allowed to be discharged in State waters or in Federal waters. Cuttings associated with WBM and SBM are not allowed to be discharged if they contain refined, mineral or formation oil. WBM and SBM associated cuttings can be discharged into marine environments if they do not contain any free oil (if they do not produce an oil sheen with the bucket sheen test).

1.3.2 Canada

Under the Canadian regulations imposed by the National Energy Board of Canada (NEBC), drill cuttings associated with SBM and OBM can be discharged into sea, only if reinjection is not technically or economically feasible. Before discharging into sea, the cuttings have to be treated with the best available technology and the concentration of the synthetic chemical concentrations should be less than 6% on wet solids. Operators may discharge untreated WBM associated cuttings under the approval of the National Energy Board.

1.3.3 Norway, UK and Netherlands

In the countries such as Norway, United Kingdom and Netherlands, offshore discharge of drilling wastes is regulated under the Convention for the Protection of the marine Environment of the North-East Atlantic (OSPAR) convention. These guidelines are applied to the regions of North Sea, Norwegian Sea and Barents Sea. Discharge of OBMs and associated cuttings were prohibited in 1996 in the OSPAR area. In order to discharge the cuttings into the sea, the associated concentration of OBM and SBM should be less than 1% by weight on dry cuttings.

2. Application of powder conveying principles in drill cuttings transportation

Due to the strict regulations, practically it is not always possible to discharge drill cuttings into the marine environments if drilling occurs with oil based drilling fluids. Therefore the cuttings have to be either transferred to onshore treatment facilities or to be re-injected. Transport methodology of the drill cuttings within the rig plays a vital role to ensure a continuous and economical drilling process, regardless of the discharge method being adopted.

2.1 Current Drill Cutting Transportation systems

Alba et al. [8] mention four basic transport methods are used in drilling rigs. They can be classified as,

1. Gravity collection methods
2. Augers belts and screw conveyors
3. Vacuum transportation
4. Pneumatic bulk transportation and storage systems

Both gravity assisted flow and the mechanical conveyors are simple and cheap methods yet become impractical in most rigs due to space limitations. Practically it is difficult to transfer drill cuttings vertically upwards and longer distances. Both these methods require significant amount of drilling fluids to lubricate the drill cuttings flow. Amount of drilling fluid associated with the drill cuttings is a significant economic factor in drill process. From one hand additional drilling fluid is required to replace the drilling muds needed for the drilling process. On the other hand high liquid content in the drill cuttings implies higher treatment costs. Hence the drilling companies prefer to have drill cuttings as dry as possible. It is impossible to add sea water to lubricate the drill cuttings flow, as water tends to form a sticky formation with the drill cuttings. Hollier et al. [9] mention that the screw conveyors cause breakdown issues, failures and injuries along with high maintenance costs. The design of the conveyors is not flexible and as a result of that while installing they might need to penetrate the deck or walls. Conventionally ship and skip method has been adopted in transporting drill cuttings from the offshore rigs to onshore/offshore treatment facilities. These operations are both time consuming and inherit significant health and safety risks which are a critical factor in offshore drilling operations.

2.2 Pneumatic and vacuum conveying systems

Several offshore drilling operators are currently considering the possibility of adopting new transport techniques to convey the drill cuttings within the rig and also from the rig to transportation vessels.

Vacuum transfer systems use vacuum blower units. According to Alba et al. [8], the main limitations of this method are the short transfer distances, the effect of the properties of the drill cuttings and the rate of drill cuttings being generated. Pneumatic conveying systems utilize positive air pressure drive which enables longer transport distances. Both these transport mechanisms are capable of conveying both wet and dry particles. Since the wetness of the particles is the major challenge in conveying drill cuttings, ability to convey wet particles is an important feature.

Schonacher et al. [10] claimed that they were able to implement a unique cuttings transport system using a pneumatic conveying system. This new method has been able transport oily clay like cuttings while replacing over 500 conventional crane lifts. The pneumatic bulk transfer system delivers cuttings in a series of blows. The time gap between the blows can be adjusted by using a level sensor.

By the work carried out by Hollier et al.[9], two gravity vacuum hoppers are used to ensure a continuous flow as typical vacuum hoppers cannot discharge and vacuum simultaneously. They also claim that this patented design is capable of handling oil based cuttings effectively.

According to Alba et al. [8], cutting re-injection process can be optimized by coupling it with a pneumatic conveying system. Their transportation system was designed in 1998 and claimed that it has been proven efficient on various kinds of rigs. Saasen et al. (2014) [11] clamed, cutting re-injection is not an environmental friendly process as a result, it is no longer a desired method. However the approach to convey drill cuttings pneumatically still holds a valid application.

All these applications of powder conveying principles ensure that they were able to achieve zero discharge conditions while transferring the cuttings effectively. Even though the basic concepts of their designs are presented, the relationship between the design parameters and the drill cutting properties are not presented. Hence a proper scientific work has to be carried out in understanding the design principles of conveying drill cuttings. Lack of understanding of the wet granular behaviour in pneumatic conveying systems, causes excessive energy consumption, frequent plugging leading to operational halts during the drilling operations. The economic impact of these issues is so significant that it is vital to study the factors influencing the transport of drill cuttings using pneumatic conveying methods.

2.3 Challenges of applying powder technology principles in drill cutting transportation

Currently powder technology principles have been applied in designing bulk conveying systems in offshore drilling rigs to store materials such as barite, cement and liquids. Due to the wetness and the continuous and random changing of the properties of the drill cuttings (size, shape, associated drilling fluid type etc.), it is a challenging task to design a similar system to convey drill cutting on the rig.

2.3.1 Wetness

Traditionally pneumatic conveying is considered to be capable of conveying any kind of dry material. When it comes to wet material, pneumatic conveying becomes challenging due to the possible blockages and excessive energy consumption. It is impossible to have dry drill cuttings on the rig. Hence this challenge has to be overcome when applying powder conveying principles in designing a drill cutting transfer system.

In a series of experiments conducted by Sheer [12] to develop models to predict the flow regimes of wet ice with air flow have come out with significant finding with regarding pneumatic conveying of wet material. Slush ice having ice content of 70-75% was unable to move in dilute phase using acceptable air velocities. But they were able to convey dispersed dense phase mixtures in small agglomerating using air velocities up to 25 m/s. When the ice content was reduced down to 65% the nature of the ice was completely changed into a semifluid. Then the flow regime was changed into slow moving longer slugs or full plugs due to low wall resistance. This shows that the liquid content has a major impact towards the flow regime.

According to Mills [13] wet or damped material can be conveyed pneumatically but the challenge is to feed them to the pipelines and to discharge from the hopper. If the material contains fine particles, wetness can be a challenge in pneumatically conveying systems as they tend to coat the pipeline and finally causing blockages. If the material is not so wet, hot air flow can be used to overcome the issue of wetness. Otherwise single plug blow tank systems have to be adopted in handling wet material. However, Hollier et al. [9] claimed that they have implemented a vacuum conveying system to convey the cuttings successfully.

2.3.2 Scaling Up

In developing a pneumatic conveying system, a reliable characterization technique is still unavailable for design calculation. The general approach is to conduct design calculations based on the data obtained by the lab scale experiments. Since the design of a pneumatic conveying system highly depends on the properties of the material being conveyed, these lab scale experimental data possess valuable information. Basically two approaches are used in scaling up the design, namely,

1. The global approach
2. The piecewise approach

In the global approach the whole conveying system is taken a single unit. The discrete position of the components of the system is not considered. Equivalent length method is adopted in designing such components. This approach is good for designing a particular conveying system but it lacks the flexibility in altering the design. On the contrary the piecewise approach considers the discrete position of the different components such as bends and vertical sections of the conveying system. Ratnayake et al [14] shows how the piecewise scaling approaches can be applied in designing bulk transfer systems to convey barite, bentonite and cement within drilling rigs. As drill cuttings can be considered as a challenging material to be handled with, piecewise approach can be considered as the most suitable one.

2.3.3 Storage

As the drill cuttings are wet and sticky, conventional single outlet silos may face the problem of blockage and rat holing. Currently, it is investigating the possibility of having mechanically assisted tanks by installing internal agitators, screw type augers or sliding tank bases. On the other hand by installing such units make the storage tanks more complex and increase the capital cost. Morris et al [15] claimed that Halliburton has come out with a new concept of designing a storage tank for cuttings having multiple outlets, calling it as the Honey comb base tank. This method has been used for storing fly ash and sewage sludge. As the compressed air is injected from the bottom and top of the tank, no additional mechanical agitation is required. They claim that this tank is capable of discharging cuttings to a horizontal distance of 102m with a rate of 48 tonnes per hour (tank pressure is 4bar). It can also transfer cuttings to a height of 55m at a rate of 30 tonnes per hour (tank pressure is 5 bar).

2.4 Development of a drill cutting transfer system

The objective of the proposed research work is to develop a scientific method to design an efficient drill cutting transfer system. As the properties of the drill cuttings vary significantly based on the location and the type of the drilling mud used, getting a representative sample is the major challenge. It will be a challenge to develop relationships and models based on the limited number of samples used in the experiments. In order to overcome this issue both theory of sampling and multivariate data analysis techniques are expected to be applied.

As the properties and the flowrate of the drill cuttings are varying while drilling a particular well, it is essential to have an online measurement system to detect the changes in the process parameters. Hence the scientific design procedure is expected to integrate process analytical tools (PAT) with the research work.

4.Conclusion

Transportation of drill cuttings within and from the offshore drill rigs is a very vital process. Even though several pneumatic conveying systems have been applied in conveying drill cuttings, no proper study has been conducted in designing an efficient drill cutting handling system. The properties of the drill cuttings significantly vary from one location to another, depending on the rock formation, drill bit type and on the type of the drilling mud used. As drill cuttings are contaminated with oil and drilling muds they possess a wet and a sticky nature. Hence designing a conveying and storage system based on the conventional powder principles is challenging. Therefore it is proposed to conduct a proper scientific research work to understand the behaviour of wet drill cuttings in pneumatically transferring systems and to develop a scientific procedure for designing an efficient drill cutting transfer system.

5.Nomenclature

5.1 Symbols

D : Diameter of the well [m]
E : Expansion factor [-] (normally ~ 0.25)
L : Length of the well [m]
V : Volume [m3]
φ : Porosity [-]

5.2Abbreviations

NADF : Non-Aqueous Drilling Fluids
OBM : Oil Based Muds
PAH : Polycyclic Aromatic Hydrocarbon
SBM : Synthetic Oil Based Muds
WBM : Water Based Muds

6.References

[1] R. Caenn, H. C. H. Darley, and G. R. Gray, Chapter 5 - The Rheology of Drilling Fluids, in *Composition and Properties of Drilling and Completion Fluids (Sixth Edition)*, R. Caenn, H. C. H. Darley, and G. R. Gray, Eds., Boston: Gulf Professional Publishing, 2011, pp. 179-269.

[2] J. M. Neff, Fate and effects of water based drilling muds and cuttings in cold water environments, May,25 2010. pp. 45-74. Available: http://s08.static-shell.com/content/dam/shell-new/local/country/usa/downloads/alaska/neff-final-draftgs072010.pdf, 'Accessed On:'[10/03/15]

[3] A. Saasen, B. Dahl, and K. Jødestøl, Particle Size Distribution of Top-Hole Drill Cuttings from Norwegian Sea Area Offshore Wells, *Particulate Science and Technology: An International Journal,* vol. 31,1 pp. 85-91, 2013. doi: 10.1080/02726351.2011.648824

[4] M. Irvine, A. d. Jong, and A. Armah, Environmental Impact Statement, Ghana Jubilee Phase 1 Development, Appendix B, Tullow Ghana Limited, 27 November 2009.

[5] S. Gerrard, A. Grant, R. Marsh, and C. London, Drill cuttings piles in the North Sea: management options during platform decommissioning,Research Report No 31, Center for Environmental risk, University of East Anglia, October 1999. pp. 14-48.

[6] J. Wills, Muddied Waters-A Survey of Offshore Oilfield Drilling Wastes and Disposal Techniques to Reduce the Ecological Impact of Sea Dumping, presented at the Ekologicheskaya Vahkta Sakhalina (Sakhalin Environment Watch), 25 May, 2000.

[7] A. Saasen, M. Berntsen, G. Løklingholm, H. Igeltjørn, and K. Åsnes, The effect of drilling fluid base-oil properties on occupational hygiene and the marine environment, *SPE Drilling & Completion,* vol. 16,03 pp. 150-153, 2001. doi: 10.2118/73193-PA

[8] A. Alba, F. Fragachan, A. Ovalle, and T. Shokanov, Environmentally Safe Waste Disposal: The Integration of Cuttings Collection, Transport, and Re-Injection, presented at the 2nd International Oil Conference and Exibition, Veracruz, Mexico, 27-30 June, 2007 pp. 528-538. doi: 10.2118/108912-MS

[9] C. Hollier and J. Reddoch, Successful optimization of advances in disposal and treatment technologies, to cost effectively meet new oil-based cuttings environmental regulations, AADE 01-NC-HO-13, presented at the AADE 2001 National drilling vonference, ¨Drilling Technology - The nest 100 years¨, Houston, Texas, 27-29, March, 2001.

[10] D. Schonacher, J. Rojas, J. Gharst, and B. Paiuk, Meeting Zero Discharge Requirements in the Gulf of Mexico Using a Unique Cuttings Transport System, SPE 80609, presented at the SPE/EPA/DOE Exploration and Production Environmental Conference, San Antonio, Texas, 10-12, March, 2003.

[11] A. Saasen, K. Jødestøl, and E. Furuholt, CO2 and NOx emissions from cuttings handling operations, presented at the SPE Bergen One Day Seminar, Grieghallen, Bergen, Norway, 2014. doi: 10.2118/169216-MS

[12] T. Sheer, Dense-phase pneumatic conveying of slush ice through plastic pipes, *Particulate Science and Technology,* vol. 26,3 pp. 273-284, May 2008.

[13] D. Mills, M. G. Jones, and V. K. Agarwal, Handbook of pneumatic conveying engineering: CRC Press, 2004, p. 23.

[14] C. Ratnayake and A. Saasen, Bulk Transfer on Oil Rigs: System Optimised Through Pilot Testing, SPE-171296-MS, presented at the SPE Russian Oil and Gas Exploration & Production Technical Conference and Exhibition, Moscow, Russia, 14-16,October, 2014.

[15] R. Morris and S. Seaton, Design and testing of bulk storage tanks for drill cuttings offers operators safer solution in zero discharge operations, AADE-06-DF-HO-17, presented at the AADE 2006 Fluids conference, Houstan, Texas, 11-12 April, 2006.

Appendix B

Experiments and simulations for horizontal pneumatic transport of dry drill cuttings

This paper has been accepted in the Chemical Engineering & Technology journal. The submitted paper is presented in this dissertation.

1. Title

Experiments and simulations for horizontal pneumatic transport of dry drill cuttings

2. Authors

Anjana Malagalage (MSc) – PhD candidate (Corresponding author)

W. K. Hiromi Ariyaratne (PhD)– Associate professor

Chandana Ratnayake (PhD) – Professor / Senior scientist

Morten C. Melaaen (PhD) – Professor / Dean

3. Author affiliations

Anjana Malagalage [1] – anjana.t.malagalage@tel-tek.no

W. K. Hiromi Ariyaratne [2,3]

Chandana Ratnayake [1,2]

Morten C. Melaaen [1,2]

1 - Department of POSTEC, Tel-Tek, Kjølnes ring 30, N-3918 Porsgrunn, Norway

2 - Faculty of Technology, Natural Sciences and Maritime Sciences, University College of Southeast Norway, Post box 235, N-3603, Norway

3 - Bilfinger Industrial Services Norway AS, Herøya Industripark, Hydrovegen 55, 3936 Porsgrunn, Norway

4. Abstract

Investigation of the possibility of using pneumatic conveying technique for the transportation of dry drill cuttings is the main objective of this study. Both pilot-scale experimental and simulation approaches were carried out for sand which is used as a model material which mimics the properties of dry drill cuttings. The simulations based on multiphase particle-in-cell method (MP-PIC) which is an Eulerian-Lagrangian model is used to predict the pressure drop and the

predictions are in good agreement with experimental results. Both approaches confirm the possibility of using pneumatic conveying technique for the transportation of dry drill cuttings under tested conditions. The study provides a foundation for further analysis of pneumatic conveying of wet drill cuttings.

5. Text

5.1 Introduction

Oil and gas drilling operation produces large amount of solid rock cuttings when drilling through different rock layers. These solid rock cuttings are brought into the surface by means of drilling fluid used for the drilling process. These solid cuttings which are contaminated with drilling fluid are called drill cuttings. The drill cutting properties such as particle size, particle shape, particle density, moisture content and oil content are dependent on the type of the drill bit used for drilling, speed of the drill bit, lithology of the rock layer and type of the drilling fluid used. Once these are brought to the surface, different solid control techniques (shale shakers, screens, etc.) are used to separate the solids from the drilling fluid, and the clean drilling fluid is pumped into the borehole again [1, 2].

Possible impacts of offshore drill cuttings (which are separated out through the solid separation techniques but still contaminated with drilling fluid) on marine life have been identified by environmental authorities, and it is categorized as a hazardous waste offshore [3, 4]. Therefore, the drill cuttings are conveyed into intermediate storage silos instead of being dumped into the sea. Eventually, these are transported to the onshore treatment facilities by the ships. However, the conveying of drill cuttings is a vital process and the current practices are facing frequent operational failures. Therefore, carrying out a proper scientific research on this topic is becoming important nowadays [5].

Since wetness, oiliness, wide particle size distribution and large particle sizes of drill cuttings are really challenging factors for pneumatic conveying; at first, a preliminary study is carried out for dry model materials representing particle size ranges of real drill cuttings. Both pilot-scale experiments and CFD simulation approaches are used for the investigation. Basically, the pressure drop results of a particular horizontal section of the rig are analyzed for a certain range of operating conditions i.e. the solid loading ratio between 2 to 4 and the superficial air velocity

at the inlet between 13 ms^{-1} to 22 ms^{-1}. More details about the experiments and the simulations are presented in the Sect. 5.2.

A detailed literature review on pneumatic conveying is presented by Malagalage [6]. It is important to conduct set of experiments which covers the whole range of desired solid mass flow rates and the potential air flow rates. The experimental pressure drop per unit length is plotted against superficial air velocity for a particular solid flow rate. Combination of such plots at different solid flow rates form a state diagram for the considered material in the considered experimental rig [7]. A typical state diagram for horizontal pneumatic conveying is shown in Fig.1

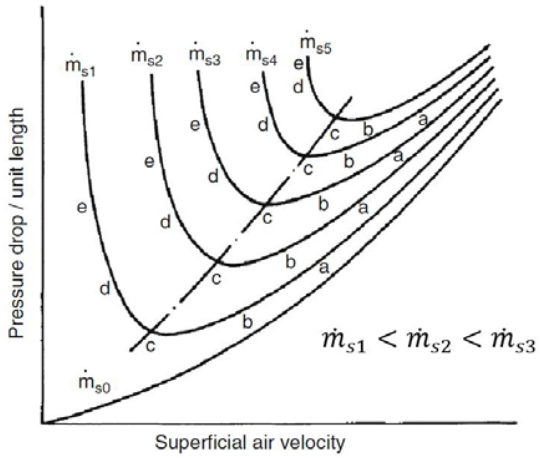

Figure 1 General state diagram for horizontal pneumatic conveying [8]

5.2 Experimental setup

A model material was selected for the experiments as the model drill cuttings, in order to overcome the problem of obtaining adequate amounts of representative samples of dry drill cuttings. A drill cutting sample was analyzed to specify the desired physical properties of the model material. The density of the sample was 2598.25 kgm^{-3}. The particle size was in the range of 0.18 mm – 8 mm and is shown in Fig.2. Sand was selected as the model material as it has equivalent density and particle size range of drill cuttings. The particle density of the sand samples was 2718.5 kgm^{-3}. Three size distributions were selected in the considered size range and their particle size distributions are shown in Fig.2. The parameters of the particle size distributions of the three sand samples and the drill cuttings are given in Tab.1. Particles larger

than sample D were not considered as it was not possible to use them in experiments as the rotary feeder would get blocked.

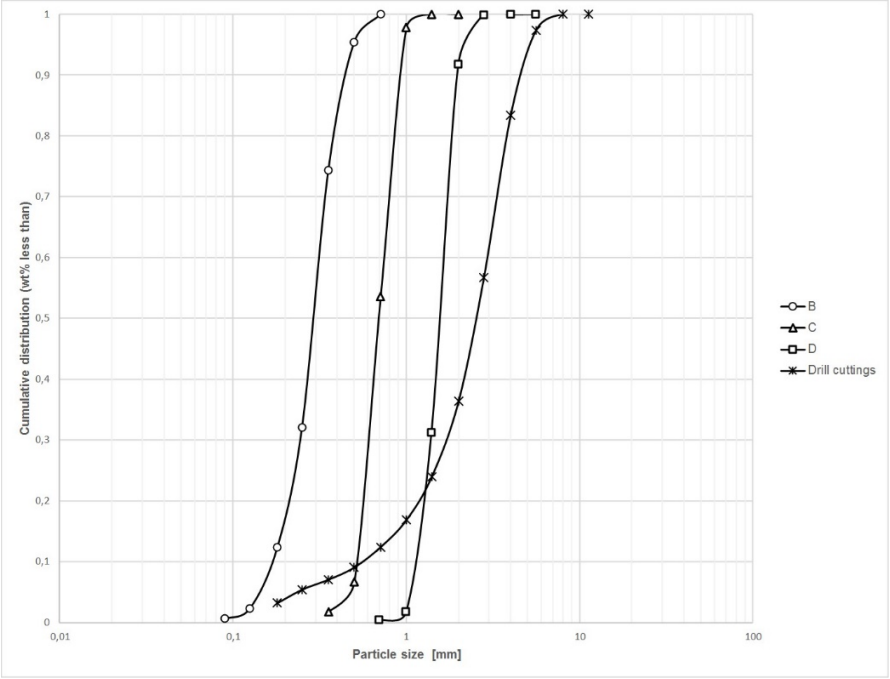

Figure 2 Cumulative particle size distribution (weight % less than) of the sand particles used for the pneumatic conveying experiments and simulations.

Table 1: Particle size distribution of the drill cuttings and model material

	Particle size		
Material	**D_{90} (mm)**	**D_{50} (mm)**	**D_{10} (mm)**
Drill cuttings	4.55	2.55	0.6
B (sand)	0.44	0.29	0.17
C (sand)	0.91	0.69	0.52
D (sand)	1.97	1.57	1.14

The experiments were carried out at the pneumatic conveying pilot rig at Tel-Tek, Norway and a schematic diagram of the rig is shown in Fig. 3. The testing material was stored in the storage tank and it was fed into the mixing chamber via a rotary feeder. In the mixing chamber, the particles were mixed with compressed air and the resulting gas-solid mixture was transported through the conveying line. The total length of the conveying line is around 40 m. During the

conveying, the local pressures at several points were measured by pressure transmitters as shown in Fig. 3. After the conveying is completed, solid particles were collected in the receiving tank. Material collected in the receiving tank can be loaded back into the storage tank to convey the material repeatedly in batch wise. It is assumed that the experiments were conducted under isothermal conditions at 290 K.

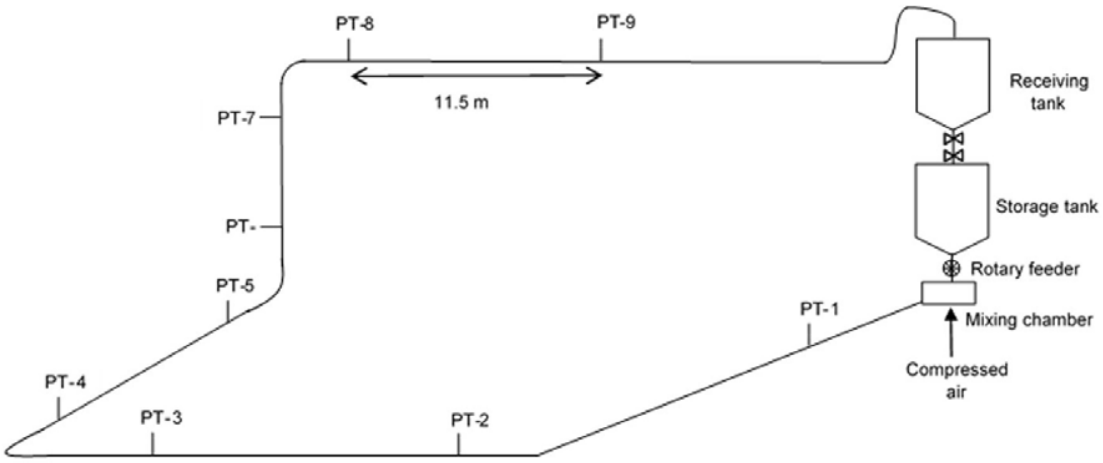

Figure 3 Schematic diagram of the pilot scale pneumatic rig used for the experiments

The experimental data from the horizontal section of PT-8 – PT-9 were selected since that section provided reproducible results under same conditions. The inside diameter of the pipe is 81.2 mm and the considered section had a length of 11.5 m. The experiments were conducted with air flow in the range of 13-22 ms^{-1} and with solid loading ratio in the range of 2-4. Solid loading ratio less than 2 was not possible to achieve as the rotary feeder tends to get stuck at low rotating speeds. Solid loading ration higher than 4 was not possible to achieve as the material discharge rate from the storage tank was not adequate.

5.3 Modelling and simulations

The experimental cases were simulated using computational particle fluid dynamics (CPFD) numerical scheme incorporated with the multiphase-particle-in-cell (MP-PIC) method. The model equations can be found elsewhere [9].

The CPFD numerical methodology incorporated in the commercially available Barracuda® 17.0.3 code was used as the platform for the modelling and simulations. The horizontal pipe section of PT-8 – PT-9 (Fig.1) was selected for the simulations as mentioned above. The particle properties and pipe dimensions were as described in the Sect. 5.2 .The air viscosity was 1.84469×10^{-5} $kgm^{-1}s^{-1}$.

The mass flow rates of the air and the particles at the inlet of the selected pipe section for different cases are specified in Tab. 2. Slip ratio between gas and particle velocities at the inlet was assumed as 1. The solid loading ratios for the all simulation cases were in the range of 3.00±0.07. At the outlet, a pressure boundary condition was adopted with experimental pressure measurements. A partial slip of the particles was assumed at wall boundary. A normal-to-wall momentum retention = 0.95, a tangent-to-wall momentum retention = 0.87 and a particle-particle restitution coefficient = 0.98 were used for the current simulations. Each simulation was run over 6 s (in flow time) to make sure the quasi-steady state.

Table 2: Details of the simulation cases

Description	**Case 1**	**Case 2**	**Case 3**	**Case 4**	Case 5
Superficial air velocity at the inlet (ms^{-1})	12.88	15.20	17.51	19.62	21.64
Solid loading ratio (kg solids/kg air)	3.07	2.98	2.95	2.97	2.98
Air mass flow rate (kgs^{-1})	0.084	0.100	0.118	0.134	0.150
Solids mass flow rate (kgs^{-1})	0.258	0.299	0.347	0.398	0.448
Solid volume fraction at the inlet (%)	0.143	0.141	0.142	0.145	0.148
Reynolds number of the flow	73972	88358	103359	117732	132198

5.4 Results and discussion

Results are discussed under two sub-sections below; “Experiments” and “Modelling and simulations”.

5.4.1 Experiments

The state diagram of the sample C that shows the pressure drop per meter in the section of PT-8 – PT-9 obtained from the experimental data is presented in Fig. 4. These data have been obtained

by averaging 3 replicate experimental data (each experiment has been time averaged). The standard deviation of the measured values are also plotted in the Fig. 4. Second order polynomial curve fitting has been used for each data series. It was not possible to obtain enough steady replicates for the points at (solid loading = 4, air velocity ~ 13 ms^{-1}) and (solid loading = 2, air velocity ~ 17ms^{-1}), hence the standard deviation values are not plotted for those two points. The pneumatic conveying state diagram of the considered model drill cutting follows the standard state diagram which is explained by Malagalage [6]. As the gas-solid mixture has a similar behavior as the air only curve at velocities higher than ~17 ms^{-1} , it can be assumed that the particles are conveyed in dilute phase. At air velocities less than ~17 ms^{-1} it can be seen that there is a tendency to increase the pressure drop per meter with reducing air velocities. This has to be verified by conducting more experimental tests. Since it was possible to get relatively better reproducible data for the considered air velocity range, data with the solid loading ratio of 3 are selected for the modelling and simulation purposes.

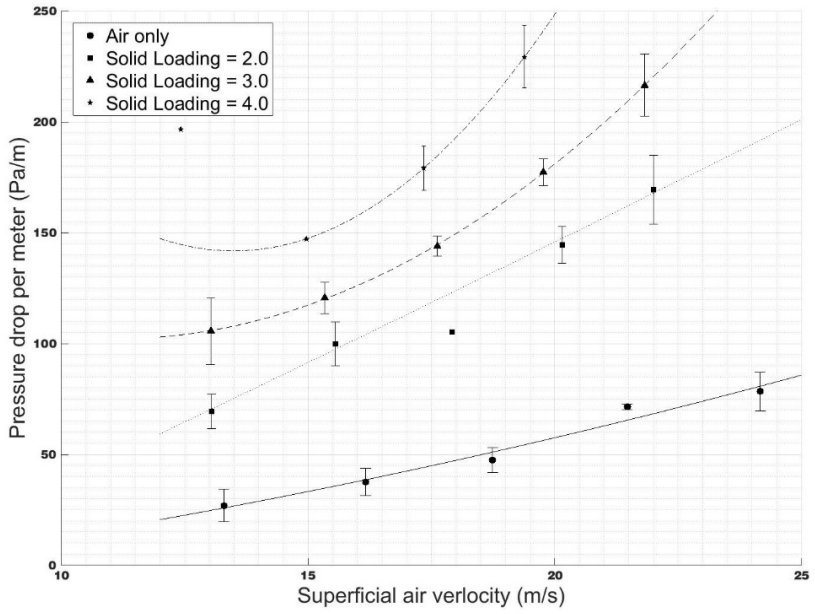

Figure 4 Experimental pressure drop per meter values in the section between pressure sensor 8 and 9 (PT8 – PT9) at different solid loading ratios

State diagrams can also be plotted for particular solid flow rates. Similar state diagrams were achieved for both sample B and D and they are presented by Malagalage [6]. For the comparison of the results, state diagram for sample C at different solid flow rates are plotted in Fig.5.

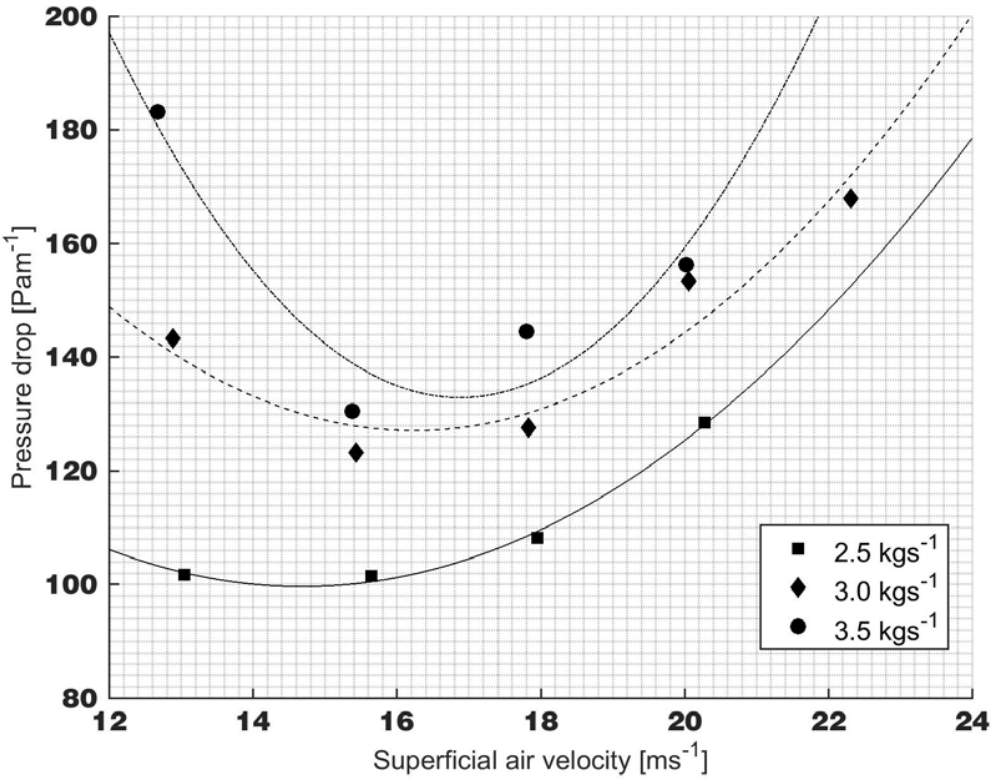

Figure 5 Experimental pressure drop per meter values in the section between pressure sensor 8 and 9 (PT8 – PT9) at different solid flow rates

According to Fig. 5 the superficial air velocities corresponding to the minimum pressure drop at different solid flow rates can be calculated. This calculation is conducted based on second order polynomial curve fitting for the experimental data. The results are tabulated in Tab.3 along with the results presented by Malagalage [6].

Table 3: Minimum pressure drop and corresponding air velocities for the sand samples

Solid flow rate (kgs^{-1})	**0.25**		**0.3**			**0.35**		
Sample	**B**	**C**	**B**	**C**	**D**	**B**	**C**	**D**
Minimum Pressure drop (Pam^{-1})	96.87	99.72	114.80	127.13	131.58	137.80	133.01	149.90
Corresponding air velocity (ms^{-1})	16.84	14.68	17.96	16.24	15.92	18.57	16.88	16.69

It is interesting to see that all three samples reach their minimum pressure drops in the same range of superficial air velocities and the corresponding minimum pressure drops lie in the same range as well. For further analysis of this behavior pressure drops the solid flow rates of 2.5 kgs^{-1}, 3 kgs^{-1} and 3.5 kgs^{-1} are plotted in Fig. 6a, Fig. 6b and Fig. 6c respectively.

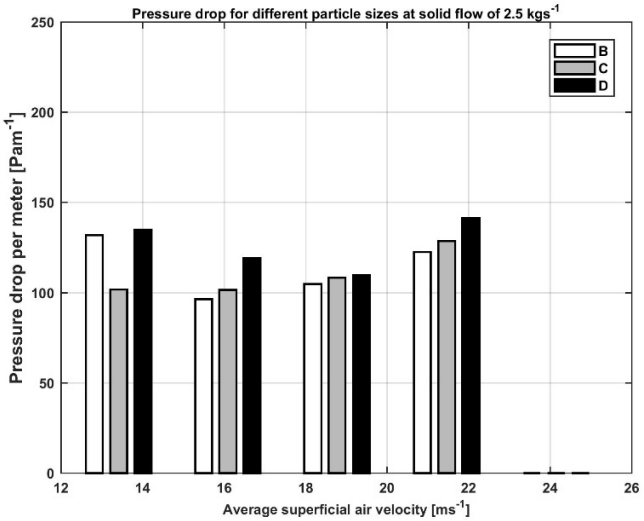

Figure 6a Comparison of pressured drops of sample B,C and D at solid flow rate of 2.5 kgs^{-1}

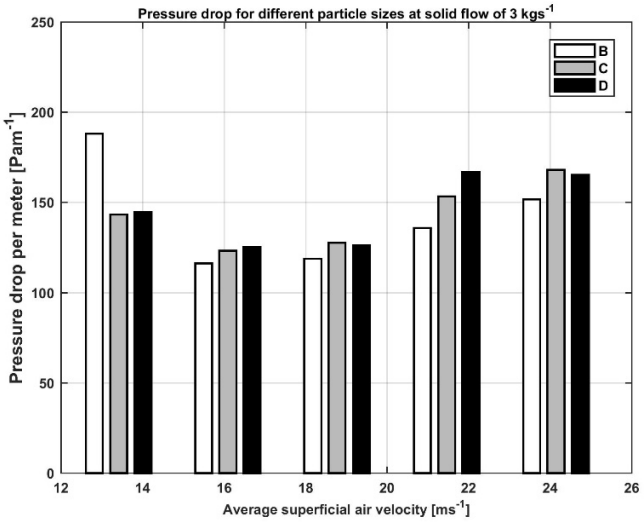

Figure 6b Comparison of pressured drops of sample B,C and D at solid flow rate of 3 kgs^{-1}

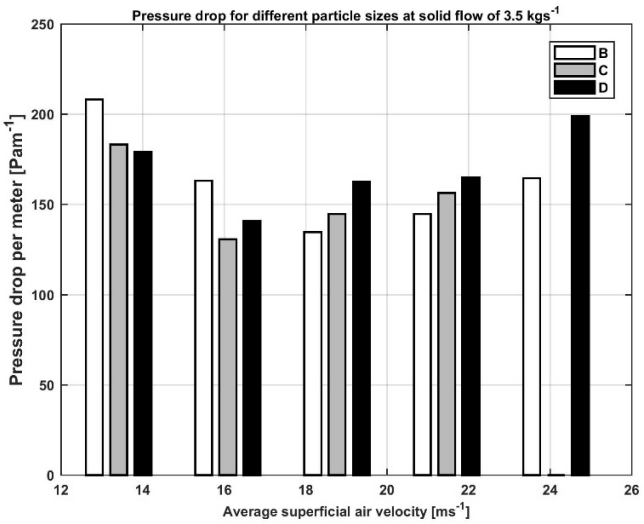

Figure 6c Comparison of pressured drops of sample B,C and D at solid flow rate of 3.5 kgs^{-1}

According to the Fig. 6 at low air velocities smaller particles (Sample B) have the highest pressure drop and at higher air velocities larger particles (Sample D) have the highest pressure drop. In between these two extreme cases all three samples reach their minimum pressure drop within a similar range of superficial air velocity. In that region the pressure drop of the three samples reach a relatively equal value regardless of the different particle sizes. Based on these results it can be concluded that when operating at the minimum pressure drop region, the impact of the particle size distribution would be minimum. This is an important phenomenon for drill cuttings conveying as the particle size distribution of the drill cuttings can fluctuate in the drilling operation.

5.4.2 Modelling and simulations

Fig. 7 shows the comparison of simulated pressure drop results with experimental data. The simulated pressure drop results are taken by time-averaging pseudo steady state data at fully developed region. For a particular solid loading ratio, the pressure drop increases with increase of superficial air velocity. This is reasonable for a dilute phase gas-solid flow in a horizontal pipe. It is because the gas phase shear is increased similar to a single-phase flow in very dilute systems.

Moreover, the predicted pressure drops are in good agreement with experimental data for the tested operating conditions. The deviation between the experiments and simulations ranges from

0% to 8%. However, it should be noted that the pressure drop results are predicted for a certain particle-wall boundary condition, and one would expect different results when the particle-wall collision parameters are changed.

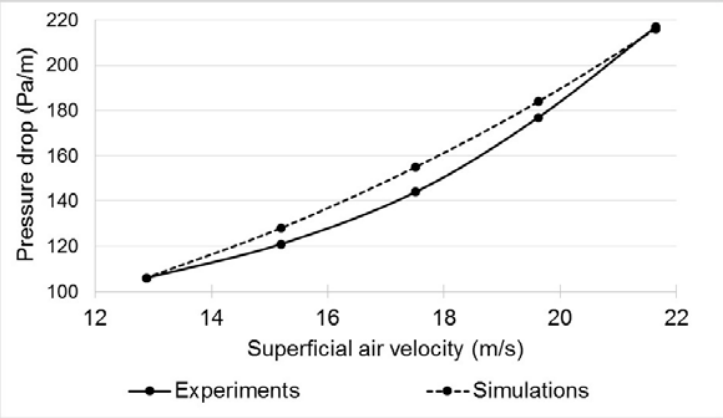

Figure 7 Comparison of simulated pressure drop per meter values with experimental data where the solid loading ratio = 3

Fig. 8 shows the solid distribution pattern after stabilizing the flow (at 6s). The flow is dilute as expected. The solid particles flow downwards after entering to the pipe due to the gravity effect. Once these particles hit the rough wall these bounce back to the core region of the pipe. Therefore, the maximum solid concentration can be found nearby central region towards bottom side.

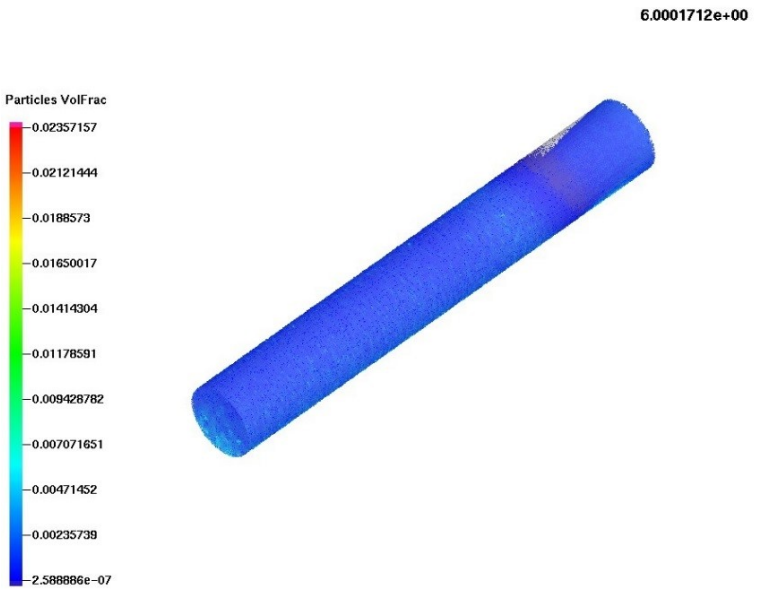

Figure 8 Predicted solids volume fraction of the pipe at time = 6s for the simulation case 5

5.5 Conclusion

As a preliminary step for investigating the possibility of using pneumatic conveying technique for the transportation of drill cuttings, experiments and simulations were carried out for conveying of a model material which mimics the dry drill cutting properties. The tested solid loading ratios were in the range of 2-4 and the superficial air velocity range was 13-22 ms^{-1}, hence the flow was dilute. Basically, the pressure drop results for a particular horizontal section of the rig are presented and analyzed.

Both experiments and simulations give physically reasonable pressure drop results. The experimental pressure drop increases when the superficial air velocity is increased from 13 ms^{-1} to 22 ms^{-1}. Moreover, the simulated pressure drop results are in good agreement with experimental results and the deviations are in the range of 0-8% for the tested conditions and for the selected particle-wall boundary conditions in the model. Simulation results also show axial and radial solid distribution patterns which are reasonable for a dilute phase conveying.

According to the experiments and simulations, it can be concluded that the dilute phase pneumatic conveying is viable and successfully used for the transportation of dry drill cuttings. By comparing the results presented by Malagalage [6] it can be seen that sand with three different particles size distributions would reach the minimum pressure drop when conveying pneumatically in the region of superficial air velocity of 15-18 ms^{-1}. The corresponding pressure drop for the three samples are significantly similar in this range and it can be concluded that for the same material, the impact of the particle size towards the minimum pressure drop and the corresponding air velocity would be minimum when the solid flow rate is in the region of 2.5-3.5 kgs^{-1}. These are some preliminary results of a scientific investigation, which is aimed enhance the knowledge on drill cuttings handling in offshore applications. Advance experiments and simulation methods are planned to investigate the influence of oil content, water content, particle size distribution and other influential properties of dill cuttings in to their transport properties and how computer simulation techniques could be used to predict the flow modes involved.

6. Acknowledgment

The authors would like to acknowledge the financial support provided by the Research Council of Norway under PETROMAKS II program and Aker BP ASA for the scientific investigation.

7. References

1. Manjula, E., et al., *A review of CFD modelling studies on pneumatic conveying and challenges in modelling offshore drill cuttings transport.* Powder Technol., **2017**. 305: p. 782-793.
2. Neff, J.M., *Fate and effects of water based drilling muds and cuttings in cold water environments.* Houston (TX): Report to Shell Exploration and Production Company, **2010**.
3. Melton, H., et al. *Environmental aspects of the use and disposal of non aqueous drilling fluids associated with offshore oil & gas operations*. in *SPE International Conference on Health, Safety, and Environment in Oil and Gas Exploration and Production*. **2004**. Society of Petroleum Engineers.
4. Forrest, J., et al., *Working document of the NPC North American resource development study-unconventional oil.* US National Petroleum Council (NPC), **2011**.
5. Malagalage, A., C. Ratnayake, and A. Saasen. *Powder Conveying Principles for Efficient Handling of Offshore Drill Cuttings*. in *The 8th International Conference for Conveying and Handling of Particulate Solids, Tel-Aviv, Israel*. **2015**.
6. Malagalage, A., et al. *Pneumatic Conveying of Model Drill Cuttings-Pilot Scale Experiments and Simulations*. in *SPE Bergen One Day Seminar*. **2017**. Society of Petroleum Engineers.
7. Mills, D., *Chapter 11 - Conveying characteristics*, in *Pneumatic Conveying Design Guide (Second Edition)*. **2004**, Butterworth-Heinemann: Oxford. p. 236-257.
8. Klinzing, G.E., et al., *Pneumatic conveying of solids: a theoretical and practical approach*. Vol. 8. **2011**: Springer Science & Business Media.
9. Ariyaratne, W.H., C. Ratnayake, and M.C. Melaaen, *Application of the MP-PIC method for predicting pneumatic conveying characteristics of dilute phase flows.* Powder Technology, **2017**. 310: p. 318-328.

Appendix C

Particle size distributions of the sand samples

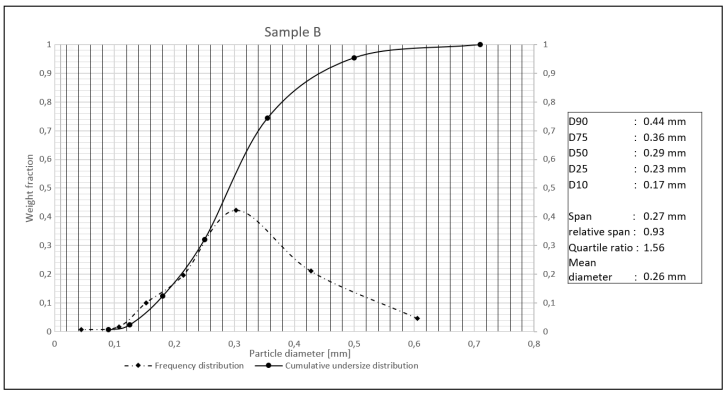

Figure C.1: Particle size distribution of mixture **B**

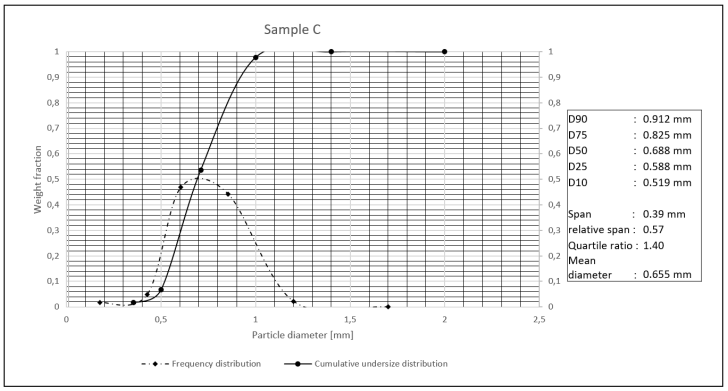

Figure C.2: Particle size distribution of mixture **C**

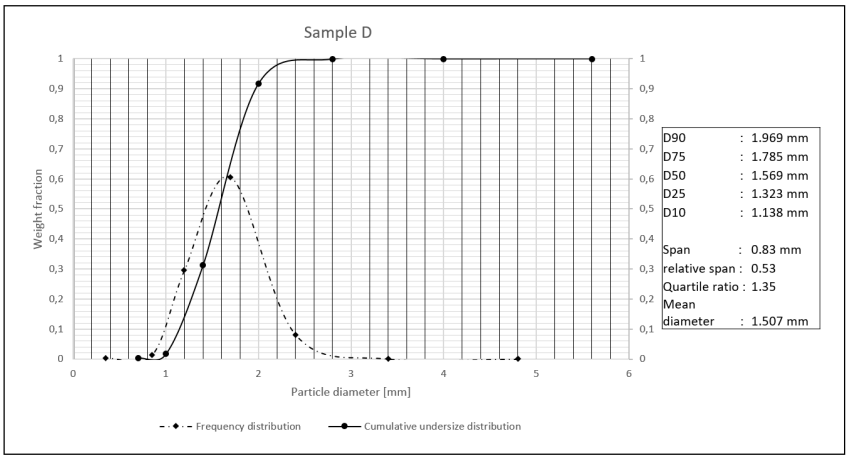

Figure C.3: Particle size distribution of mixture **D**

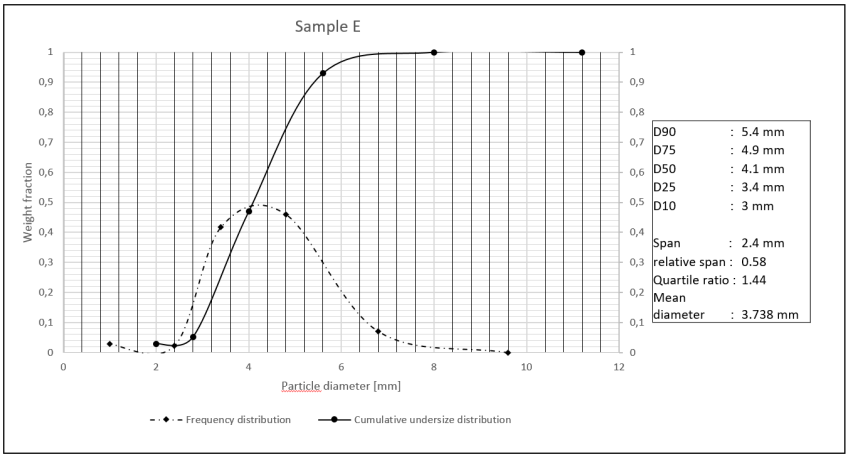

Figure C.4: Particle size distribution of mixture **E**

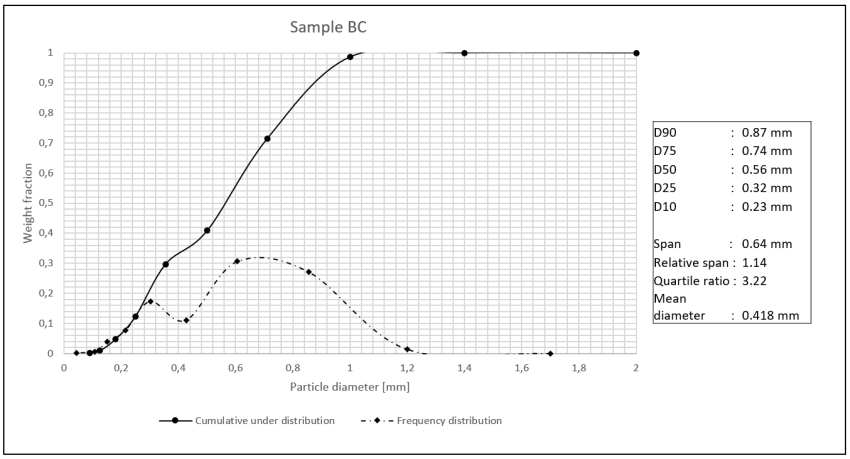

Figure C.5: Particle size distribution of mixture **BC**

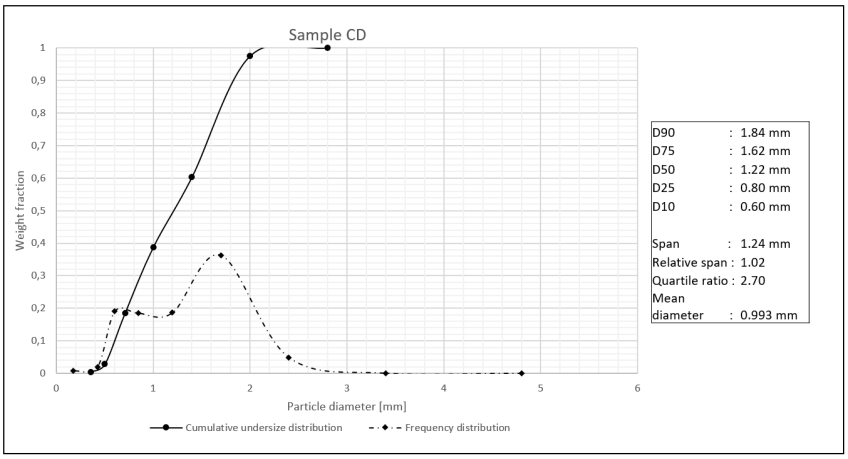

Figure C.6: Particle size distribution of mixture **CD**

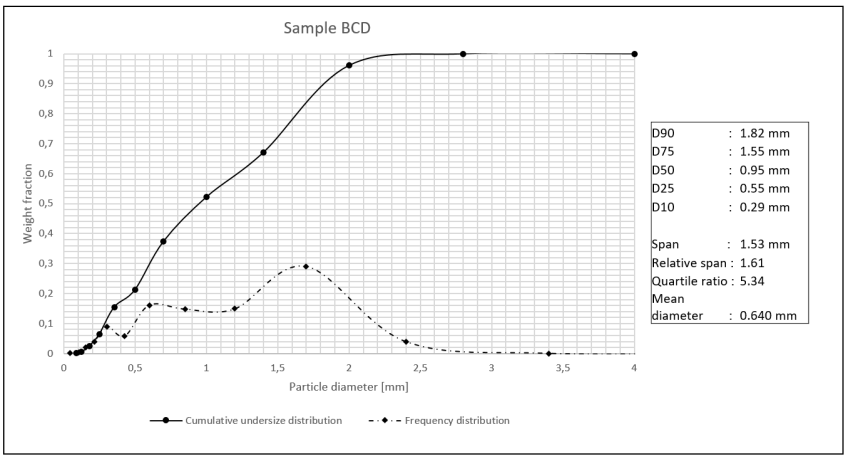

Figure C.7: Particle size distribution of mixture **BCD**

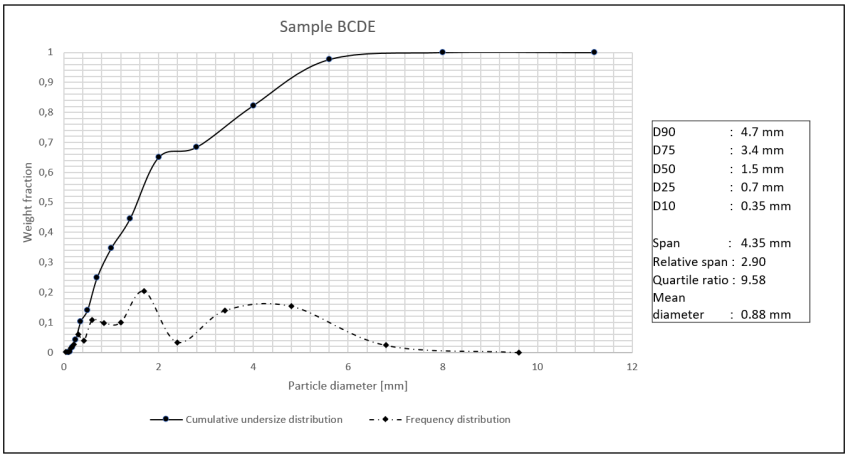

Figure C.8: Particle size distribution of mixture **BCDE**

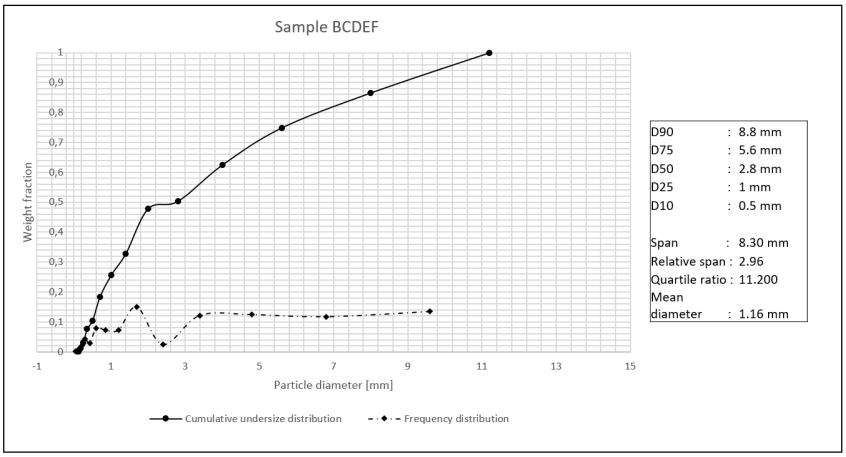

Figure C.9: Particle size distribution of mixture **BCDEF**

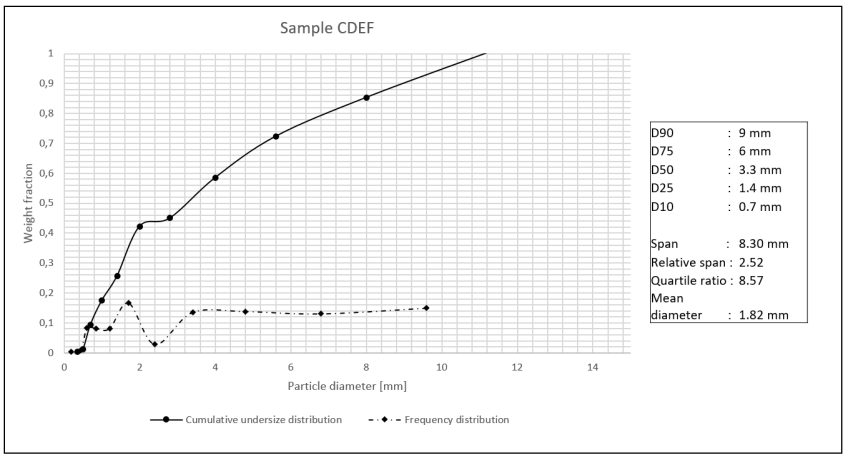

Figure C.10: Particle size distribution of mixture **CDEF**

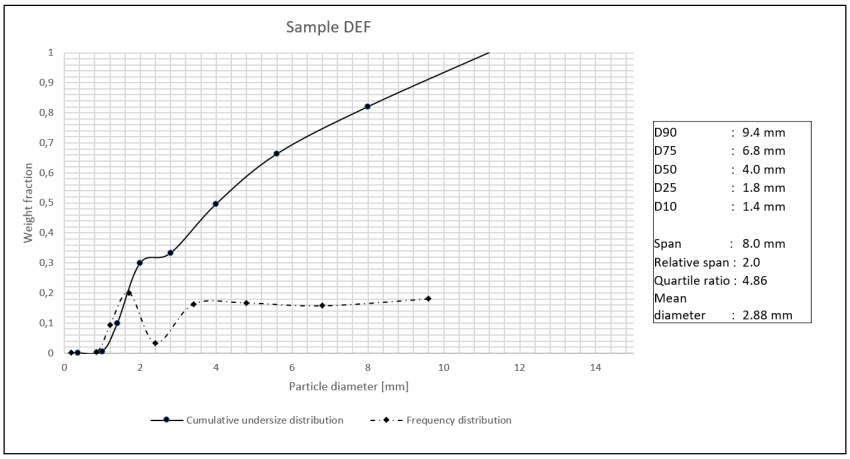

Figure C.11: Particle size distribution of mixture **DEF**

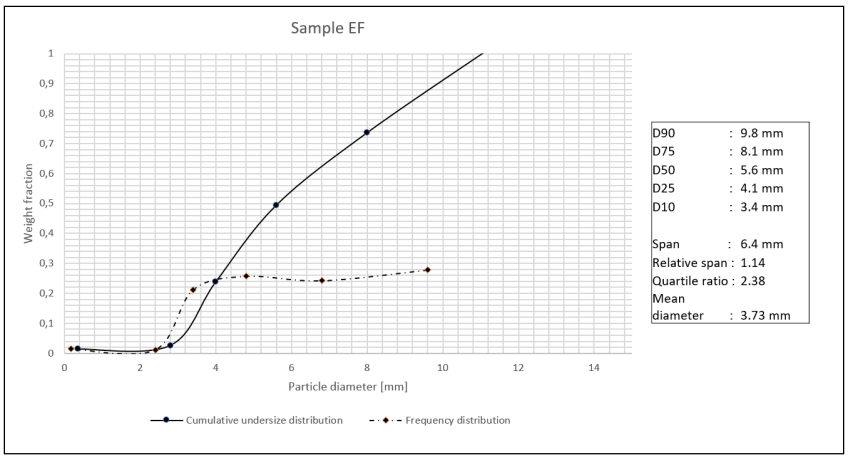

Figure C.12: Particle size distribution of mixture **EF**

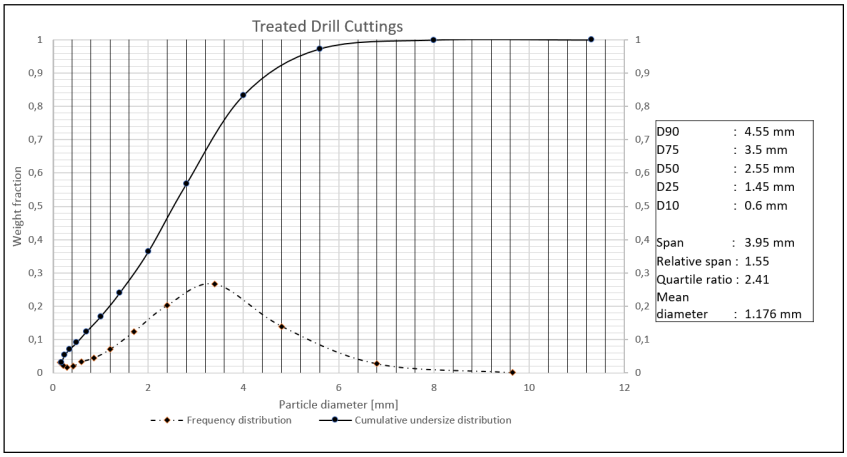

Figure C.13: Particle size distribution of the treated drill cuttings sample

Appendix D

Fluidization curves for dry sand samples

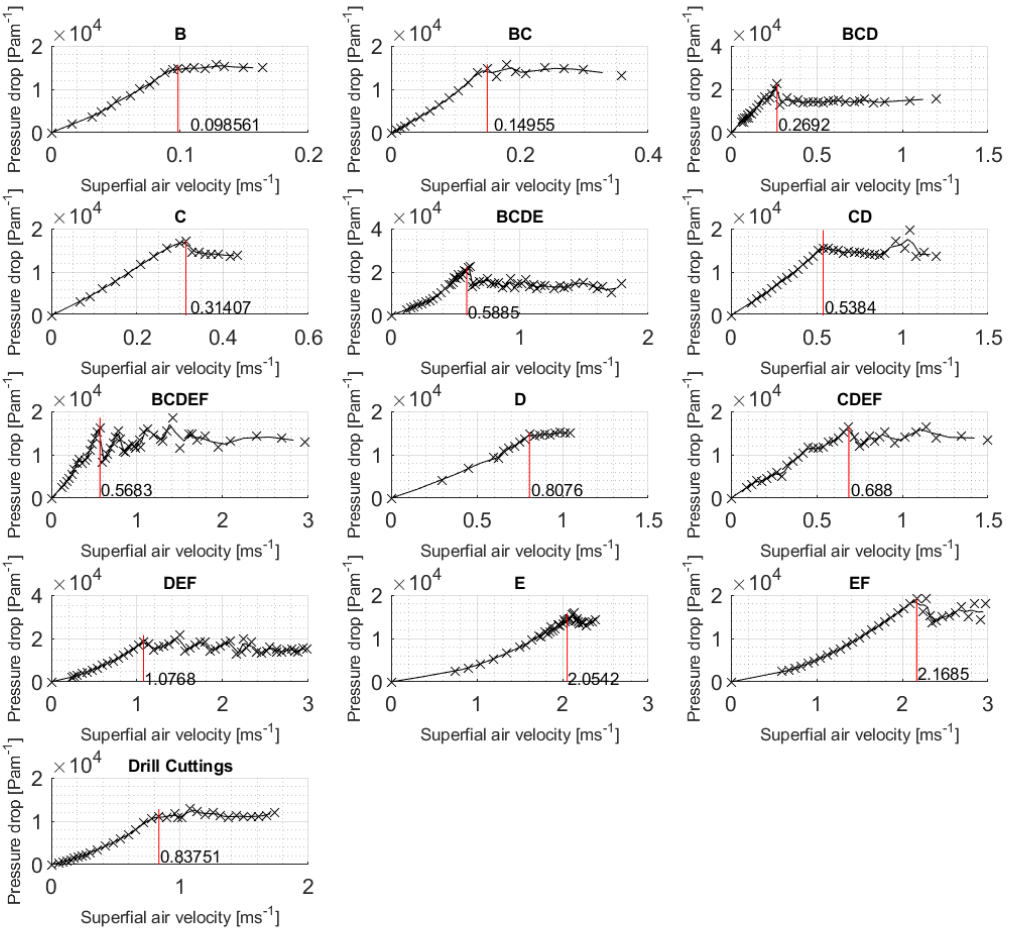

Appendix E

Fluidization curves for oily sand samples

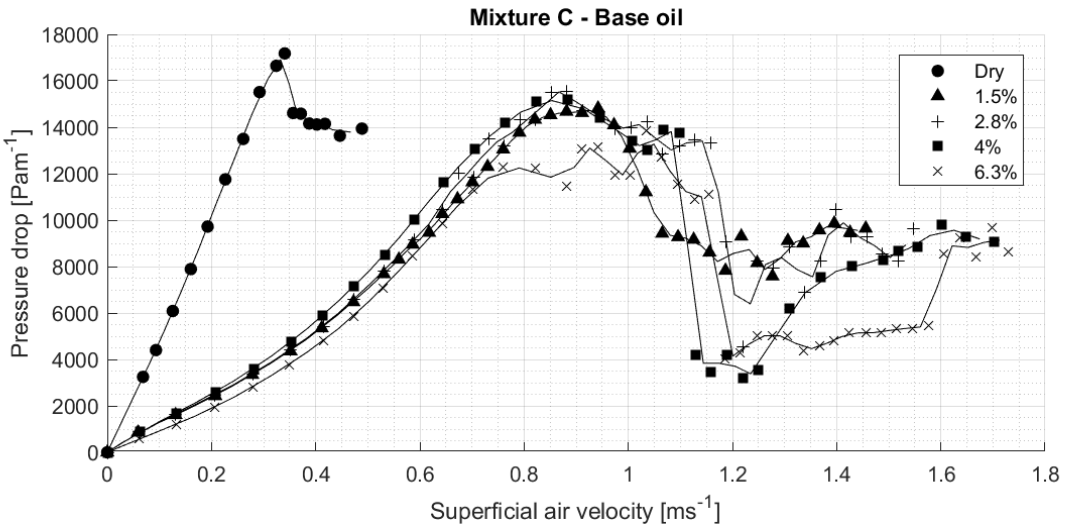

Figure E.1: Fluidization curves for the **C**- base oil mixtures

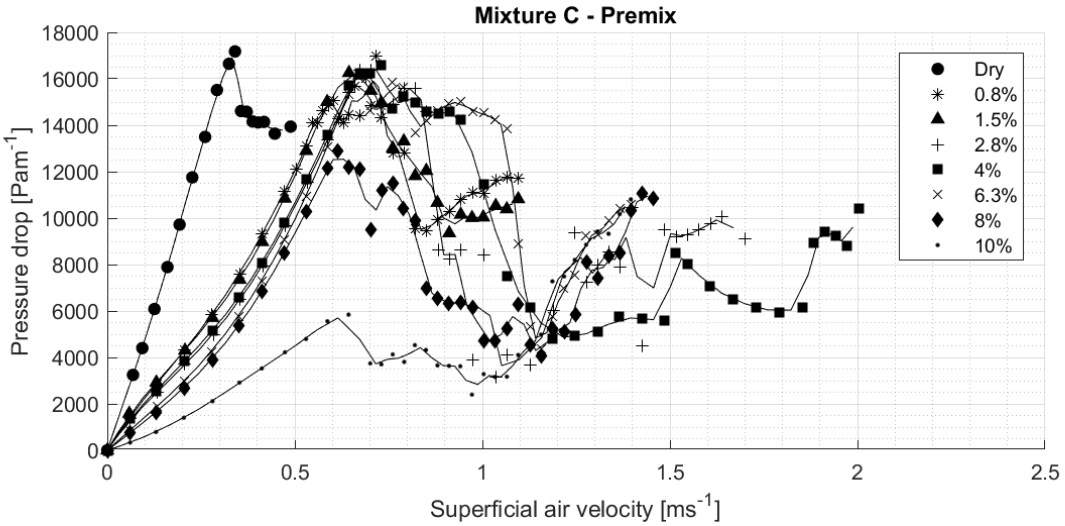

Figure E.2: Fluidization curves for the **C**-premix mixtures

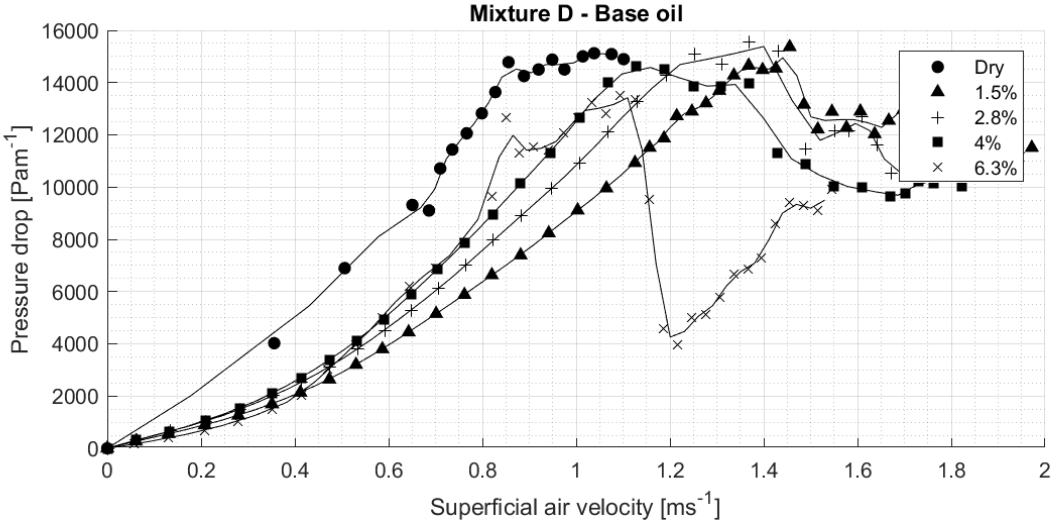

Figure E.3: Fluidization curves for the **D**- base oil mixtures

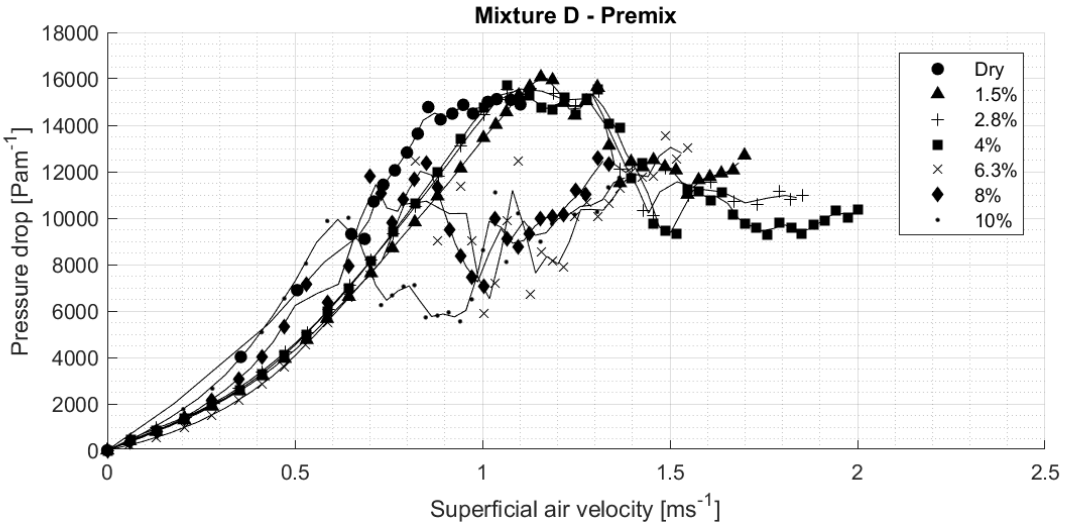

Figure E.4: Fluidization curves for the **D**-premix mixtures

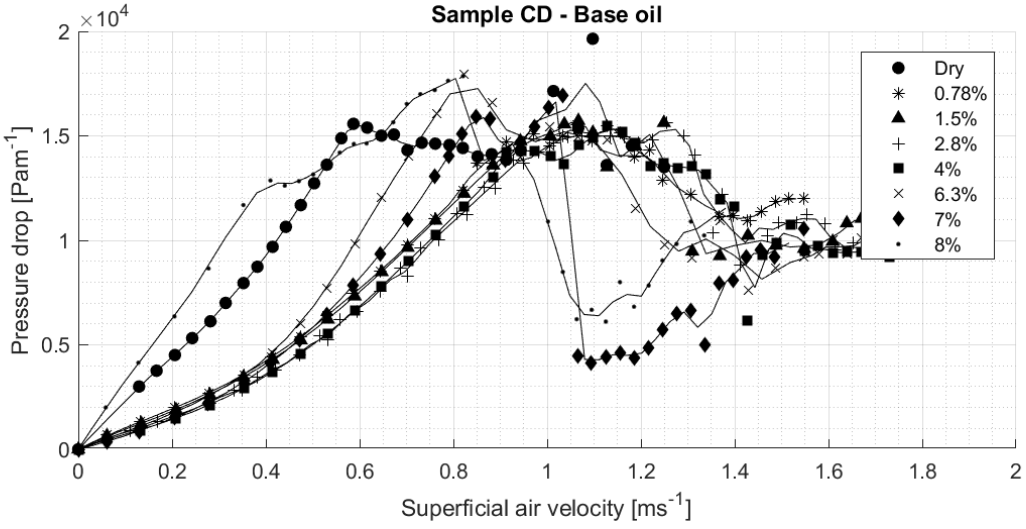

Figure E.5: Fluidization curves for the **CD**- base oil mixtures

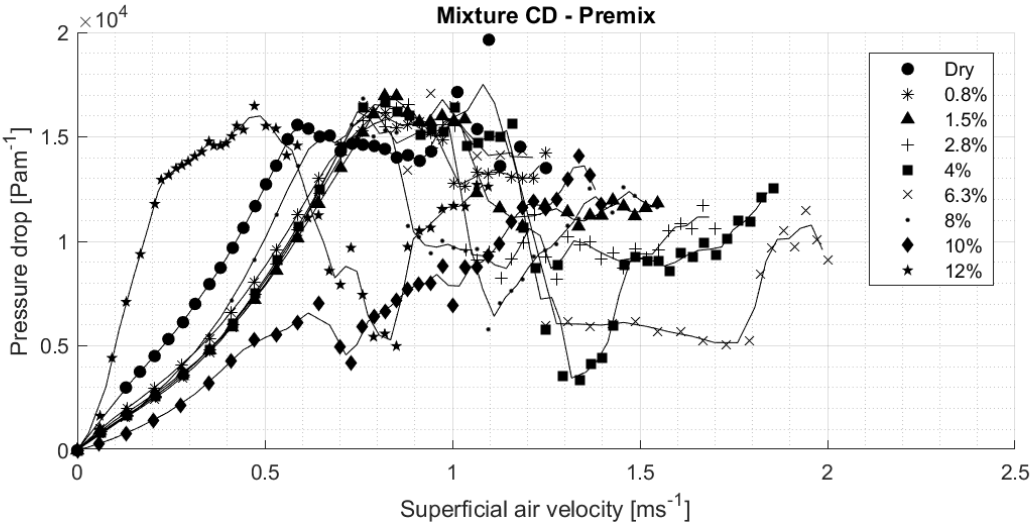

Figure E.6: Fluidization curves for the **CD**- premix mixtures

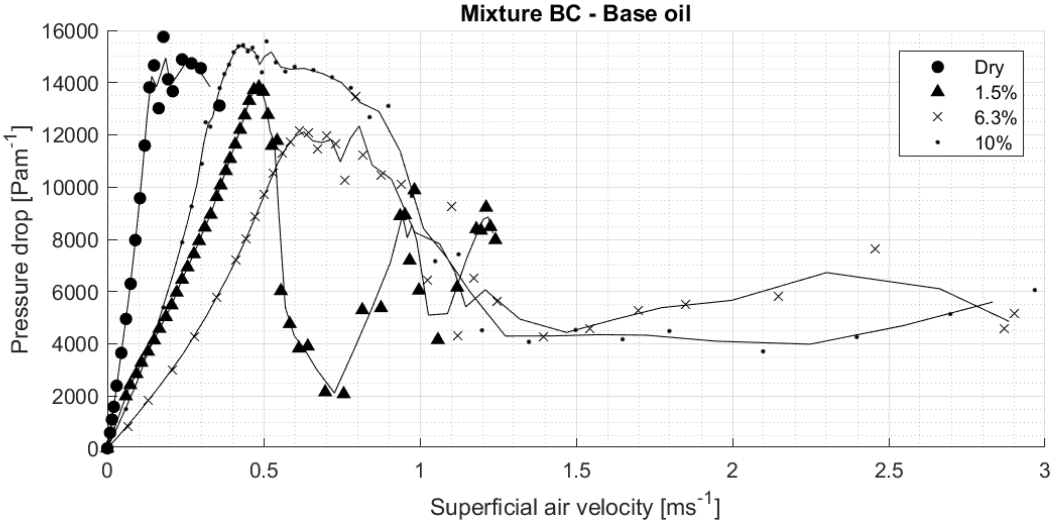

Figure E.7: Fluidization curves for the **BC**- base oil mixtures

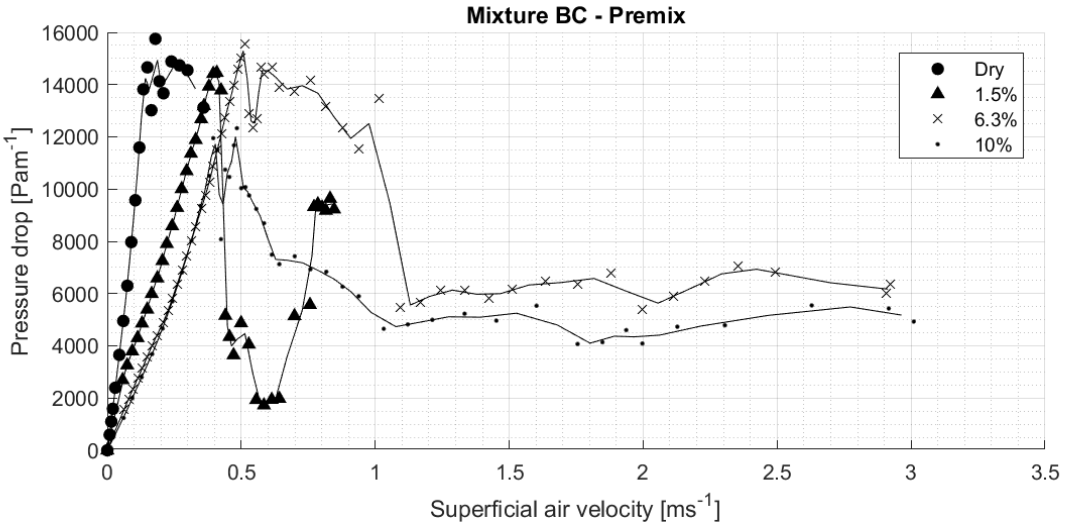

Figure E.8: Fluidization curves for the **BC**- premix mixtures

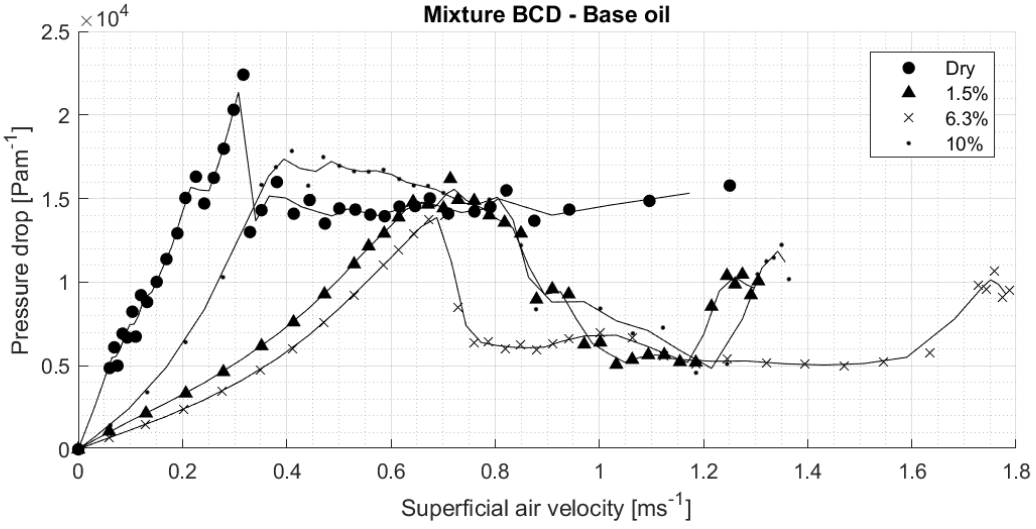

Figure E.9: Fluidization curves for the **BCD**- base oil mixtures

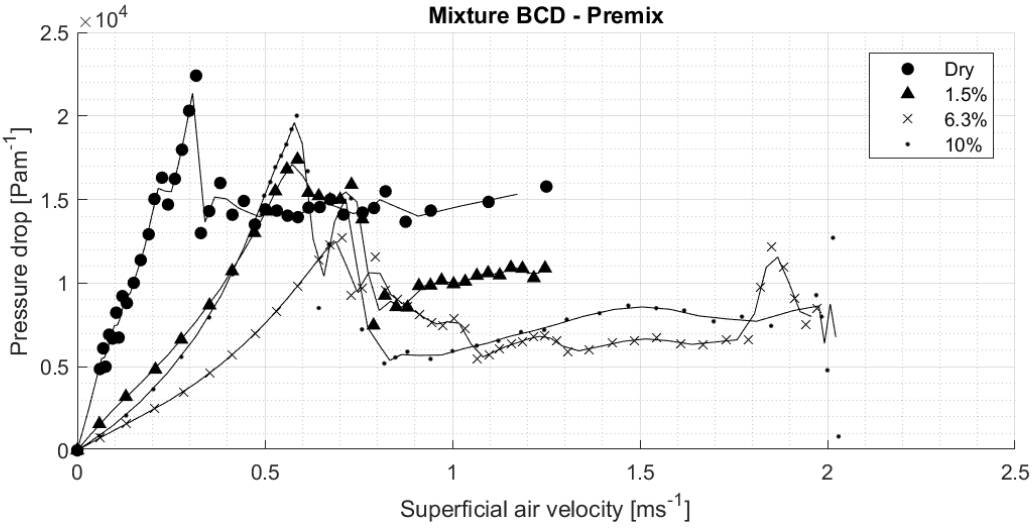

Figure E.10: Fluidization curves for the **BCD**- base oil mixtures

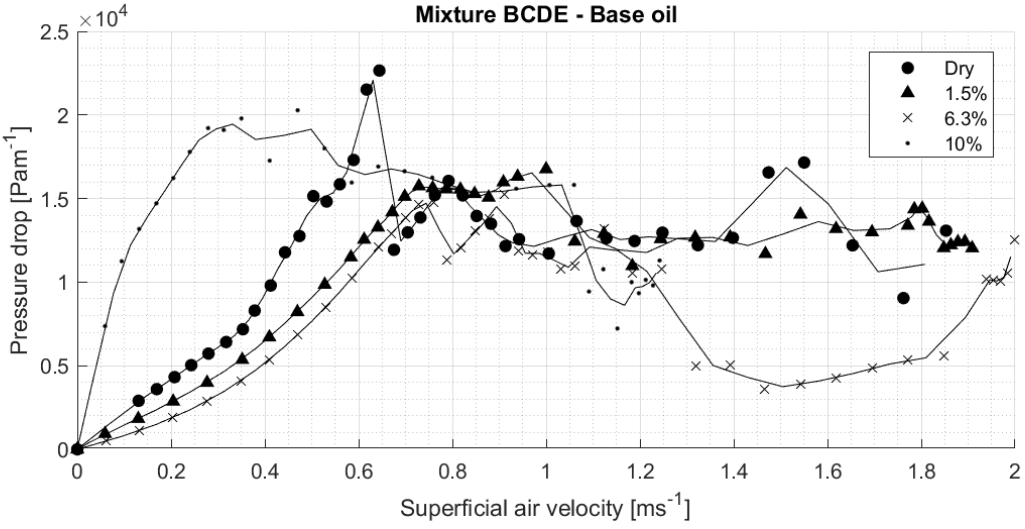

Figure E.11: Fluidization curves for the **BCDE**- base oil mixtures

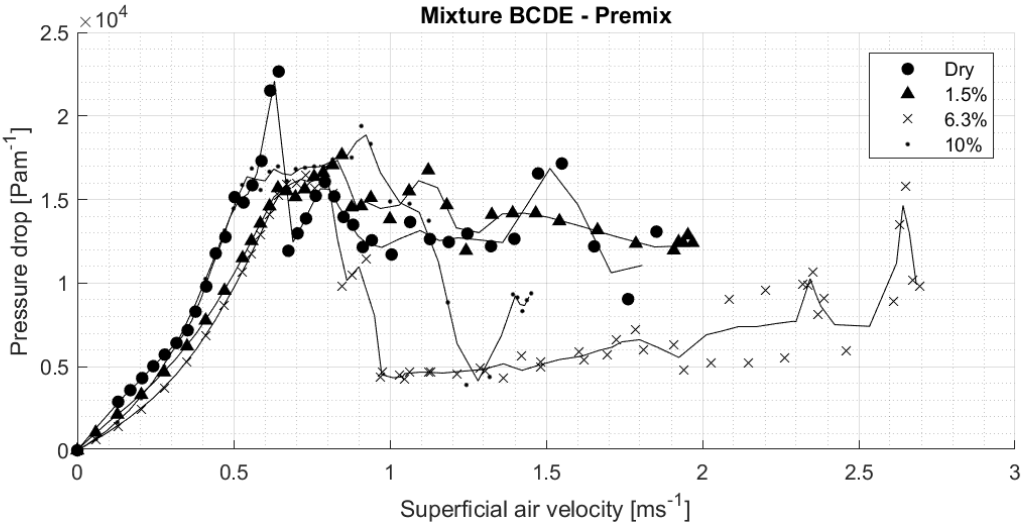

Figure E.12: Fluidization curves for the**BCDE**- premix mixtures

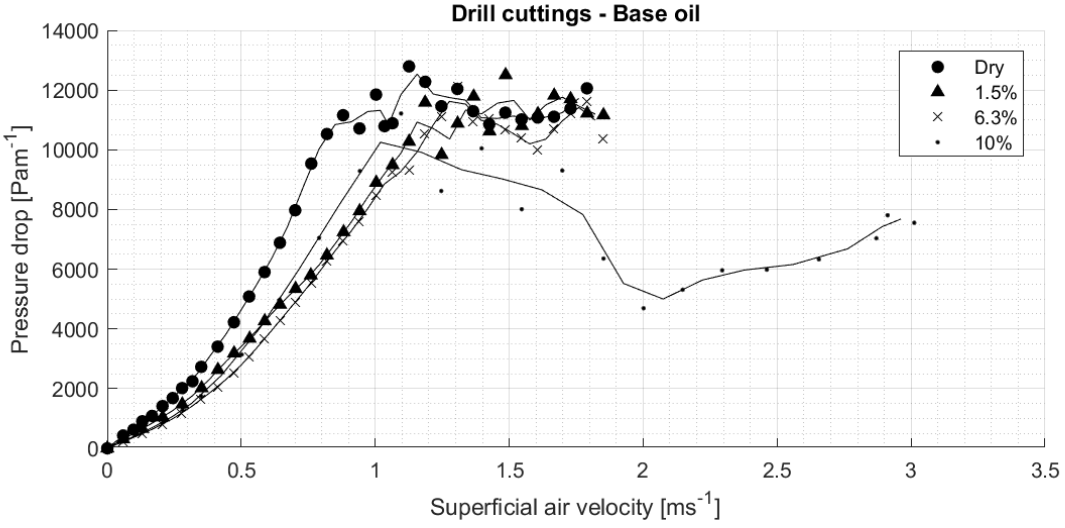

Figure E.13: Fluidization curves for the drill cuttings- base oil mixtures

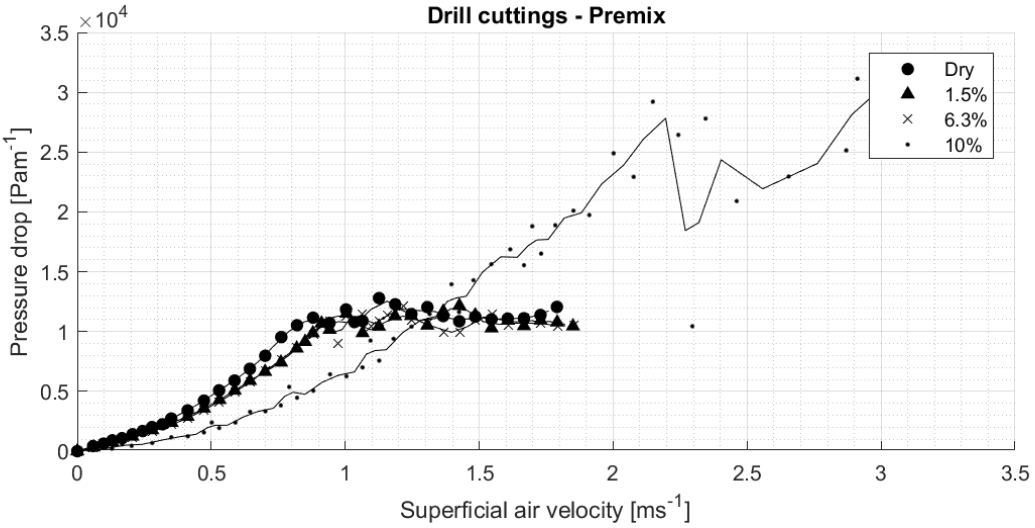

Figure E.14: Fluidization curves for the drill cuttings - premix mixtures

Appendix F

Fluidization curves at different drilling fluid concentrations

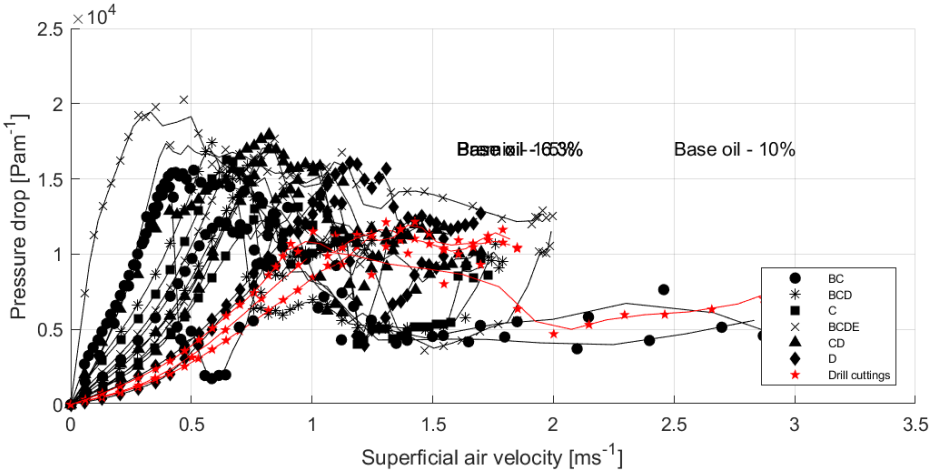

Figure F.1: Fluidization curves for mixtures with 1.5% of premix

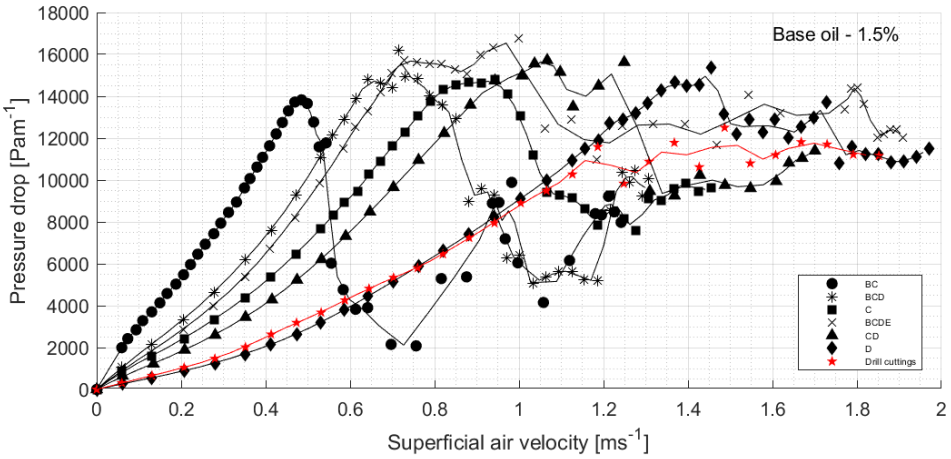

Figure F.2: Fluidization curves for mixtures with 1.5% of base oil

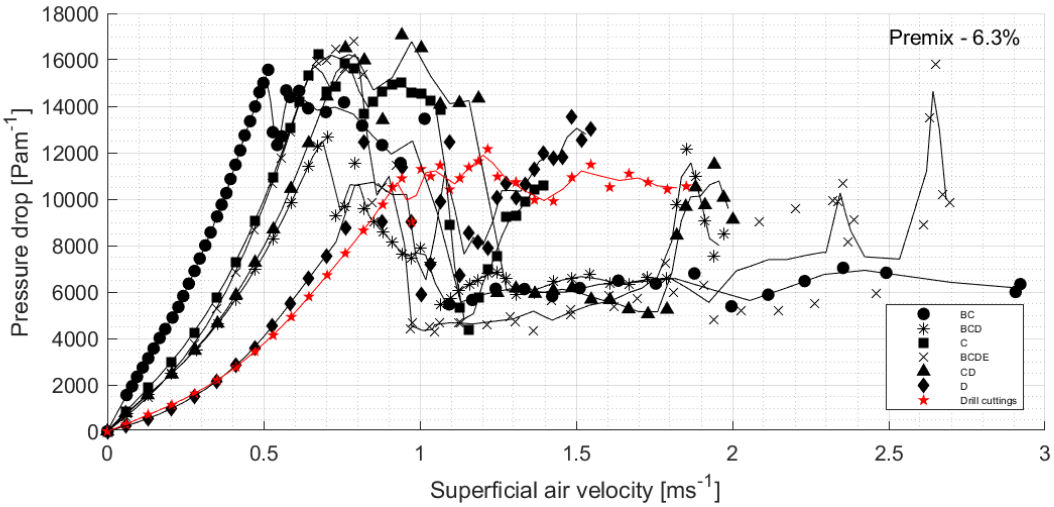

Figure F.3: Fluidization curves for mixtures with 6.3% of premix

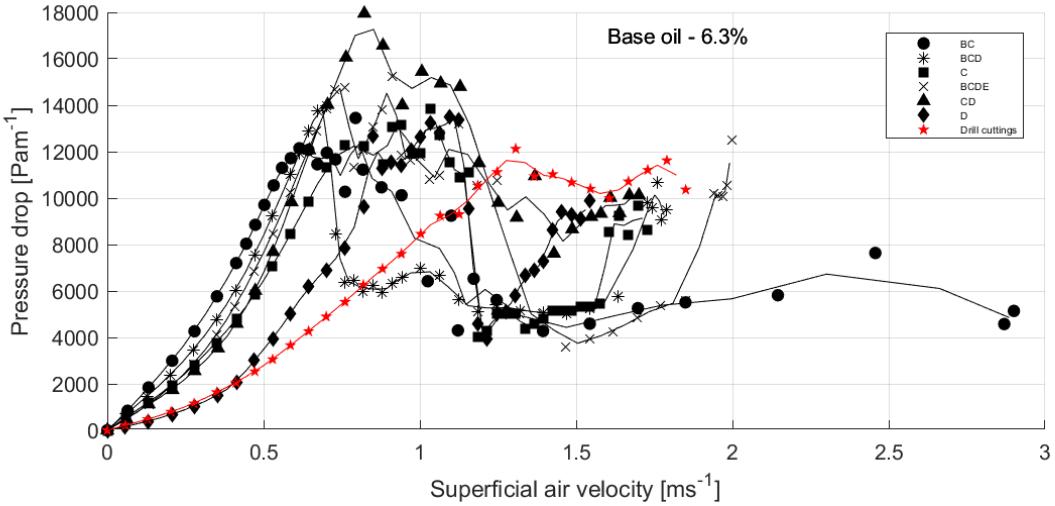

Figure F.4: Fluidization curves for mixtures with 6.3% of base oil

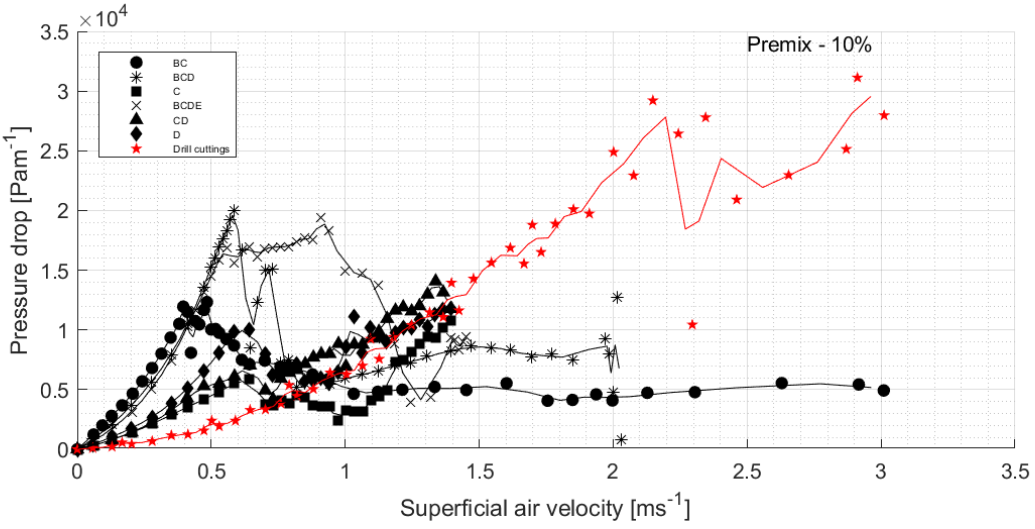

Figure F.5: Fluidization curves for mixtures with 10% of premix

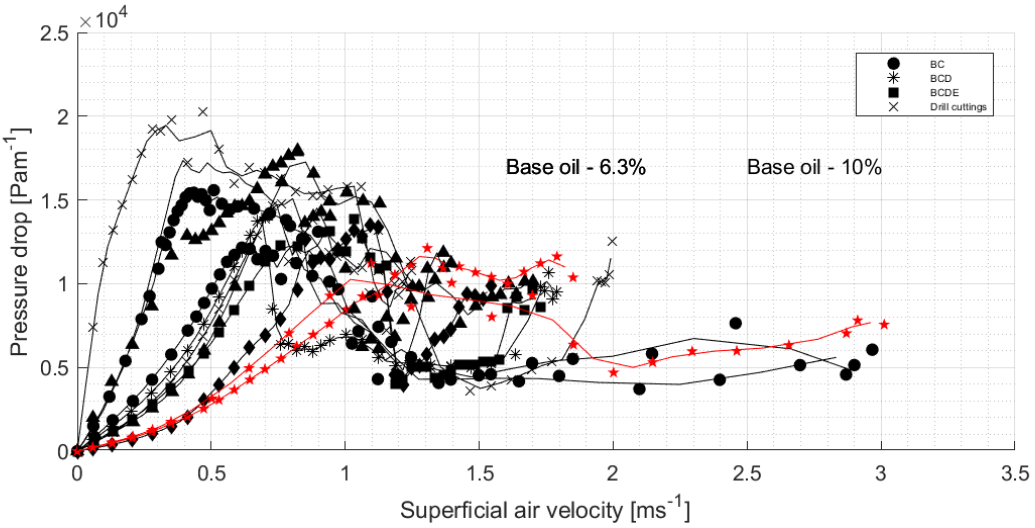

Figure F.6: Fluidization curves for mixtures with 10% of base oil

Appendix G

Pneumatic conveying state diagrams

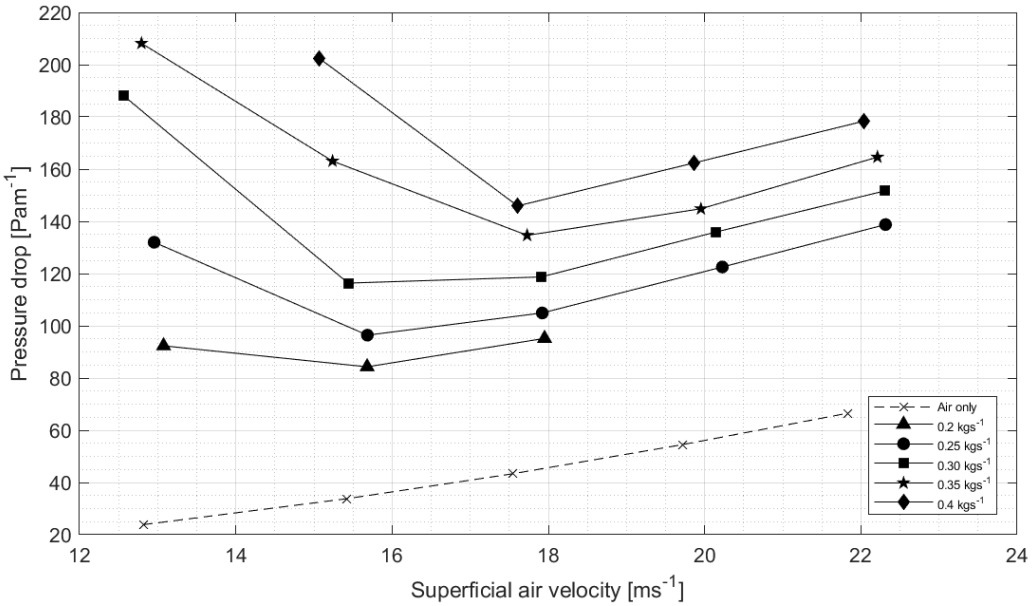

Figure G.1: Pneumatic conveying state diagram for mixture **B** (dry)

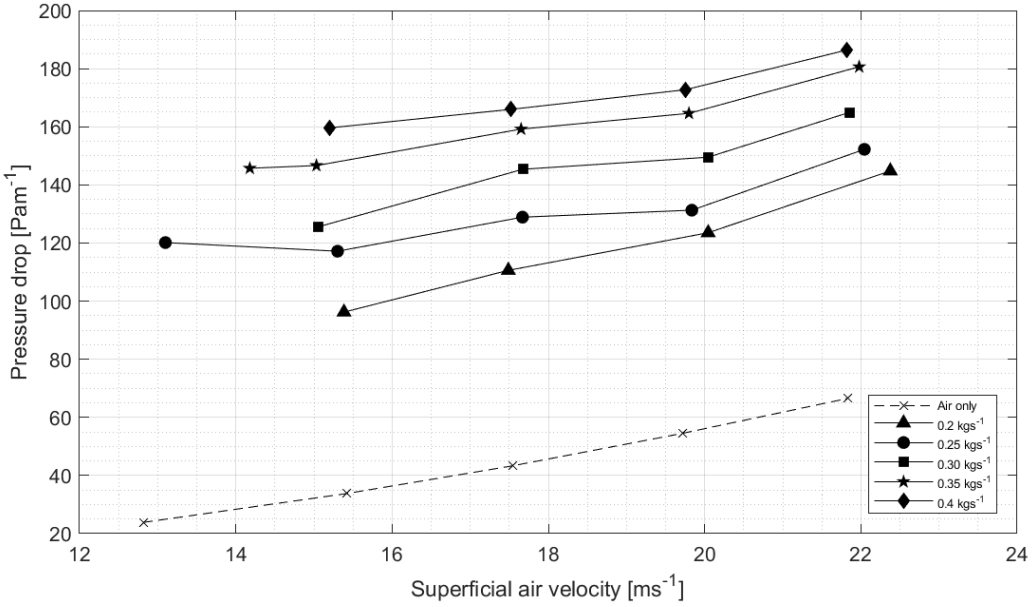

Figure G.2: Pneumatic conveying state diagram for mixture **BC** (dry)

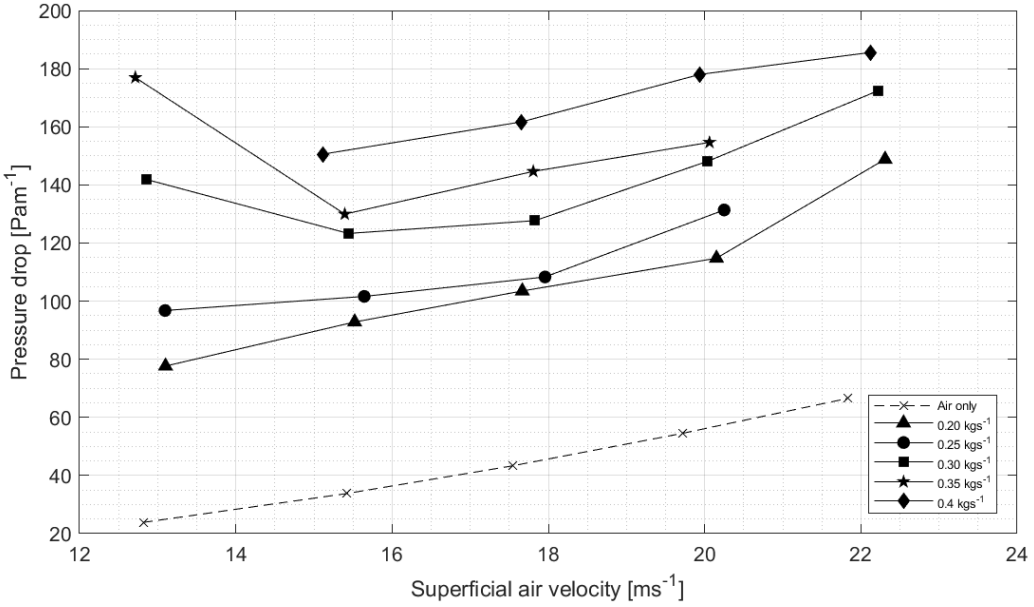

Figure G.3: Pneumatic conveying state diagram for mixture **C** (dry)

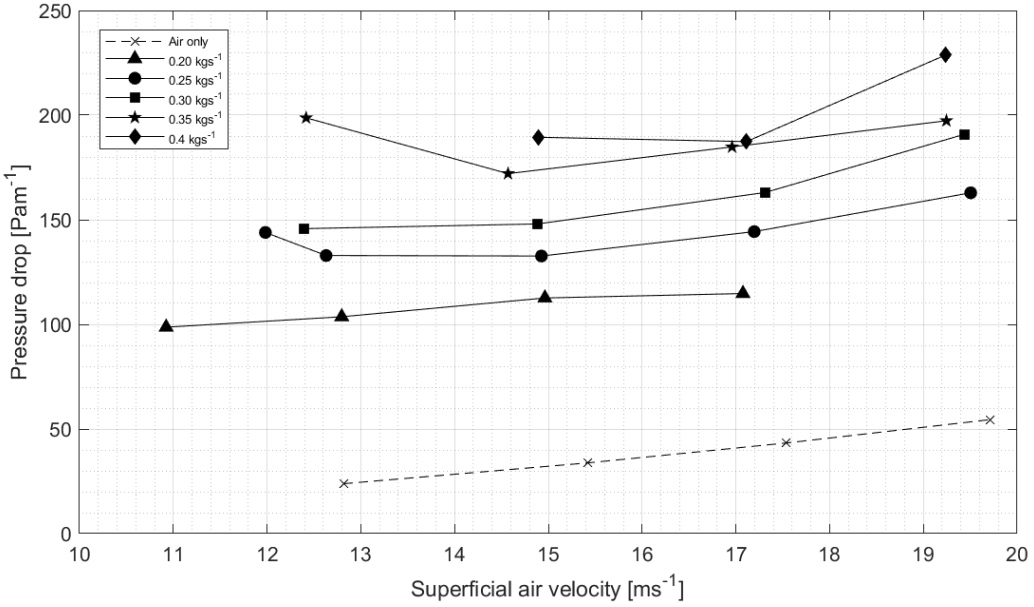

Figure G.4: Pneumatic conveying state diagram for mixture **CD** (dry)

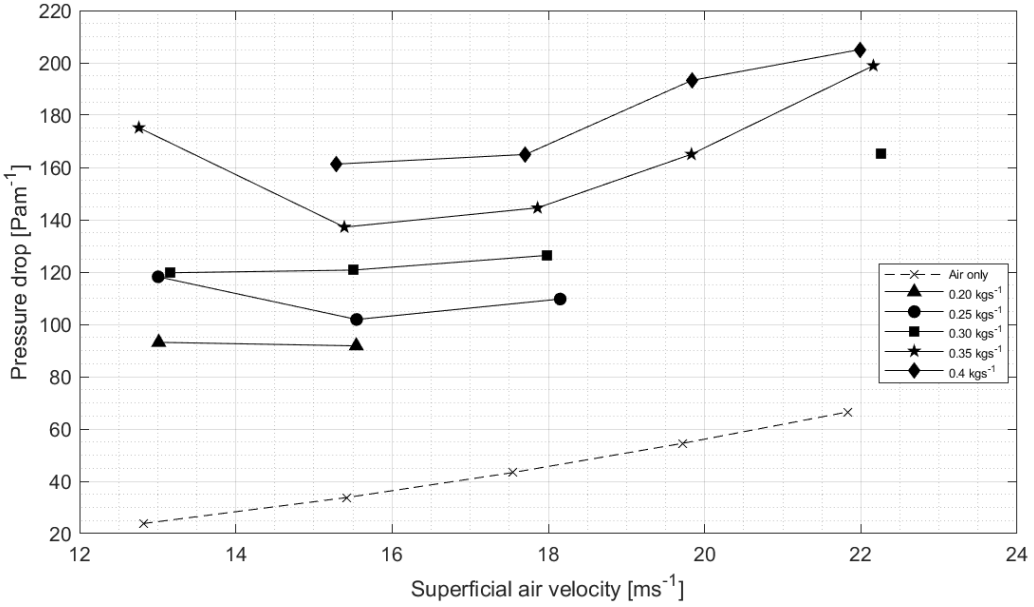

Figure G.5: Pneumatic conveying state diagram for mixture **D** (dry)

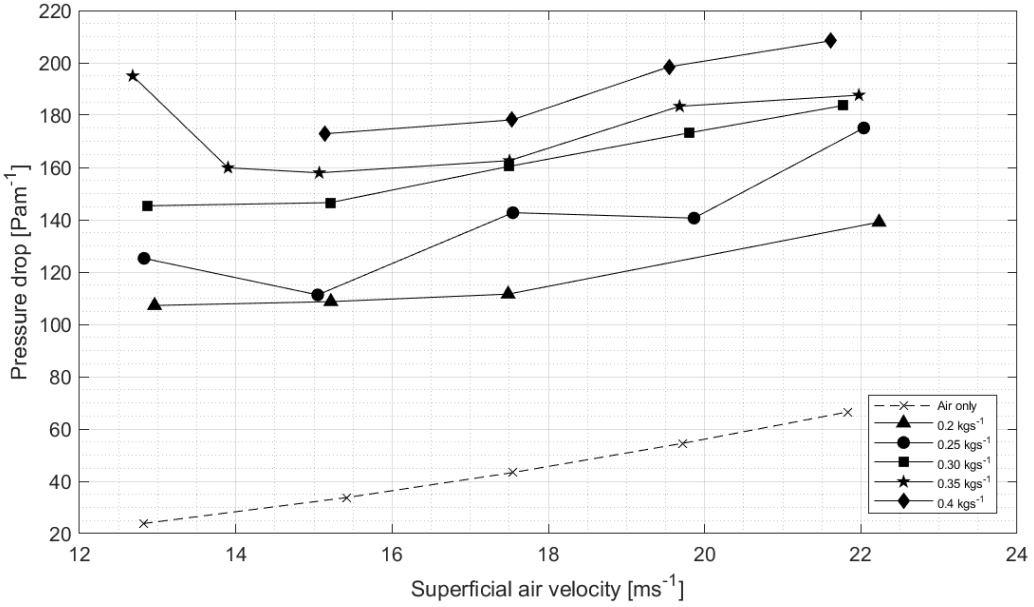

Figure G.6: Pneumatic conveying state diagram for mixture **BCD** (dry)

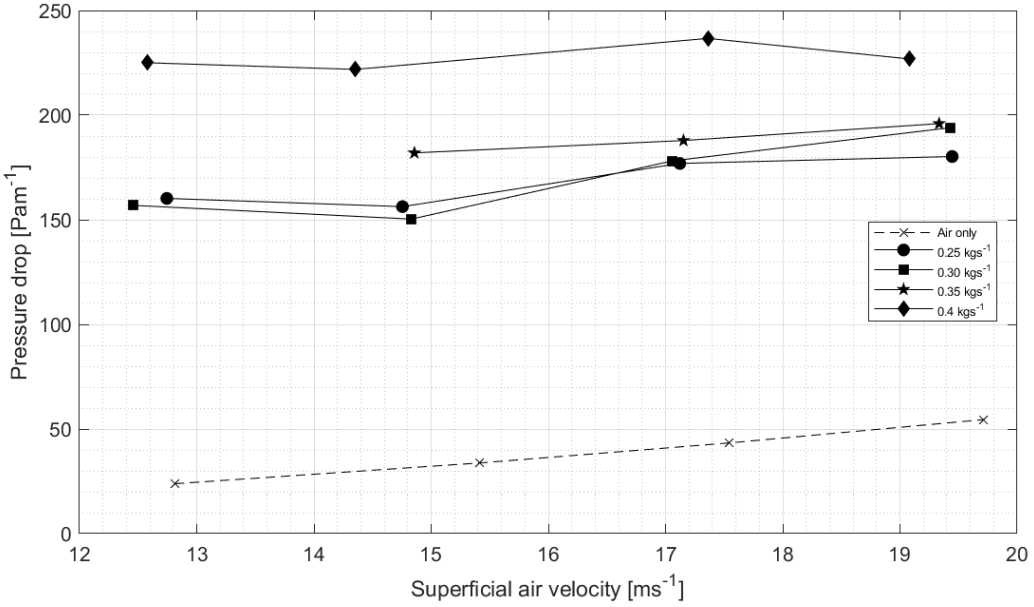

Figure G.7: Pneumatic conveying state diagram for mixture **BCDE** (dry)

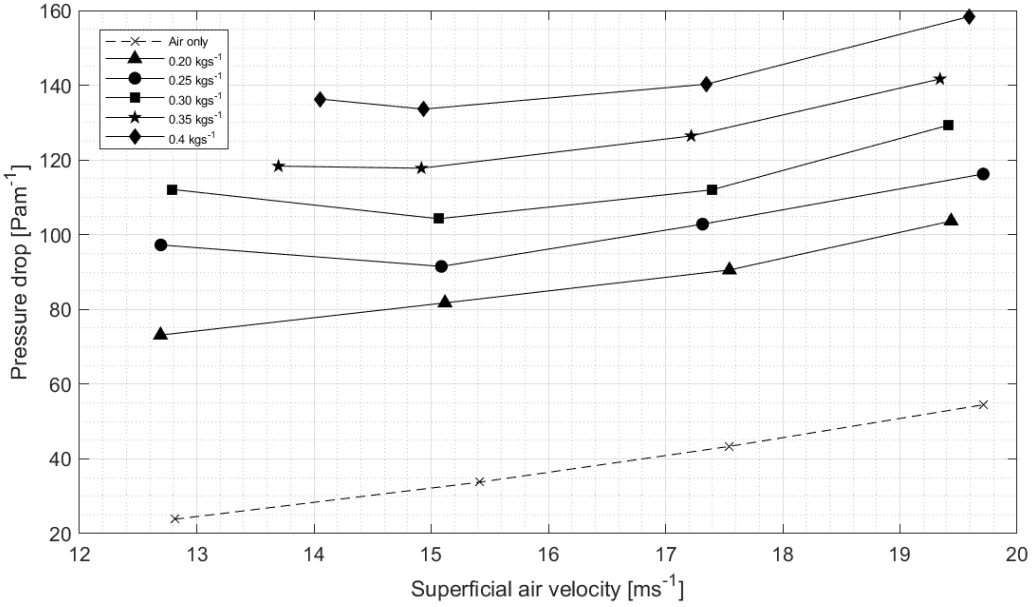

Figure G.8: Pneumatic conveying state diagram for mixture **BC**- Premix 1.5%

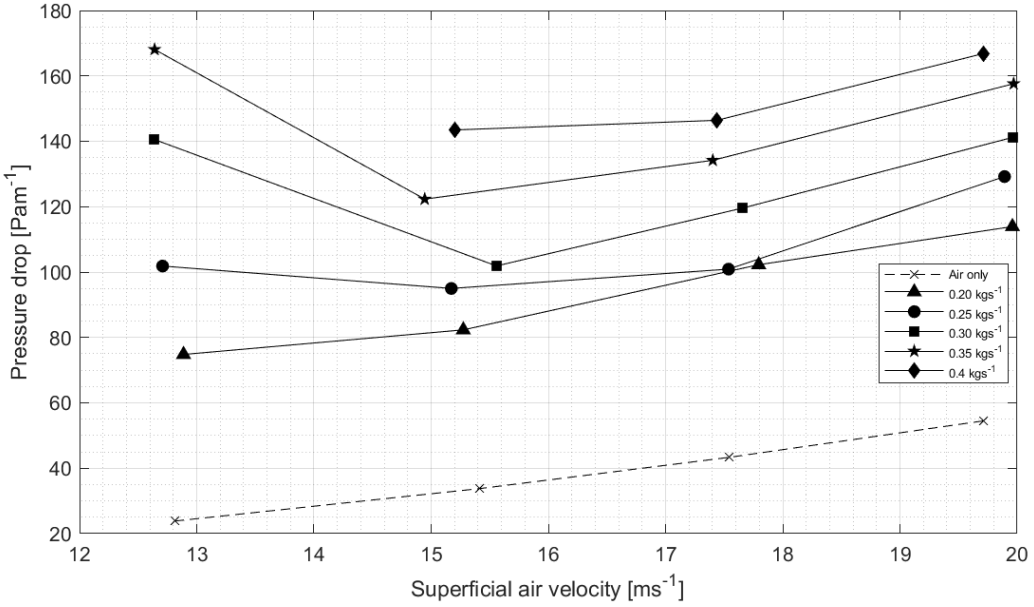

Figure G.9: Pneumatic conveying state diagram for mixture **CD**- Premix 1.5%

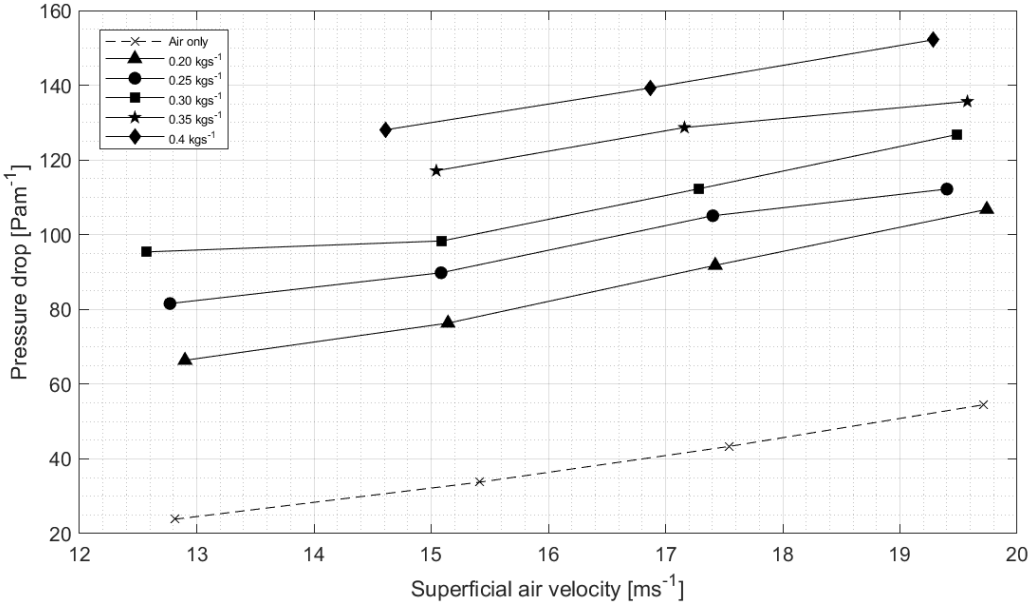

Figure G.10: Pneumatic conveying state diagram for mixture **BCD**- Premix 1.5%

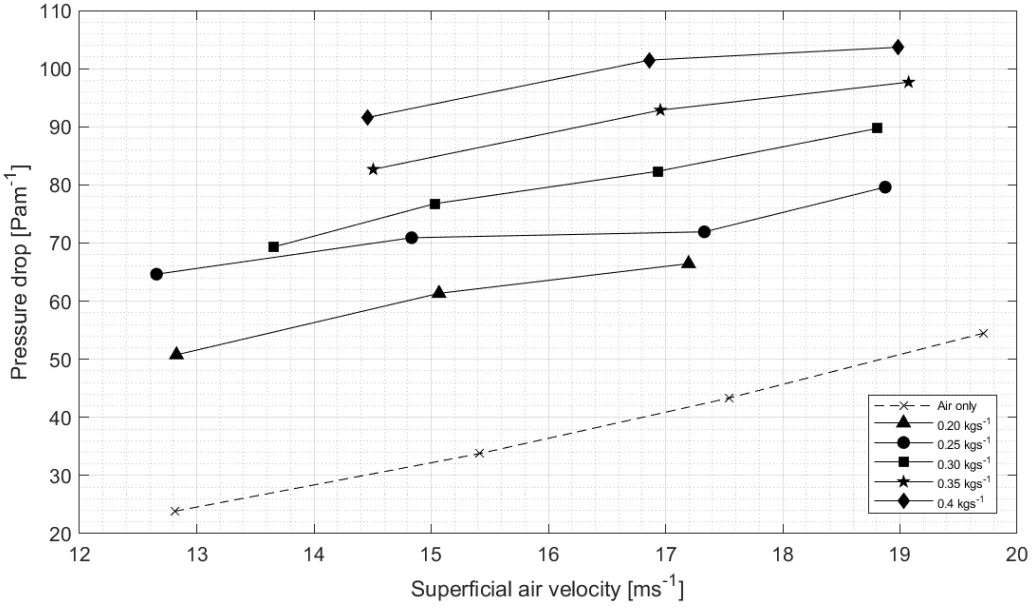

Figure G.11: Pneumatic conveying state diagram for mixture **BCDE**- Premix 1.5%

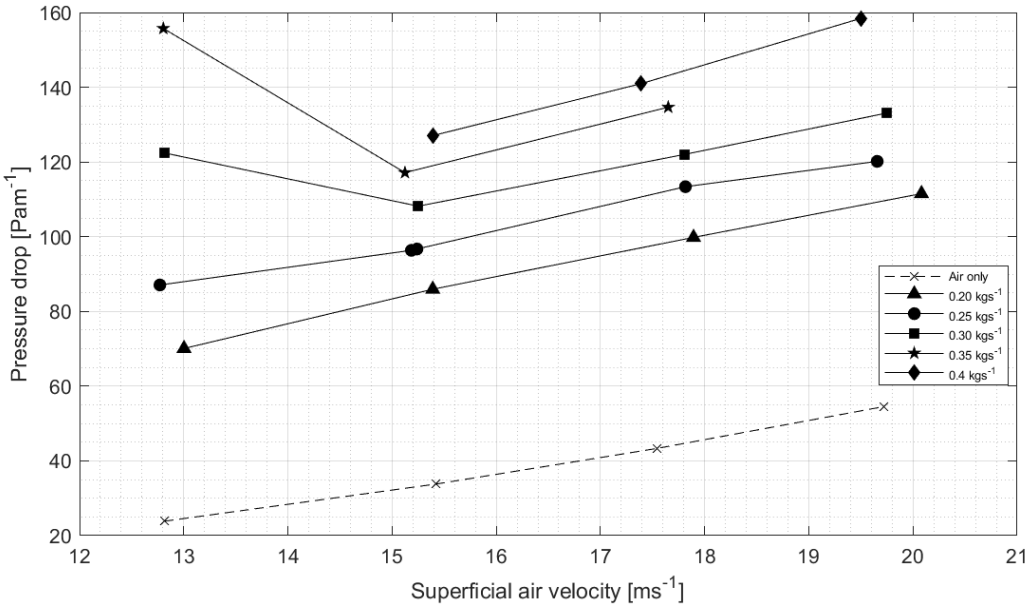

Figure G.12: Pneumatic conveying state diagram for mixture **CD**- Premix 6.3%

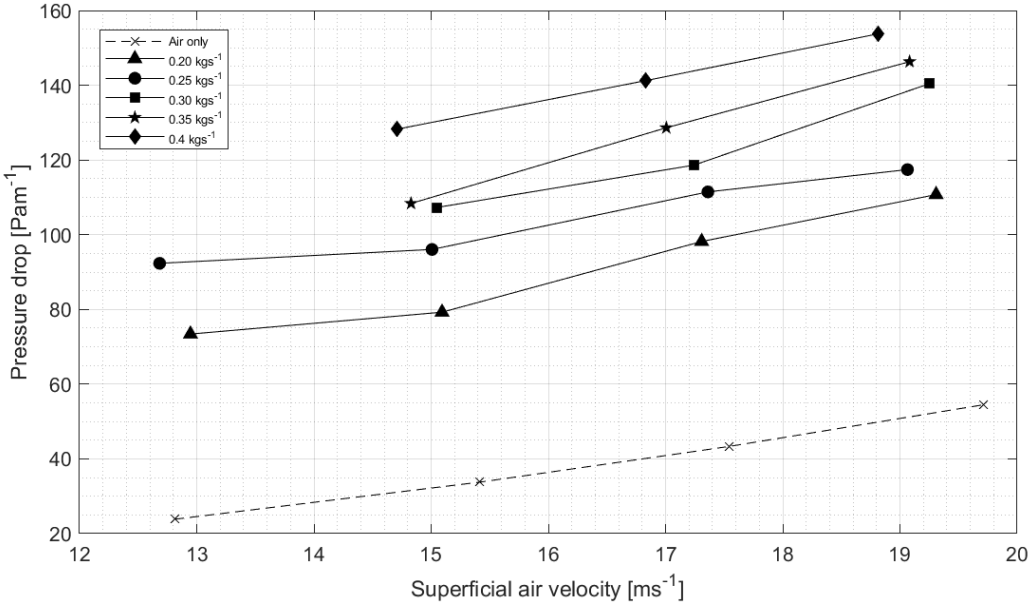

Figure G.13: Pneumatic conveying state diagram for mixture **BCD**- Premix 6.3%

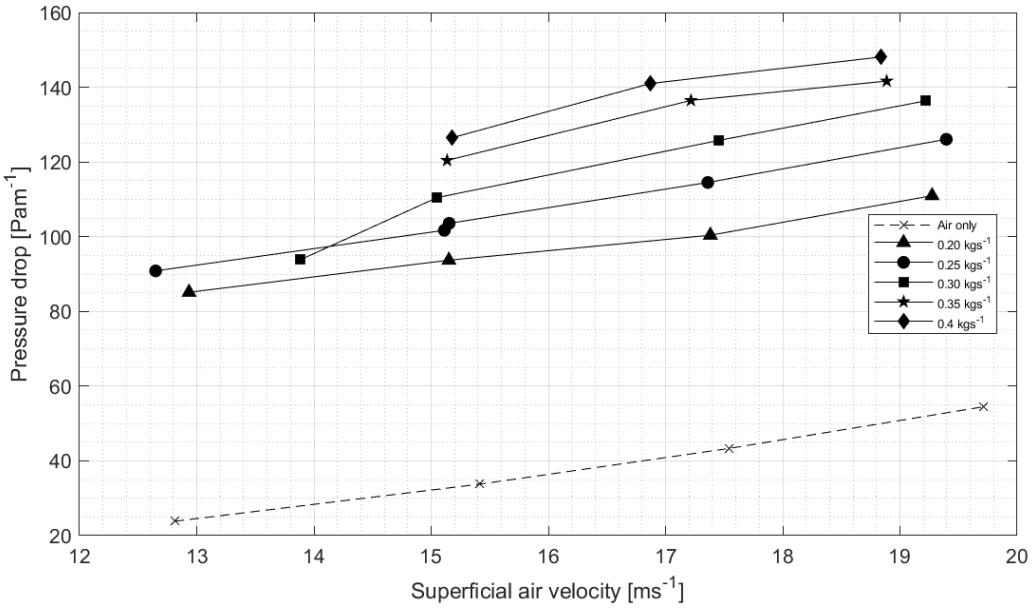

Figure G.14: Pneumatic conveying state diagram for mixture **BCDE**- Premix 6.3%

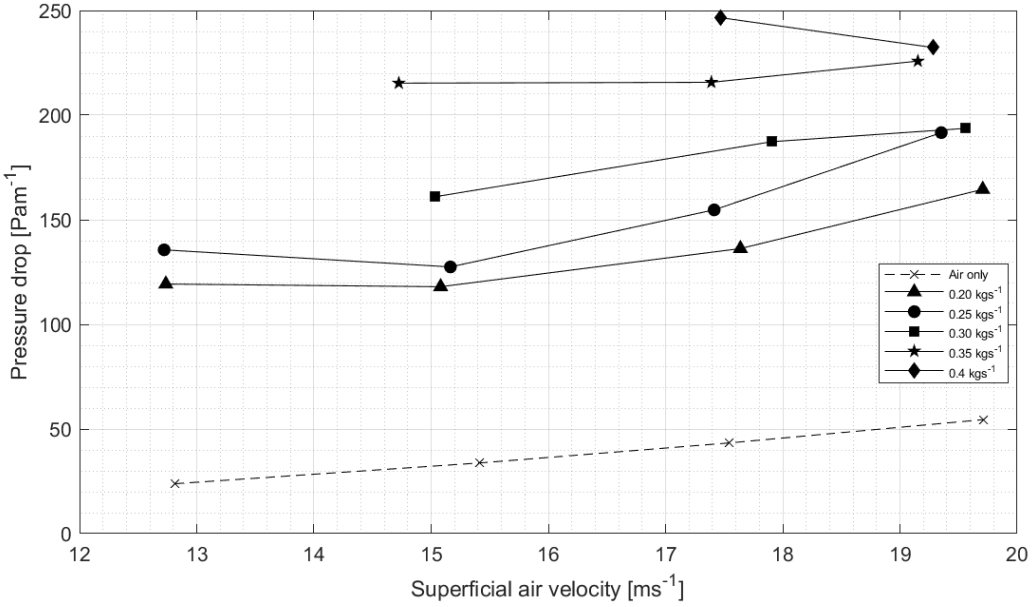

Figure G.15: Pneumatic conveying state diagram for mixture **CD**- Premix 10%

Appendix H

Comparison of pressure drop change and MFV drop

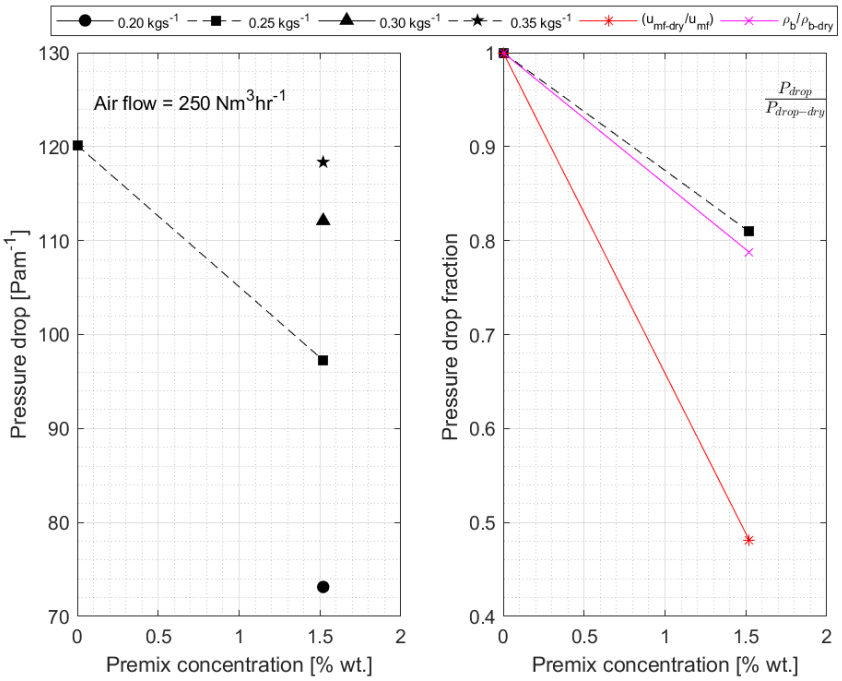

Figure H.1: Pressure drop vs. drilling fluid concentration for the mixture **BC** at air flow of 250 $\mathrm{Nm^3hr^{-1}}$

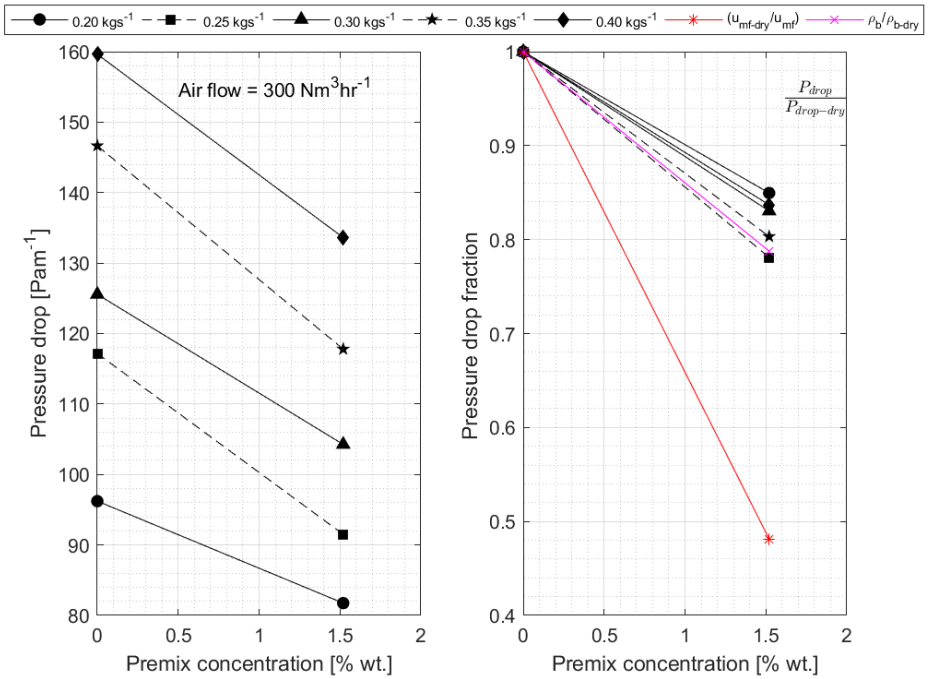

Figure H.2: Pressure drop vs. drilling fluid concentration for the mixture **BC** at air flow of 300 Nm^3hr^{-1}

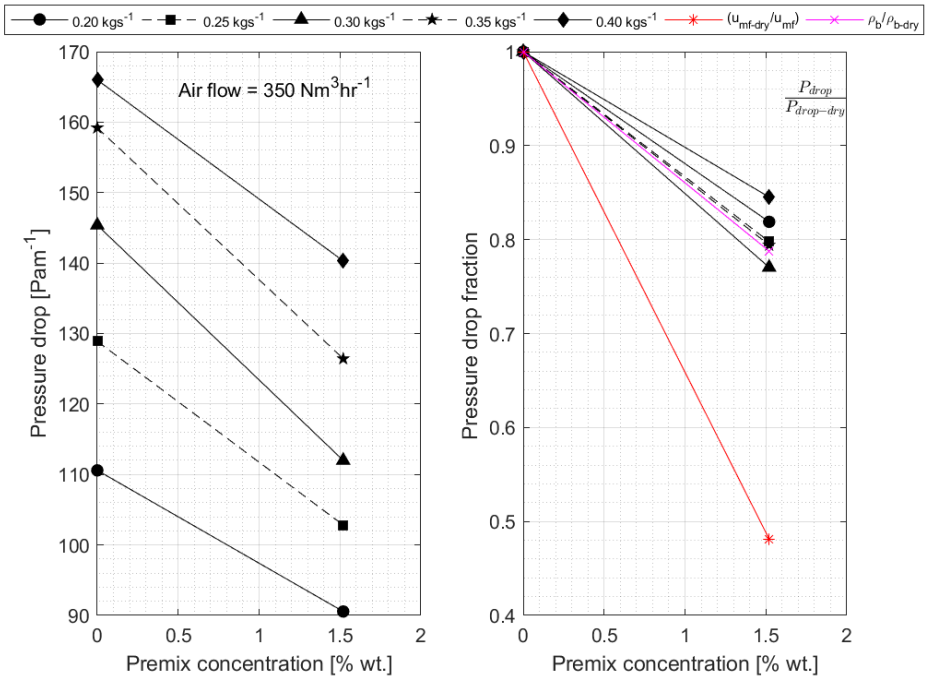

Figure H.3: Pressure drop vs. drilling fluid concentration for the mixture **BC** at air flow of 350 Nm^3hr^{-1}

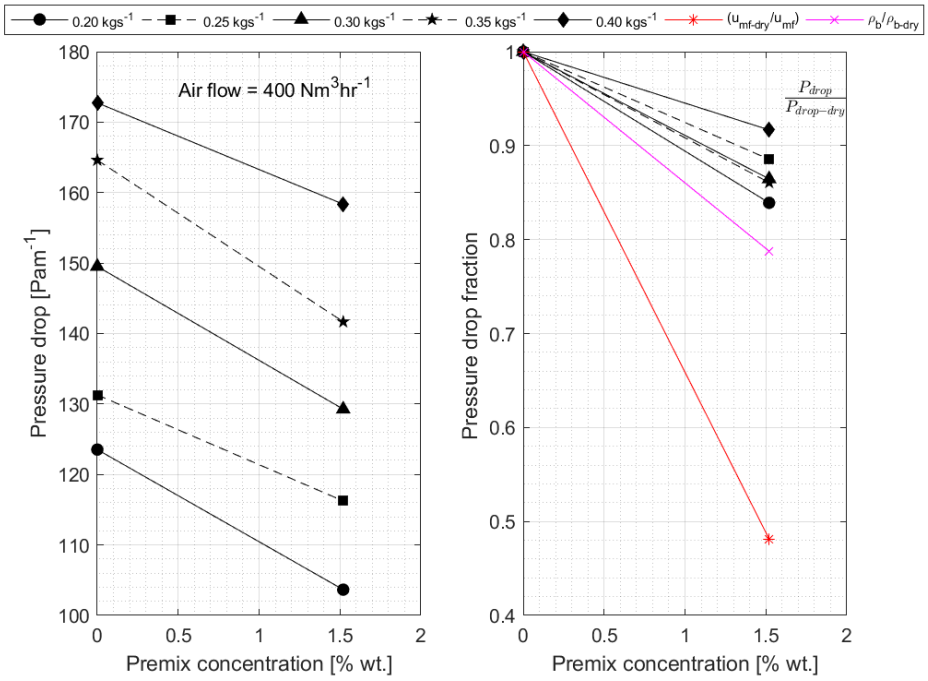

Figure H.4: Pressure drop vs. drilling fluid concentration for the mixture **BC** at air flow of 400 $\mathrm{Nm^3hr^{-1}}$

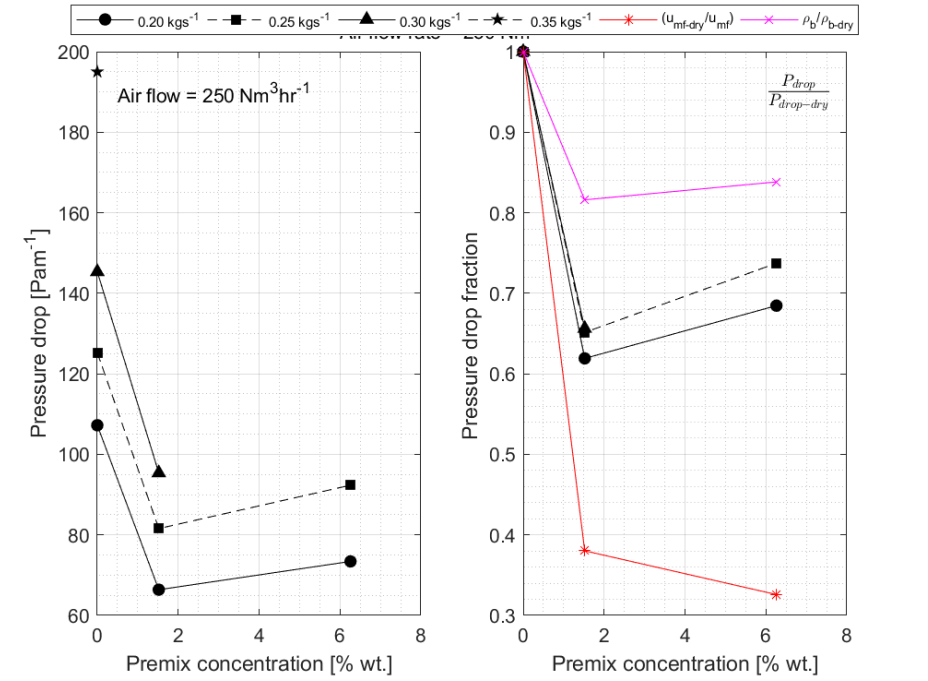

Figure H.5: Pressure drop vs. drilling fluid concentration for the mixture **BCD** at air flow of 250 $\mathrm{Nm^3hr^{-1}}$

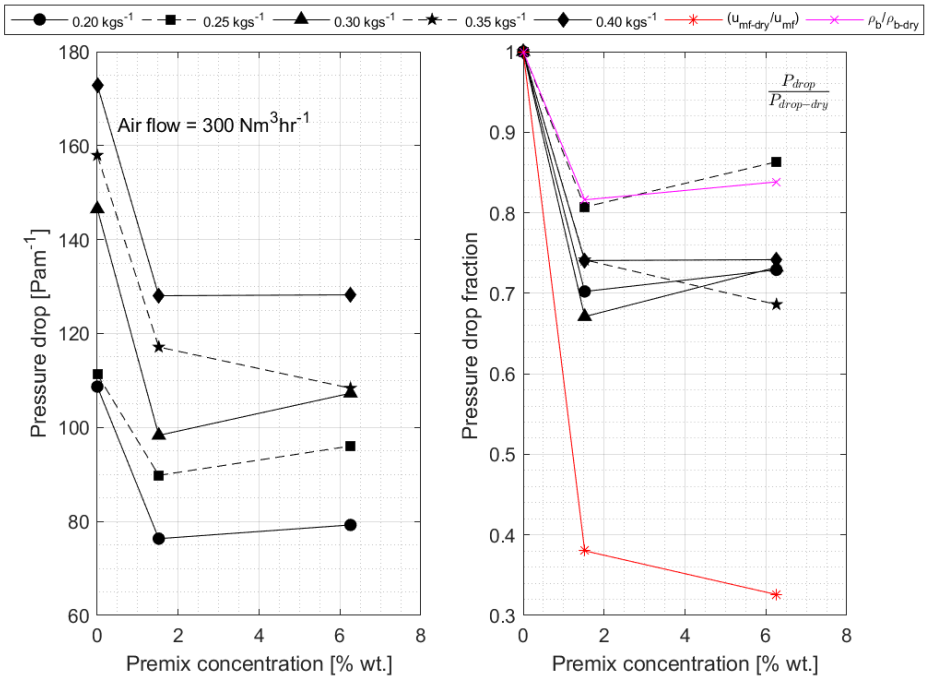

Figure H.6: Pressure drop vs. drilling fluid concentration for the mixture **BCD** at air flow of 300 $\mathrm{Nm^3hr^{-1}}$

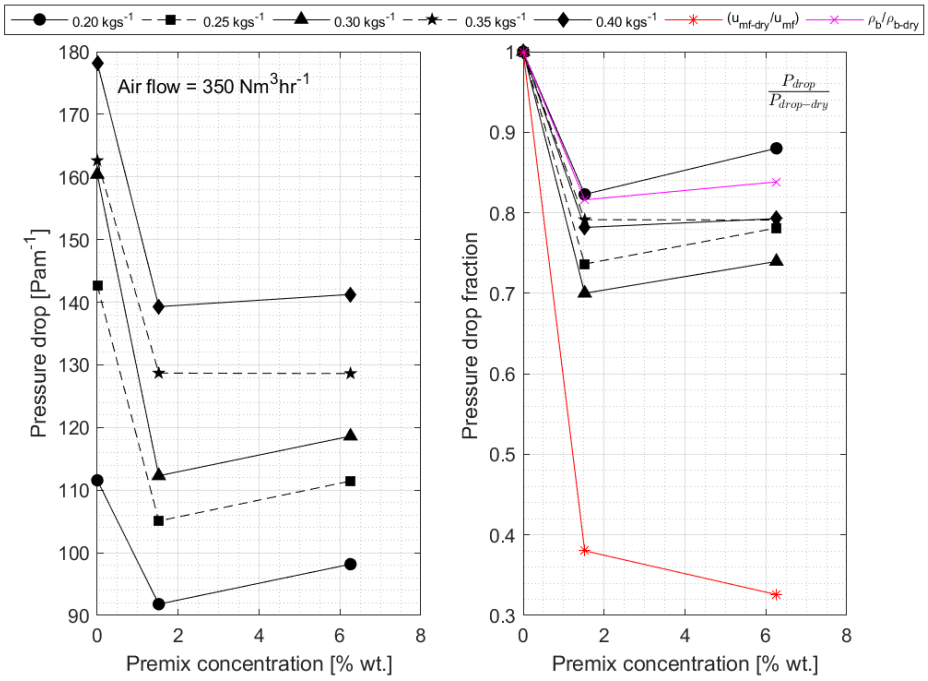

Figure H.7: Pressure drop vs. drilling fluid concentration for the mixture **BCD** at air flow of 350 $\mathrm{Nm^3hr^{-1}}$

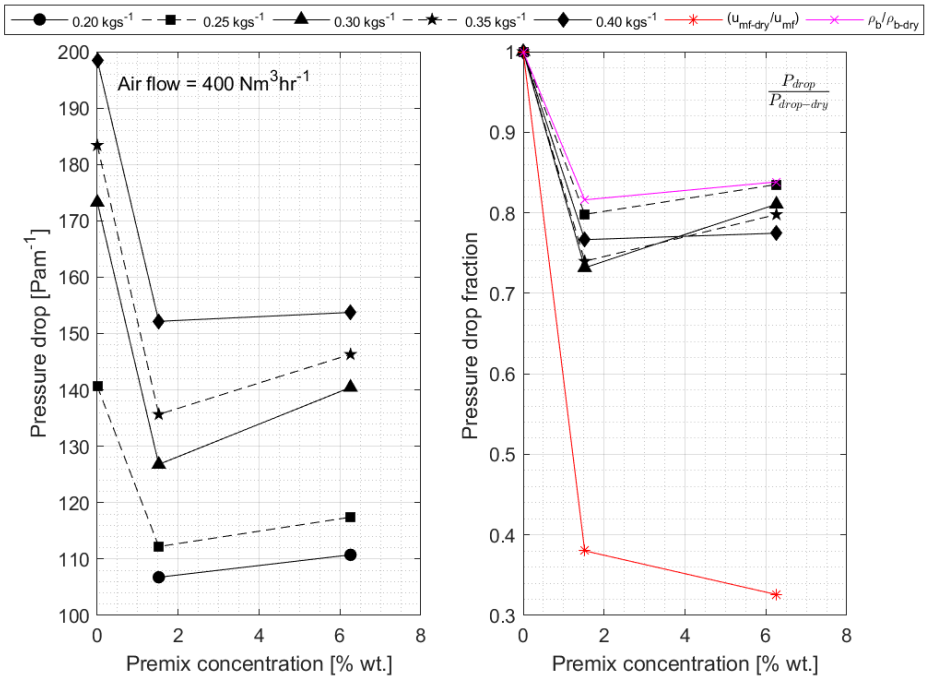

Figure H.8: Pressure drop vs. drilling fluid concentration for the mixture **BCD** at air flow of 400 $\mathrm{Nm^3hr^{-1}}$

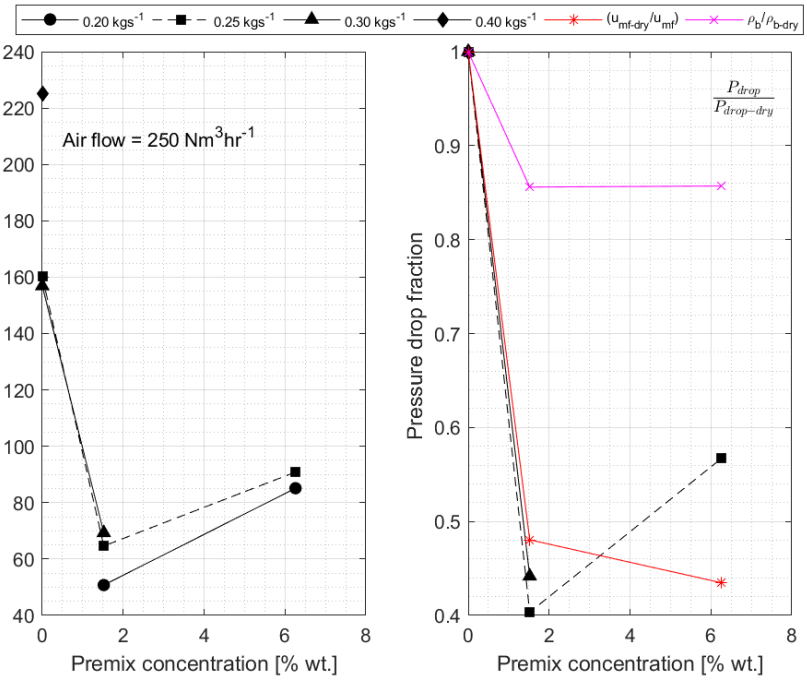

Figure H.9: Pressure drop vs. drilling fluid concentration for the mixture **BCDE** at air flow of 250 $\mathrm{Nm^3hr^{-1}}$

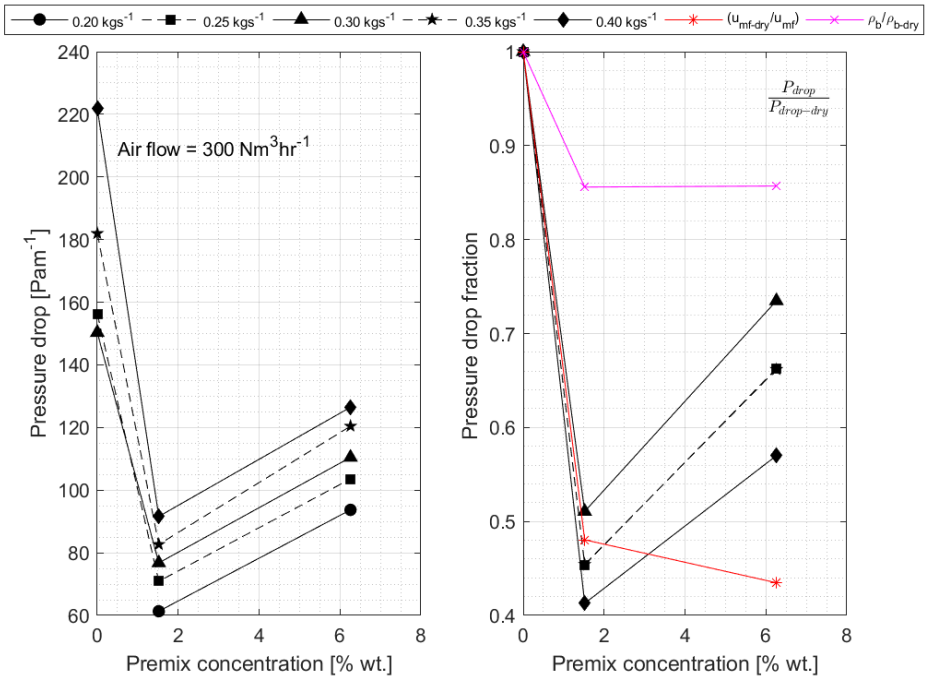

Figure H.10: Pressure drop vs. drilling fluid concentration for the mixture **BCDE** at air flow of 300 Nm^3hr^{-1}

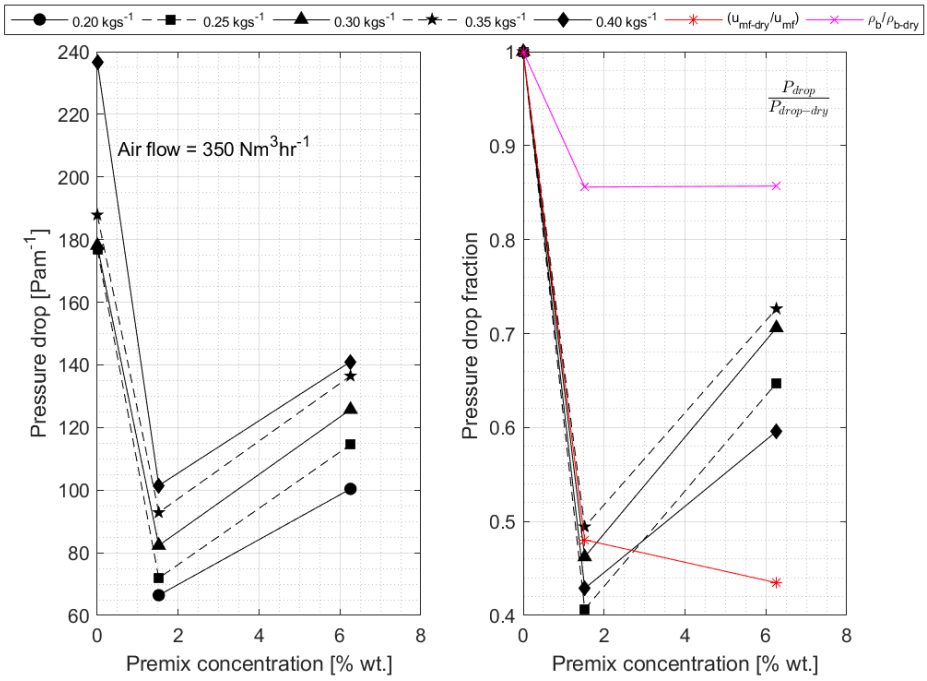

Figure H.11: Pressure drop vs. drilling fluid concentration for the mixture **BCDE** at air flow of 350 Nm^3hr^{-1}

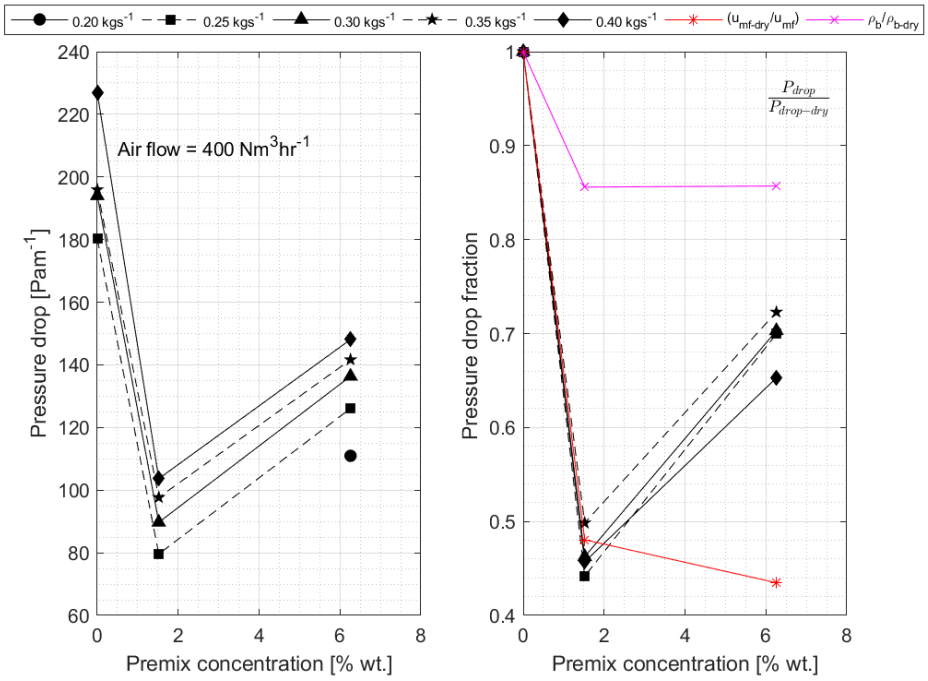

Figure H.12: Pressure drop vs. drilling fluid concentration for the mixture **BCDE** at air flow of 400 Nm^3hr^{-1}

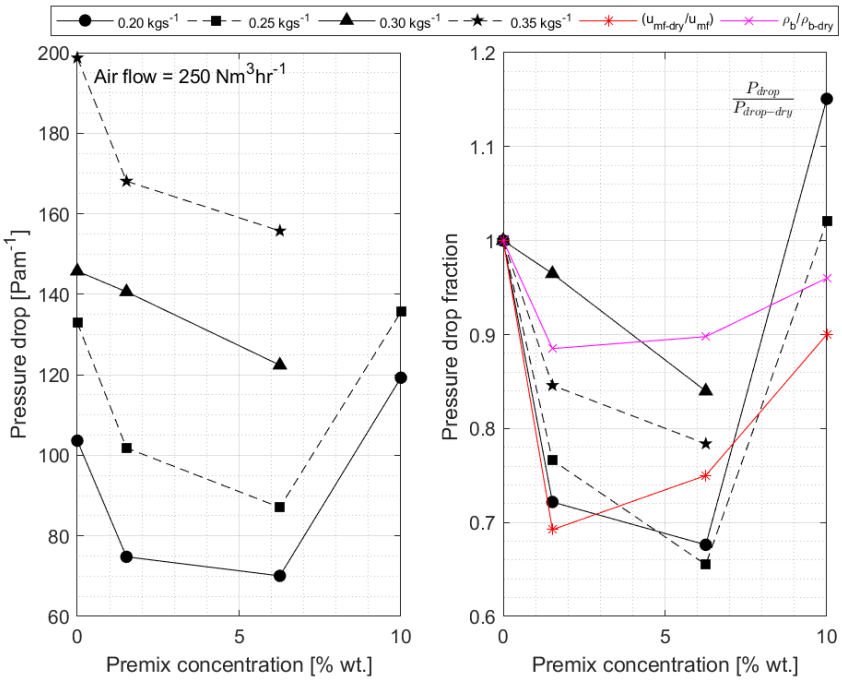

Figure H.13: Pressure drop vs. drilling fluid concentration for the mixture **CD** at air flow of 250 Nm^3hr^{-1}

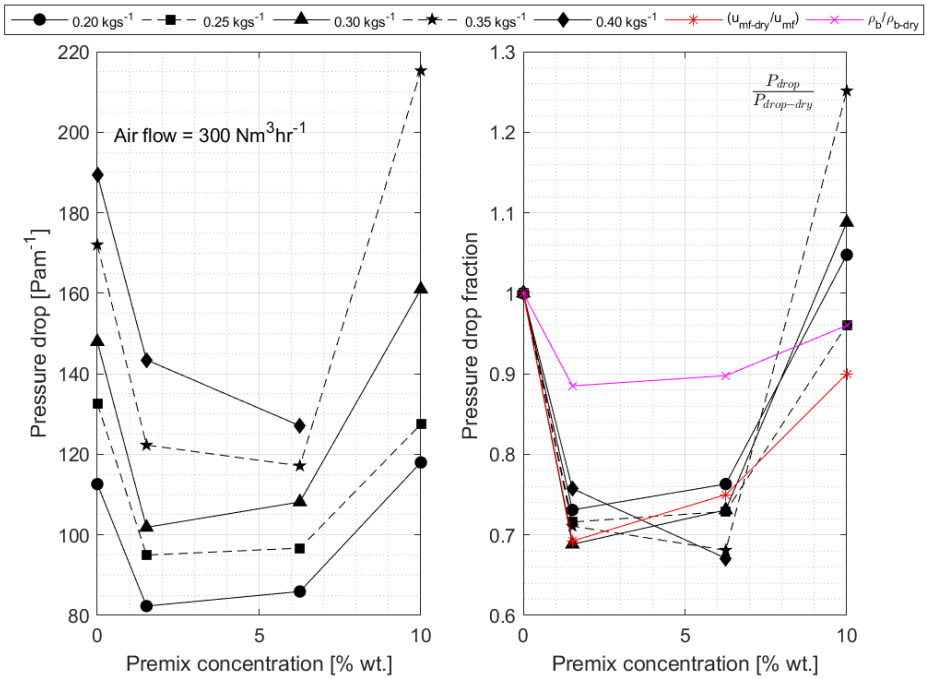

Figure H.14: Pressure drop vs. drilling fluid concentration for the mixture **CD** at air flow of 300 $\mathrm{Nm^3hr^{-1}}$

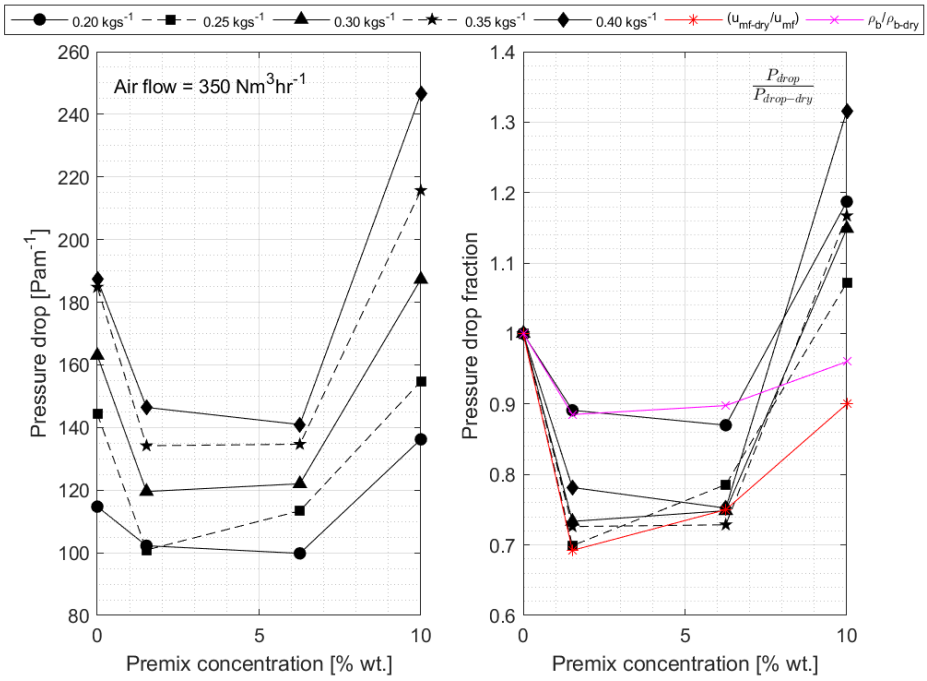

Figure H.15: Pressure drop vs. drilling fluid concentration for the mixture **CD** at air flow of 350 $\mathrm{Nm^3hr^{-1}}$

Doctoral dissertation no. 7
2018

—

Pneumatic conveying and storage of wet particles to illustrate offshore drill cutting handling

Dissertation for the degree of Ph.D

—

Anjana Malagalage

—

ISBN: 978-82-7206-481-4 (print)
ISBN: 978-82-7206-482-1 (online)

usn.no

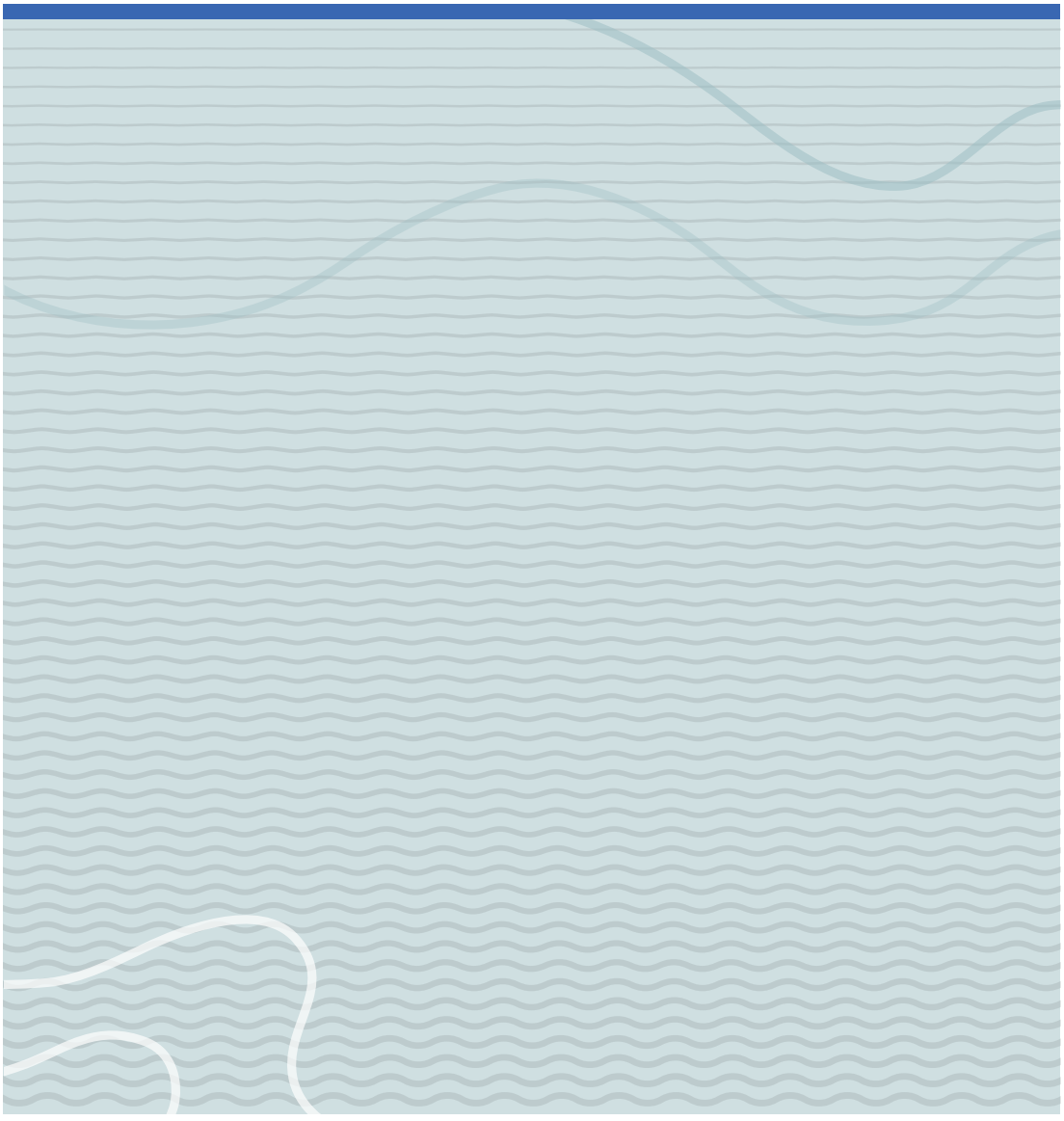

- **Pneumatic conveying and storage of wet particles to illustrate offshore drill cutting handling** - Anjana Malagalage

University of South-Eastern Norway
Faculty of Technology, Natural Sciences and Maritime Studies

Doctoral dissertation no. 7
2018

Anjana Malagalage

N l c s k _rga am l t cwg l e _ l b qrmp_ec md u cr n_prgajcq rm gjj s qrp_rc mddq f mpc bpgjj a s rrg l e f _ l bjg l e